

Quantum Spin Liquid States

Yi Zhou,¹ Kazushi Kanoda,² and Tai-Kai Ng³

¹*Department of Physics and Zhejiang Institute of Modern Physics,
Zhejiang University,
Hangzhou, 310027,
P. R. China*

²*Department of Applied Physics,
University of Tokyo,
Hongo 7-3-1, Bunkyo-ku,
Tokyo 113-8656,
Japan*

³*Department of Physics,
Hong Kong University of Science and Technology,
Clear Water Bay Road,
Kowloon, Hong Kong,
China*

This article is an introductory review on the physics of quantum spin liquid states (QSLs). Quantum magnetism is a fast evolving field, and recent developments show that the ground states and low energy physics of frustrated spin systems may develop lot of exotic behaviors once we get out of the regime of semi-classical approaches. The aim of this article is to introduce this development. The article starts by explaining how the semi-classical approaches fail once quantum mechanics become important, and then describes the alternative approaches to tackle the problem. We shall discuss mainly spin 1/2 systems and spend most of our time on one particular set of plausible spin liquid states in this article where spins are represented by fermions. These states are spin-singlet states and may be viewed as extension of Fermi liquid states to Mott insulators, and are usually classified under the category of so-called $SU(2)$, $U(1)$ or Z_2 spin liquid states. We shall review the basic theory for these states and the extensions of these states to include the effect of spin-orbit coupling, and higher spin ($S > 1/2$) systems. Two other important approaches with strong influences on the understanding of spin liquid states are also introduced; (i) The Matrix Product states and Projected Entangled Pair States, and (ii) the Kitaev honeycomb model. Experimental progresses for spin liquid states in realistic materials including anisotropic triangular lattice systems (κ -(ET)₂Cu₂(CN)₃ and EtMe₃Sb[(Pd(dmit)₂)₂]; Kagome-lattice systems (ZnCu₃(OH)₆Cl₂) and Hyperkagome-lattice systems (Na₄Ir₃O₈) are reviewed and compared with theories.

PACS numbers: 75.10.Kt, 71.10.-w, 71.10.Ay, 71.30.+h

CONTENTS

I. Introduction	2	III.4.1. One dimensional lattice	20
II. From semi-classical to non-linear-sigma model approaches for quantum antiferromagnets	3	III.4.2. Triangular lattice	21
II.1. Two-spin problem	3	III.4.3. Kagome lattice	21
II.2. Berry's phase	4	III.5. Classification of spin liquid states: Quantum Order and Projective Symmetry Groups	23
II.3. Non-linear- σ -model	4	IV. Beyond RVB approaches	24
II.3.1. Topological term	5	IV.1. RVB and its generalization to spin systems with strong spin-orbit coupling	24
II.4. Quantum spin chains and Haldane conjecture	6	IV.2. RVB approach to $S > 1/2$ systems	26
II.4.1. Integer spin chains	6	IV.3. Matrix Product States (MPS) and Projected Entangled Pair States (PEPS)	28
II.4.2. Half-odd-integer spin chains	7	IV.3.1. Valence Bond Solid and MPS states in one dimension	29
II.4.3. Open spin chains and end states	7	IV.3.2. PEPS states in higher dimensions and beyond	30
II.5. Higher dimensions and frustrated quantum antiferromagnets	8	IV.4. Kitaev honeycomb model and related issues	31
III. Resonant Valence Bond (RVB) States	8	V. Spin Liquid States in Real Materials	34
III.1. RVB and Gauge Theory	11	V.1. Anisotropic triangular lattice systems: κ -(ET) ₂ Cu ₂ (CN) ₃ and EtMe ₃ Sb[(Pd(dmit) ₂) ₂]	35
III.2. U(1) gauge fluctuations	14	V.2. Kagome-lattice system: ZnCu ₃ (OH) ₆ Cl ₂	40
III.2.1. Mott transition: relation between Fermi- and spin- liquids	15	V.3. Hyperkagome-lattice system: Na ₄ Ir ₃ O ₈	43
III.3. Z_2 spin liquid states	17	V.4. Experimental summary	45
III.4. Numeric Realization of Gutzwiller Projection: Variational Monte Carlo Method and Some Results	18	VI. Summary	47

Acknowledgments	49
A. Path integral for a single spin	49
References	50

I. INTRODUCTION

Quantum spin liquid states (QSLs) in dimensions $d > 1$ has been a long sought dream in condensed matter physics. The general idea is that when acting on spin systems, quantum mechanics may lead to exotic ground states and low energy behaviors which cannot be captured by traditional semi-classical approaches. The difficulty in implementing this idea is that we have no natural place to start with once we are out of the comfort zone of semi-classical approaches, at least at dimensions larger than one. Except for a few exactly solvable models, we have to rely heavily on numerical or variational approaches to “guess” the correct ground state wavefunctions and a combination of sophisticated numerical and analytical techniques to understand the corresponding low energy excitations.

There exist some excellent reviews on quantum spin liquids (Balents, 2010; Lee, 2008a) and frustrated magnetism (Diep, 2004; Lacroix *et al.*, 2011). This article complements the ones mentioned above by attempting to give a pedagogical introduction to this subject and reviews the current status of the field. We shall explain in an introductory level why sophisticated approaches are needed to study quantum spin liquid states, how they are implemented in practice, and what are the expected new physics that may appear. The experimental side of the story and the drawbacks or pitfalls in the theoretical approaches will also be discussed. We shall concentrate mainly on spin 1/2 systems, and shall study in detail one particular set of plausible spin liquid states usually termed Resonant Valence Bond (RVB) states in this article. The spins are treated as fermions in these states and the states may be viewed as extension of Fermi liquid states to Mott insulators. They are usually classified under the category of $SU(2)$, $U(1)$ or Z_2 spin liquid states. Because of intrinsic limitations in the fermionic RVB approach, many other approaches to spin liquid states have been developed by different authors. These approaches often lead to other exotic possibilities not covered by the simple fermionic approach. Two of these approaches will be introduced in this article for completeness; (i) The Matrix Product states and Projected Entangled Pair States, and (ii) the Kitaev honeycomb model.

The article is organized in the following way: in section II we introduce the semi-classical approach for simple quantum antiferromagnets, explain the importance of spin Berry phase and how one can include it in a semi-classical description to obtain the correct theory. In particular, we show how it leads to the celebrated Haldane

conjecture. The existence of end excitations as a natural consequence of the low energy effective theory of these systems will be discussed. One-dimensional quantum spin systems are of strong interests nowadays because they provide some of the simplest realizations of Symmetry Protected Topological phases (SPT) in strongly correlated systems.

The limitation of the semi-classical approach when applying to systems with frustrated interaction will be pointed out in section III where we introduce the alternative idea of constructing variational wavefunctions directly. We shall introduce Anderson’s famous idea of Resonant Valence Bond (RVB) wavefunction for spin 1/2 systems and discuss how this idea can be implemented in practice. The difficulty of incorporating $SU(2)$ spin algebra in our usual many-body perturbation theory is pointed out and the trick of representing spins by particles (fermions or bosons) with *constraints* to avoid the difficulty is introduced. The non-trivial $SU(2)$ gauge structure in the fermion representation of RVB states and the resulting rich structure in low energy effective field theories for these spin states ($SU(2)$, $U(1)$ and Z_2 spin liquids) are discussed. An interesting linkage of the $U(1)$ spin liquid state to the (metallic) Fermi liquid state through a Mott metal-insulator transition is introduced.

The difficulty of finding controllable approaches to study spin liquid states has led to extension of the RVB approach and the search of alternative approaches. Some of these approaches are reviewed briefly in section IV, including (i) the extension of RVB to include the effect of spin-orbit coupling and higher spin ($S > 1/2$) systems, (ii) The Matrix Product states and Projected Entangled Pair States, and (iii) the Kitaev honeycomb model. The main message of this section is that a larger variety of exotic spin states become possible when we go out of the paradigm of spin-1/2 systems with rotational symmetry. The $U(1)$ and Z_2 spin liquid states belong to just a very small corner of plausible exotic states once we get out of the paradigm of semi-classical approaches.

Section V is devoted to an experimental survey for spin liquid states. Special attention is paid to the $U(1)$ spin liquid state, where most experimental efforts were devoted to. The best studied examples are a family of organic compounds $\kappa-(ET)_2Cu_2(CN)_3$ (ET) (Shimizu *et al.*, 2003) and $Pd(dmit)_2(EtMe_3Sb)$ (dmit salts) (Itou *et al.*, 2008). Both materials are Mott insulators in proximity to the metal-insulator transition and become superconductor (ET) or metal (dmit) under modest pressure. Despite the large magnetic exchange $J \approx 250$ K observed in these systems, there is no experimental indication of long range magnetic ordering down to temperature ~ 30 mK. Linear temperature dependence of the specific heat and Pauli-like spin susceptibility were found in both materials at low temperature suggesting that the low energy excitations are spin-1/2 fermions with a Fermi surface (Watanabe *et al.*, 2012;

Yamashita *et al.*, 2008b). This Fermi liquid-like behavior is further supported by their Wilson ratios which are close to one. Besides ET and dmit-salt, the Kagome compound $ZnCu_3(OH)_6Cl_2$ (Helton *et al.*, 2007), and the three dimensional hyper-Kagome material $Na_4Ir_3O_8$ (Okamoto *et al.*, 2007) are also considered to be candidates for QSLs with gapless excitations. Experimental surveys on these quantum spin liquid candidate materials are presented in this article, including thermodynamics, thermal transport and various spin spectra. We also briefly introduce the discoveries of a few new materials, and discuss the existing discrepancies between experiments and theories. The paper is summarized in section VI.

II. FROM SEMI-CLASSICAL TO NON-LINEAR-SIGMA MODEL APPROACHES FOR QUANTUM ANTIFERROMAGNETS

We consider here simple Heisenberg antiferromagnets on bi-partite lattices (with sublattices A and B) with Hamiltonian

$$H = J \sum_{\langle i,j \rangle} \mathbf{S}_i \cdot \mathbf{S}_j, \quad (1)$$

where $J > 0$ and $\langle i,j \rangle$ describes a pair of nearest neighbor sites on the bi-partite lattice. For a bipartite lattice, two nearest neighbor sites always belong to different sublattices. \mathbf{S} is a quantum spin with magnitude $S = n/2$, where $n =$ positive integer. Examples of bi-partite lattices include 1D spin chain, 2D square or honeycomb lattices, and 3D cubic lattices.

II.1. Two-spin problem

The semi-classical approach starts from the assumption that the quantum spins are “close” to classical spins and it is helpful to start from first analyzing the corresponding classical spins problem. For simplicity, we start by considering only two classical spins coupled by the Heisenberg interaction

$$H = J \mathbf{S}_A \cdot \mathbf{S}_B. \quad (J > 0)$$

The classical spins obey the Euler’s equation of motion

$$\frac{\partial \mathbf{S}_{A(B)}}{\partial t} = J \mathbf{S}_{B(A)} \times \mathbf{S}_{A(B)}. \quad (2)$$

The equation can be solved most easily by introducing the magnetization and staggered magnetism vectors $\mathbf{M}(\mathbf{N}) = \mathbf{S}_A + (-)\mathbf{S}_B$, where it is easy to show from Eq. (2) that

$$\begin{aligned} \frac{\partial \mathbf{M}}{\partial t} &= 0, \\ \frac{\partial \mathbf{N}}{\partial t} &= J \mathbf{M} \times \mathbf{N}, \end{aligned} \quad (3)$$

indicating that classically the staggered magnetization vector \mathbf{N} rotates around the (constant) total magnetization vector \mathbf{M} . Denoting $\mathbf{S}_{A(B)} = S_{A(B)} \hat{r}_{A(B)}$, where $S_{A(B)}$ are the magnitudes of spins $\mathbf{S}_{A(B)}$ and $\hat{r}_{A(B)}$ are unit vectors indicating the directions of $\mathbf{S}_{A(B)}$, the classical ground state has $\hat{r}_A = -\hat{r}_B$ with $\mathbf{M} = 0$, i.e. the two spins are antiferromagnetically aligned. Notice that the equation of motion (3) implies $\frac{\partial(\mathbf{N}^2)}{\partial t} = 0$, i.e. the magnitude of \mathbf{N} remains unchanged during its motion. Therefore, writing $\mathbf{N} = N \hat{n}$, where N is the magnitude of \mathbf{N} and \hat{n} is the unit vector denoting its direction, we find that only \hat{n} changes under the equation of motion (3),

The effects of quantum mechanics can be seen most easily by observing that the equations of motion (3) describes the dynamics of a free rotor (a hard rod with one end fixed and the rod can rotate freely around the fixed end otherwise). A free rotor is represented by a vector $\mathbf{r} = r_0 \hat{r}$, where $r_0 =$ constant is the length of the rod, and \hat{r} is the unit radial vector describing the orientation of the rod. The rod has angular momentum

$$\mathbf{L} = \mathbf{r} \times \mathbf{p} = r_0 \hat{r} \times \mathbf{p}, \quad (4)$$

where $\mathbf{p} = m r_0 \dot{\hat{r}}$ is the momentum, and m is the mass. Using Eq. (4), we obtain

$$\dot{\hat{r}} \times \mathbf{L} = -r_0 \mathbf{p} = -mr_0^2 \dot{\hat{r}}. \quad (5a)$$

We also have

$$\dot{\mathbf{L}} = 0 \quad (5b)$$

(conservation of angular momentum). Comparing equations (3) and (5), we find that the equations of motion for two spins is equivalent to the equation of motions for free rotor if we identify $\mathbf{L} \rightarrow \mathbf{M}$, $\hat{r} \rightarrow \hat{n}$ and $J = I^{-1}$, where $I = mr_0^2$ is the moment of inertia of the rotor.

The quantum Hamiltonian of the free rotor is

$$H_{rotor} = \frac{1}{2I} \mathbf{L}^2,$$

and its solution is well known. The eigenstates are spherical harmonics $Y_{lm}(\theta, \phi)$ (θ and ϕ specifies the direction of unit vector \hat{r}) with eigenvalues

$$\mathbf{L}^2 = l(l+1)\hbar^2, \quad L_z = m\hbar,$$

and corresponding energies $E_l = l(l+1)\hbar^2/2I$, l, m are integers with $l \geq 0$ and $l \geq |m|$. In particular, the ground state of the quantum rotor has $\mathbf{L}(\mathbf{M}) = 0$, but the direction of the vector $\mathbf{r}(\mathbf{N})$ is completely uncertain ($Y_{00}(\theta, \phi) = \frac{1}{\sqrt{4\pi}}$) as a result of quantum fluctuations, indicating a breakdown of classical solution where \mathbf{n} is fixed at the ground state. (Alternatively, one can understand this from the Heisenberg uncertainty principle $\langle \delta \hat{r} \rangle \langle \delta \mathbf{L} \rangle > \hbar$. With $\mathbf{L} = 0$ in the ground state, $\delta \mathbf{L} \equiv 0$

and $\delta\hat{r} \rightarrow \infty$, the direction of the vector \hat{r} becomes completely uncertain.)

A moment of thought indicates that our mapping of spin problem to rotor problem cannot be totally correct. How about if \mathbf{S}_A is an integer spin and \mathbf{S}_B is a half-odd-integer spin? Elementary quantum mechanics tells us that the ground state should carry half-odd-integer angular momentum. This is missing in our rotor mapping where the spin magnitudes $S_{A(B)}$ do not enter!

II.2. Berry's phase

The missing piece in our mapping of two-spin problem to rotor model is the Berry's phase (Berry, 1984) carried by spins which is absent in rotors. The correct spin-quantization rule is recovered only after this piece of physics is added properly to the rotor problem. To begin with, we first review the Berry's phase carried by a single spin.

We recall that for a spin tracing out a close path \mathbf{C} on the surface of the unit sphere, the spin wavefunction acquires a Berry's phase $\gamma(\mathbf{C}) = S\Omega(\mathbf{C})$, where S is the spin magnitude and $\Omega(\mathbf{C})$ is the surface area under the close path \mathbf{C} on the unit sphere (see Fig. 1). $S\Omega(\mathbf{C})$ can be represented more conveniently by imagining the spin trajectory as the trajectory of a particle carrying unit charge moving on the surface of the unit sphere. In this case, the Berry's phase is just the phase acquired by the charged particle if a magnetic monopole of strength S (i.e. $\mathbf{B}(\mathbf{r}) = (S/r^2)\hat{r}$) is put at the center of the sphere. The Berry's phase acquired is the magnetic flux enclosed by the close path \mathbf{C} .

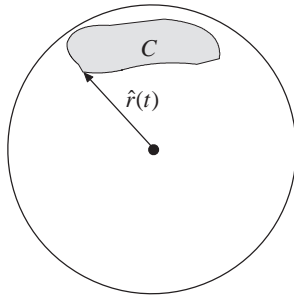


FIG. 1 Berry's phase with a magnetic monopole.

Let $S\mathbf{A}_M(\mathbf{r})$ be the vector potential associated with the monopole, i.e. $\nabla \times \mathbf{A}_M = \hat{r}/r^2$, then in the “charge + gauge field” representation, the effect of Berry's phase can be described by a vector-potential term in the action

$$S_B = \hbar S\Omega(C) = \hbar S \int dt \mathbf{A}_M(\hat{r}) \cdot \dot{\hat{r}}. \quad (6)$$

This is an example of Wess-Zumino term for quantum particles. A more rigorous derivation of the Wess-Zumino

action is given in Appendix A where the action for a single spin in magnetic field is derived *via* a path integral approach.

We now revisit the two-spin problem. With the Berry's phases included, the Lagrangian of the corresponding rotor problem becomes

$$L = \frac{1}{2J}(\hat{n} \times \dot{\hat{n}})^2 + \hbar S_A \mathbf{A}_M(\hat{r}_A) \cdot \dot{\hat{r}}_A + \hbar S_B \mathbf{A}_M(\hat{r}_B) \cdot \dot{\hat{r}}_B, \quad (7)$$

where $\mathbf{N} = N\hat{n} = \mathbf{S}_A - \mathbf{S}_B$. To simplify the problem we make the semi-classical approximation $\hat{r}_A = -\hat{r}_B$ in the Berry's phase terms, which is a reasonable approximation for states close to the classical ground state. With this approximation, we obtain

$$L \rightarrow \frac{1}{2J}(\hat{n} \times \dot{\hat{n}})^2 + \hbar \Delta S \mathbf{A}_M(\hat{n}) \cdot \dot{\hat{n}}, \quad (8)$$

where $\hat{n} = \hat{r}_A$, $\Delta S = S_A - S_B$. The Hamiltonian of the system is

$$H_M = \frac{J}{2} (\mathbf{\Pi} - \hbar \Delta S \mathbf{A}_M(\hat{n}))^2 \quad (9)$$

where $\mathbf{\Pi} = \dot{\hat{n}}/J$ is the canonical momentum of the rotor.

H_M is the Hamiltonian of a charged particle moving on the surface of a unit sphere with a magnetic monopole of strength $|\Delta S|$ located at the center of the sphere. The eigenstates of the Hamiltonian are well known and are called the monopole spherical harmonics (Wu and Yang, 1976). The most interesting feature of monopole spherical harmonics is that it allows half-odd-integer angular momentum states (which happens when $|\Delta S|$ is a half-odd-integer). The ground state carries angular momentum $L = |\Delta S|$ and is $(2|\Delta S| + 1)$ fold degenerate, corresponding to the degeneracy of a quantum spin of magnitude $|\Delta S|$, in agreement with exact result for the two-spin problem.

II.3. Non-linear- σ -model

The two-spin problem tells us that there are two important elements we have to keep track of when a classical spin problem is replaced by the corresponding quantum spin problem, a) quantum fluctuations, originated from the (non)-commutation relation between canonical coordinates (\mathbf{N}) and momenta (\mathbf{M}), and b) Berry's phase, which dictates the quantization of spins. In the following we shall generalize the rotor approach to the many-spin systems described by the antiferromagnetic (AFM) Heisenberg model, keeping in mind the above two elements.

Following Haldane (Haldane, 1983a,b), we consider here Heisenberg antiferromagnets on a bi-partite lattice described by Hamiltonian (1). As in the two-spin problem we introduce the magnetization vectors $\mathbf{M}(\mathbf{x}_i)$ and

staggered magnetization vectors $\mathbf{N}(\mathbf{x}_i)$ such that

$$\begin{aligned}\mathbf{S}_i^A &= \mathbf{M}(\mathbf{x}_i) + \mathbf{N}(\mathbf{x}_i), \\ \mathbf{S}_i^B &= \mathbf{M}(\mathbf{x}_i) - \mathbf{N}(\mathbf{x}_i),\end{aligned}\quad (10)$$

where $\mathbf{S}^{A(B)}$ denotes spins on the $A(B)$ -sublattices of the bipartite lattice. We shall assume that the ground state of the quantum system is "classical-like" with almost anti-parallel spins on two nearest neighboring sites such that $\mathbf{M}(\mathbf{x}_i) \ll \mathbf{N}(\mathbf{x}_i)$, with both $\mathbf{M}(\mathbf{x})$ and $\mathbf{N}(\mathbf{x})$ very slowly varying function in space. (We shall see how this assumption can be justified in the following.) The classical equation of motion for the spin at lattice site i is

$$\frac{\partial \mathbf{S}_i^{A(B)}}{\partial t} = J \left(\sum_{j=\text{NN}(i)} \mathbf{S}_j^{B(A)} \right) \times \mathbf{S}_i^{A(B)}, \quad (11)$$

where $j = \text{NN}(i)$ means that j represents nearest neighbor sites of i .

Using Eq. (10) we obtain after some straightforward algebra and taking the continuum limit,

$$\begin{aligned}\frac{\partial \mathbf{N}(\mathbf{x})}{\partial t} &\sim Jz\mathbf{M}(\mathbf{x}) \times \mathbf{N}(\mathbf{x}), \\ \frac{\partial \mathbf{M}(\mathbf{x})}{\partial t} &\sim -\frac{Ja^2}{2}(\nabla^2 \mathbf{N}(\mathbf{x})) \times \mathbf{N}(\mathbf{x}),\end{aligned}\quad (12)$$

where a = lattice spacing, and $z = 2d$ is the coordination number. We have assumed a square (cubic) type lattice and have made the slowly varying approximation

$$\mathbf{M}(x_{i+1}) + \mathbf{M}(x_{i-1}) \sim 2\mathbf{M}(x_i),$$

$$\mathbf{N}(x_{i+1}) + \mathbf{N}(x_{i-1}) \sim 2\mathbf{N}(x_i) + a^2 \partial_x^2 \mathbf{N}(x_i),$$

etc. in deriving the above result. We have also assumed $\mathbf{M}(\mathbf{x})$ to be small and neglected all the non-linear terms in $\mathbf{M}(\mathbf{x})$ in deriving (12).

To proceed further we consider the situation where all spins have the same magnitude S . Then it is easy to see from Eq. (10) that $\mathbf{N}(\mathbf{x})^2 + \mathbf{M}(\mathbf{x})^2 = S^2$ and $\mathbf{N}(\mathbf{x}) \cdot \mathbf{M}(\mathbf{x}) = 0$. Assuming $M = |\mathbf{M}(\mathbf{x})| \ll N = |\mathbf{N}(\mathbf{x})| \sim S$, we obtained from Eq. (12) that $M \sim \omega/(zJ)$ and $\omega \sim \sqrt{z}JaS|\mathbf{k}|$, where ω and \mathbf{k} are the frequency and wavevector of the fluctuations in \mathbf{N} . In particular, $M \ll N$ when $ak \ll \sqrt{z}$, i.e. when $\mathbf{N}(\mathbf{x})$ is slowly varying in space.

In the following we shall approximate $N \sim S$ and write $\mathbf{N}(\mathbf{x}) = S\hat{\mathbf{n}}(\mathbf{x})$, where $\hat{\mathbf{n}}^2 = 1$. Eliminating $\mathbf{M}(\mathbf{x})$ from Eq. (12), we obtain

$$\frac{\partial^2 \hat{\mathbf{n}}(\mathbf{x}, t)}{\partial t^2} = \frac{z(SJa)^2}{2} \nabla^2 \hat{\mathbf{n}}(\mathbf{x}, t), \quad (13a)$$

corresponding to the following classical action for the vector field $\hat{\mathbf{n}}$

$$S_\sigma = \frac{1}{2} \int dt \int d^d x \left(\frac{1}{J} \left(\frac{\partial \hat{\mathbf{n}}}{\partial t} \right)^2 - \frac{zJ(Sa)^2}{2} (\nabla \hat{\mathbf{n}})^2 \right), \quad (13b)$$

with constraint $\hat{\mathbf{n}}^2 = 1$. S_σ is the non-linear- σ -model (NL σ M) for the unit vector field $\hat{\mathbf{n}}(\mathbf{x})$.

Comparing Eqs. (13b) and (8) we see that the NL σ M can be viewed as a continuum model describing coupled rotors $\hat{\mathbf{n}}(\mathbf{x})$. The first term in the action gives the kinetic energy for the rotors which we have discussed in detail for the two-spin model. The second term represents coupling between nearest rotors in the lattice spin model. We note that the coupling term between rotors has magnitude $\sim S^2$ and dominates over the kinetic energy in the large S limit.

A more systematic derivation of the NL σ M starting from Eq. (10) can be achieved by writing

$$\mathbf{S}_i = \eta_i S \hat{\mathbf{n}}(x_i) \sqrt{1 - \left| \frac{\mathbf{M}(x_i)}{S} \right|^2} + \mathbf{M}(x_i)$$

where $\eta_i = e^{i\pi x}$ and we still have $\mathbf{N}(\mathbf{x}) \cdot \mathbf{M}(\mathbf{x}) = 0$. Assuming that $\mathbf{M}(\mathbf{x})$ is small, we can integrating out $\mathbf{M}(\mathbf{x})$ in a power series expansion of $\mathbf{M}(\mathbf{x})$ in the path integral. The NL σ M for $\hat{\mathbf{n}}(\mathbf{x})$ is obtained to the leading (Gaussian) order (Auerbach, 1994).

II.3.1. Topological term

We next consider the Berry's phase contribution to the action. Following Appendix A, the total Berry's phase contribution to the action is

$$S_T = \sum_i S_B(\hat{r}_i) \sim \hbar S \sum_i (-1)^i \Omega(\hat{n}_i) \quad (14)$$

where $S\Omega(\hat{r}_i) = S \int dt \mathbf{A}_M(\hat{r}_i) \cdot \dot{\hat{r}}_i$ is the Berry's phase for a single spin and $(-1)^i = 1(-1)$ for sites on even (odd) sublattice. We have assumed that the spins are almost antiparallel in the last step. In the continuum limit, we obtain

$$S_T \sim \frac{\hbar S}{2^d} \int d^d x \left(\frac{\partial}{\partial x^1} \cdots \frac{\partial}{\partial x^d} \right) \Omega(\hat{n}(\mathbf{x})). \quad (15)$$

S_T is sensitive to boundary condition (see discussion below) and we shall assume close (periodic) boundary condition in the following. The case of open boundary condition will be discussed afterward. For periodic boundary condition, it is easy to see that S_T is zero unless the integrand has a non-trivial topological structure.

To evaluate $\partial_x \Omega$, we recall that $\Omega(\hat{n})$ measures the area on the surface of sphere bounded by the trajectory $\hat{n}(t)$. Thus the variation $\delta\Omega(\hat{n})$ due to a small variation in the trajectory $\delta\hat{n}$ is simply

$$\delta\Omega(\hat{n}) = \int dt \delta\hat{n} \cdot (\hat{n} \times \partial_t \hat{n})$$

and

$$S_T = \frac{\hbar S}{2^d} \int d^d x \int dt \left[\left(\frac{\partial}{\partial x^1} \cdots \frac{\partial}{\partial x^d} \right) \hat{n} \right] \cdot (\hat{n} \times \partial_t \hat{n}). \quad (16)$$

The total effective action describing the quantum anti-ferromagnet is $S = S_\sigma + S_T$.

The topological term is nonzero in one dimension, and is usually written in the form

$$\frac{S_T}{\hbar} = \frac{\theta}{8\pi} \sum_{\mu,\nu=0,1} \int d^2x \varepsilon_{\mu\nu} \hat{n} \cdot (\partial_\mu \hat{n} \times \partial_\nu \hat{n}) \quad (17a)$$

where $x_0 = t, x_1 = x$, $\theta = 2\pi S$ and $\varepsilon_{\mu\nu}$ is the rank-2 Levi-Civita antisymmetric tensor (Affleck, 1986; Haldane, 1985). The Pontryagin index

$$Q = \frac{1}{8\pi} \sum_{\mu,\nu=0,1} \int d^2x \varepsilon_{\mu\nu} \hat{n} \cdot (\partial_\mu \hat{n} \times \partial_\nu \hat{n}) = \text{integer} \quad (17b)$$

measures how many times the $2[=1(\text{space})+1(\text{time})]$ -dimensional spin configuration \hat{n} has wrapped around the unit sphere. At two dimensions

$$S_T \rightarrow \frac{\hbar\theta}{2} \int dy \frac{\partial Q(y)}{\partial y} = 0,$$

where $Q(y)$ is the Pontryagin index coming from summing over all spin configurations in the y^{th} column of the two dimensional lattice. The sum is zero for smooth spin configurations since Q is an integer which cannot “change smoothly” (Dombre and Read, 1988; Fradkin and Stone, 1988; Haldane, 1988b; Wen and Zee, 1988). For the same reason S_T vanishes at any dimension greater than one. However one should be cautioned that this conclusion is valid only when we restrict ourselves to smooth spin configurations $\hat{n}(\mathbf{x}, t)$ in computing S_T . The Berry’s phase may have non-zero contributions if we allow also singular spin configurations in the theory. This is the case in $2 + 1d$ where monopole-like spin configurations are allowed in $3d$ space (Haldane, 1988b; Read and Sachdev, 1990).

II.4. Quantum spin chains and Haldane conjecture

We now study the predictions of the effective action for quantum spin chains. In one-dimension, the quantum spin chains are described by the path integral

$$\int D[\hat{n}(x, t)] e^{\frac{i}{\hbar} (S_\sigma(\hat{n}) + S_T(\hat{n}))}.$$

We first consider the topological term. We note that $S_T = 2\hbar\pi S Q$ and $e^{\frac{i}{\hbar} S_T} = (-1)^{2SQ}$ ($Q = \text{integer}$). In particular, $e^{\frac{i}{\hbar} S_T} \equiv 1$ for integer spin chains and the Berry’s phase has no effect in the effective action. On the other hand, $e^{\frac{i}{\hbar} S_T} = \pm 1$ for half-odd-integer spin chains, depending on whether Q is even or odd. There is no further distinction between spin chains with different spin value S ’s in S_T . This result leads to the first part of the Haldane conjecture, that there exist fundamental differences between integer and half-odd-integer spin chains

(Haldane, 1988b). To proceed further, we first consider integer spin chains where $e^{\frac{i}{\hbar} S_T} \equiv 1$ and the system is described by the “pure” NL σ M S_σ .

II.4.1. Integer spin chains

We start by asking the question: what are the plausible ground states described by S_σ ? For this purpose it’s more convenient to consider a lattice version of S_σ ,

$$S_\sigma \rightarrow \frac{1}{2} \int dt \sum_i \left(\frac{1}{J} \left(\frac{\partial \hat{n}_i}{\partial t} \right)^2 + JS^2 \hat{n}_i \cdot \hat{n}_{i+1} \right), \quad (18)$$

with corresponding Hamiltonian

$$H_\sigma = \frac{J}{2} \sum_i ((\mathbf{L}_i)^2 - S^2 \hat{n}_i \cdot \hat{n}_{i+1}), \quad (19)$$

where \mathbf{L}_i is the angular momentum operator for the i^{th} rotor. The Hamiltonian has two competing terms and we expect that it may describe two plausible phases, a strong-coupling phase where the kinetic energy (first) term dominates, and a weak-coupling phase, where the potential energy (second) term dominates. A natural control parameter for this analysis is the spin magnitude S , which dictates the magnitude of the potential energy. In the first case (small S) where the potential energy term is small, we expect that the ground state can be viewed in a first approximation as a product of local spin-singlets, i.e. $\mathbf{L} = 0$ states,

$$|G\rangle = |0\rangle_1 |0\rangle_2 \cdots |0\rangle_N,$$

where $|0\rangle_i$ represents the $\mathbf{L} = 0$ state for the rotor on site i . The lowest energy excitations are $\mathbf{L} = 1$ states separated from the ground state by an excitation gap $\sim \hbar^2 J$. This picture is believed to be correct as long as the magnitude of the potential energy term is much smaller than the excitation energy for the $\mathbf{L} = 1$ state. In the second case where the potential energy term dominates (large S), we expect that the ground state is a magnetically ordered (Néel state) with $\hat{n}_i = \hat{n}_0$ at all sites i , the excitations are Goldstone modes of the ordered state (spin waves).

It turns out that this naive expectation is valid only at dimensions $d > 1$. At one dimension the magnetically ordered state is not stable because of quantum fluctuations associated with the Goldstone mode (Mermin-Wigner Theorem) and the ground state is always quantum disordered (Mermin and Wagner, 1966), i.e. a spin liquid state. This result can be shown more rigorously by a renormalization group (RG) analysis of the NL σ M. We shall not go through this analysis in this article but shall just assume that this is the case and examine its consequences. Readers interested at the RG analysis can

look at, for example, references (Brézin and Zinn-Justin, 1976; Polyakov, 1987, 1975).

Physically, this result means that after some renormalization, the ground state of integer spin chains can always be viewed as a product state of local spin singlets, irrespective of spin magnitude S . The lowest energy excitations are gapped spin triplet ($\mathbf{L} = 1$) excitations. This is the Haldane conjecture for integer spin chains.

II.4.2. Half-odd-integer spin chains

The RG analysis cannot be applied to half-odd-integer spin chains straightforwardly because of appearance of the topological term S_T . To understand why, let's assume that the RG again flows to the strong coupling limit and examine what happens in this case.

To zeroth order the Hamiltonian of the system consists of the kinetic energy term only. However, the rotors are moving under the influence of effective monopole potentials coming from S_T . In particular all half-odd-integer spin chains have the same S_T with effective magnetic monopole strength $1/2$, corresponding to that of a spin- $1/2$ chain. In this case, the ground state of a single rotor has angular momentum $\mathbf{L} = 1/2$ and is two-fold degenerate (see discussion after Eq.(9)). The total degeneracy of ground state is 2^N , where N =number of lattice sites. This huge degeneracy implies that the coupling between rotors cannot be neglected when we consider the rotor Hamiltonian (19), and the strong coupling expansion just tell us that the system behaves like a coupled-spin- $1/2$ chain (Shankar and Read, 1990).

Fortunately the antiferromagnetic spin- $1/2$ chain can be solved by the exact Bethe Ansatz technique (Giamarchi, 2003). The exact Bethe Ansatz solution tells us that the antiferromagnetic spin- $1/2$ Heisenberg chain is critical, namely, the ground state has no long-ranged magnetic order but has a gapless excitation spectrum. Unlike integer spin chains where the lowest energy excitations carry spin $S = 1$, the elementary excitation of the system has spin $S = 1/2$. Combining this with the continuum theory leads to the Haldane conjecture for half-odd integer spin chains, that they are all critical with elementary $S = 1/2$ excitations.

II.4.3. Open spin chains and end states

The Haldane conjecture has been checked numerically in quantum spin chains with different spin magnitudes and was found to be correct in all cases that people have study so far. One may wonder whether the difference in spin magnitudes may show up in some low energy properties of quantum spin chains at all. The answer is yes, when we consider open spin chains.

Recall that we have always assumed periodic boundary

condition in deriving S_T . In fact, a periodic boundary condition is needed to define the Pontryagin index for the topological term S_T . For an open chain of length L , S_T is replaced by (Affleck, 1990; Haldane, 1983a; Ng, 1994)

$$\begin{aligned} S_T^{(o)} &= \frac{\hbar}{2} \int_0^L d^d x \frac{\partial S_B(\hat{n}(x))}{\partial x} \\ &= 2\pi\hbar S Q + \frac{\hbar S}{2} (\Omega(\hat{n}(L)) - \Omega(\hat{n}(0))), \end{aligned} \quad (20)$$

where $2\pi S Q = \theta Q$ is the usual topological θ -term we obtain when $\Omega(\hat{n}(0)) = \Omega(\hat{n}(L))$, i.e. when we consider periodic boundary condition. The open chains differ from the close chains by the existence of additional boundary Berry's phase terms with effective spin magnitude $S/2$.

We now examine the effect of this additional Berry's phase term. First we consider integer spin chains. Following previous discussion, we expect that the spin chain is described by the strong coupling limit of the effective Hamiltonian (19), except that the rotors at the two ends of the spin chain are subjected to monopole potentials of strength $S/2$, resulting in effective free spins with magnitude $S/2$ located at the ends of the spin chain. The two spins are coupled by a term $J_{eff} \sim JS^2 e^{-L/\xi}$ when the coupling between rotors are taken into account, where $\xi \sim E_g^{-1}$ is the correlation length, E_g is the spin gap. These end states can be understood also from a wavefunction proposed by Affleck, Lieb, Kennedy and Tasaki (AKLT) for $S = 1$ spin chains (Affleck *et al.*, 1987) (see section IV) and were observed experimentally in $S = 1$ spin chain materials (Glarum *et al.*, 1991). In modern terminology, the end states at integer spin chains are manifestation of symmetry-protected topological order (SPT) (Chen *et al.*, 2012; Gu and Wen, 2009; Pollmann *et al.*, 2012), which manifests itself as a boundary action which is protected by rotational (SO(3)) symmetry.¹

For half-odd-integer spin chains the analysis is a bit more complicated. We start by rewriting Eq. (20) for $S_T^{(o)}$ as (Ng, 1994)

$$\begin{aligned} S_T^{(o)} &= \frac{\hbar}{2} \left(4\pi \frac{1}{2} Q + S (\Omega(\hat{n}(L)) - \Omega(\hat{n}(0))) \right) \\ &= \frac{\hbar}{2} \left(4\pi \frac{1}{2} Q + \frac{1}{2} (\Omega(\hat{n}(L)) - \Omega(\hat{n}(0))) \right. \\ &\quad \left. + (S - \frac{1}{2}) (\Omega(\hat{n}(L)) - \Omega(\hat{n}(0))) \right) \end{aligned} \quad (21)$$

where we have replaced S by $1/2$ in the usual topological (Pontryagin index) term and have divided the boundary Berry's phase term into two parts: the first part

¹ For $S = 1$ chains, the $S = 1/2$ end states are protected by a weaker $Z_2 \times Z_2$ symmetry (Chen *et al.*, 2011a,b)

when combined with the Pontryagin index term is the total Berry's phase contribution for an open $S = 1/2$ spin chain, and the second part is the additional contribution when $S > 1/2$. Performing the strong-coupling expansion as before, we find that the system behaves as an open spin-1/2 chain coupled to two end spins with magnitude $\frac{1}{2} + \frac{1}{2}(S - \frac{1}{2})$. The problem of impurity end spin coupled to a spin-1/2 chain has been analyzed using bosonization technique where it was found that after screening by the spin-1/2 chain (essentially a Kondo effect), a free spin with magnitude $\frac{1}{2}(S - \frac{1}{2})$ is left at each end of the spin chain (Eggert and Affleck, 1992). Notice that the existence of end states in half-odd-integer spin chains is rather non-trivial because the bulk spin excitations are *gapless*. As a result, the end spins at the two ends of half-odd-integer spin chains are coupled by a term $J_{eff} \sim JS^2/(L \ln L)$, $L =$ length of spin chain. The excitation energy of the end state is logarithmically lower than the energy of bulk spin excitations, which has energies $\sim J/L$ (Ng, 1994). These predictions for open chains and end states base on the NL σ M plus topological θ term analysis has been verified numerically by density matrix renormalization group calculation (Qin *et al.*, 1995).

II.5. Higher dimensions and frustrated quantum antiferromagnets

The NL σ M approach to quantum antiferromagnets has been extended to higher dimensions and to frustrated quantum antiferromagnets. For simple antiferromagnets S_T vanishes at dimensions $d > 1$ and we only have to consider the NL σ M, i.e. S_σ . As discussed before S_σ describes two plausible phases, the weak-coupling phase where the ground state is antiferromagnetically ordered and the strong-coupling phase, where the ground state is gapped. The weak-coupling phase is favored for large spin magnitude S . Different numerical and analytical studies have agreed that the ground state is always Néel ordered for simple quantum antiferromagnets on a 2d square lattice even for the smallest possible spin value $S = 1/2$ (Manousakis, 1991). For this reason physicists have turned to frustrated spin models to look for exotic spin liquid states.

The NL σ M approach has generated interesting results when applied to weakly frustrated spin models where the main effect of frustration is to reduce the effective coupling strength between rotors (for example, $J_1 - J_2$ models where a next-nearest neighbor antiferromagnetic coupling is added to the Heisenberg model on square lattice). In this case, it has been shown that spin-Peierls order can be obtained when discontinuous monopole-like spin configurations are included in the calculation of S_T (Read and Sachdev, 1990). However, the method becomes questionable when applied to strongly frustrated spin systems where effective rotors become difficult to

define locally, for example, the antiferromagnetic Heisenberg model on Kagome lattice.

Generally speaking, a continuum theory is reliable only if the short-distance physics is captured correctly by the classical or mean-field theory behind. The continuum theory becomes unreliable if the short-distance physics it assumes is not correct. This seems to be the case of the NL σ M approach when applied to strongly frustrated spin systems. We shall consider alternative methods of treating quantum spin systems in the coming sections, keeping in mind the physics we learnt.

III. RESONANT VALENCE BOND (RVB) STATES

The semi-classical approach based on fluctuations around presumed classical (Néel) order is difficult to carry out in frustrated lattice models. The difficulties mainly come from two reasons. Firstly, different degenerate or quasi-degenerate classical ground states may exist in a frustrated spin system. It is difficult to include these quasi-degenerate classical ground states in the NL σ M description. Secondly, the effect of Berry phases become intractable because of the complicated (classical) spin trajectory.

The term geometric frustration (or frustration in short) was introduced by Gerard Toulouse in the context of frustrated magnetic systems (Toulouse, 1977; Vannimenus and Toulouse, 1977). Indeed, frustrated magnetic systems had been studied long before. Early work includes a study of the classical Ising model on a triangular lattice with nearest-neighbor spins coupled antiferromagnetically, by G. H. Wannier (Wannier, 1950), which serves as the simplest example of geometric frustration (Diep, 2004). Due to the AFM coupling, two nearest neighboring spins A and B tend to be anti-parallel. Then the third spin C which is a neighbor of both A and B is *frustrated* because its two possible orientations, up and down, give the same energy. The classical ground state has numerous degeneracy. As a result we cannot choose a classical spin order as the starting point to construct the NL σ M for the quantum $S = 1/2$ XXZ model

$$H = J_z \sum_{\langle i,j \rangle} S_i^{(z)} S_j^{(z)} + J_\perp \sum_{\langle i,j \rangle} \left(S_i^{(x)} S_j^{(x)} + S_i^{(y)} S_j^{(y)} \right)$$

with $J_z \gg J_\perp$ because there exists infinite spin configurations with the same classical energy. We note that the spin-spin correlation was found to decay in power law at zero temperature in the exact solution for the classical Ising model (Stephenson, 1970).

In this case, an alternative approach is variational wavefunction, where we have to more-or-less *guess* the ground state wavefunction based on experience or physical intuition. A very important idea along this line is the idea of Resonant Valence Bond (RVB) for spin-1/2

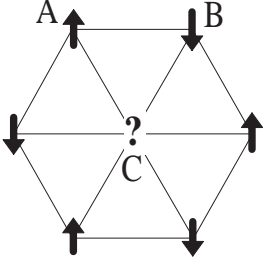


FIG. 2 Geometric frustration. The spin C is frustrated because either up or down orientation will give rise to the same energy in the AFM Ising limit.

systems suggested by Anderson. The term RVB was first coined by Pauling (Pauling, 1949) in the context of metallic materials. Anderson revived the interest in this concept in 1973 when he constructed a non-degenerate quantum ground state for $S = 1/2$ AFM on a triangular lattice (Anderson, 1973). A valence bond is a spin singlet state constructed by two $S = 1/2$ spins at site i and j given by

$$(i, j) = \frac{1}{\sqrt{2}}(|\uparrow_i \downarrow_j\rangle - |\downarrow_i \uparrow_j\rangle), \quad (22)$$

and a RVB state is a tensor product of valence bond states whose wavefunction is given by

$$|\Psi_{RVB}\rangle = \sum_{i_1 j_1 \dots i_n j_n} a_{(i_1 j_1 \dots i_n j_n)} |(i_1, j_1) \dots (i_n, j_n)\rangle, \quad (23)$$

where $(i_1, j_1) \dots (i_n, j_n)$ are dimer configurations covering the whole lattice. The wavefunction sums over all possible arrangements of dividing the lattice into pairs of lattice sites (i.e. dimers). $a_{(i_1 j_1 \dots i_n j_n)}$ are variational parameters determined by minimizing the ground state energy of a given Hamiltonian. For a Quantum disordered antiferromagnet, it was proposed that the valence bond pairs in the RVB construction are dominated by short ranged pairs, resulting in liquid like states with no long range spin order. The corresponding spin correlation function $\langle \mathbf{S}_i \cdot \mathbf{S}_j \rangle$ in the RVB state may be short ranged with a finite correlation length (usually called sRVB) or decay with distance in a power law (algebraic spin liquid states). The state is called a Valence Bond Solid (VBS) state if a single dimer configurations dominates in the ground state. The algebraic spin liquid state is usually invariant under all the symmetry operations allowed by the lattice, whereas the VBS states usually break lattice translational or rotational symmetry.

The wavefunction (23) parameterized by $a_{(i_1 j_1 \dots i_n j_n)}$ has too many variational degrees of freedom even after taking into account translational and rotational symmetries of the wavefunction and has to be simplified for practical purposes. A solution was proposed by Baskaran, Zou and Anderson (Baskaran *et al.*, 1987) who noted

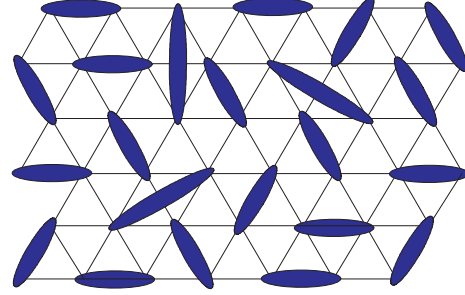


FIG. 3 A configuration of spin singlet dimer covering over a lattice. A RVB state is a superposition of such configurations.

that the BCS states for superconductors are direct product states of spin-singlet Cooper pairs, and suggested that good RVB wavefunctions can be constructed from BCS wavefunctions by Gutzwiller projection P_G ,

$$|\Psi_{RVB}\rangle = P_G |\Psi_{BCS}\rangle, \quad (24)$$

$$|\Psi_{BCS}\rangle = \prod_{\mathbf{k}} (u_{\mathbf{k}} + v_{\mathbf{k}} c_{\mathbf{k}\uparrow}^\dagger c_{-\mathbf{k}\downarrow}^\dagger) |0\rangle,$$

where $c_{\mathbf{k}\uparrow}^\dagger$ and $c_{-\mathbf{k}\downarrow}^\dagger$ are electron creation operators and the numerical coefficients $u_{\mathbf{k}}$ and $v_{\mathbf{k}}$ are determined from a trial BCS mean-field Hamiltonian H_{BCS} through the Bogoliubov-de Gennes equations, i.e. the RVB wavefunction is fixed by the parameters determining H_{BCS} . The electron number at each lattice site may take values of 0, 1 or 2 in the original BCS wavefunctions. The Gutzwiller projection P_G removes all the wavefunction components with double occupied sites from the BCS state and freezes the charge degrees of freedom. A Mott insulator state at half filling is obtained if the total number of electron is equal to the number of lattice sites. We note that the technique of Gutzwiller projection is now widely applied to other mean-field wavefunctions $|\Psi_{MF}\rangle$ to study Mott insulating states in diverse physical systems. Interesting and energetically favorable wavefunctions are often obtained when $|\Psi_{MF}\rangle$ is chosen properly.

Besides representing spins by electrons or fermions, one may also use Schwinger bosons to represent spins to construct RVB wavefunctions (see also discussion after Eq. (27)). It is easy to recognize that in general almost any mean field wavefunction $|\Psi_{MF}\rangle$ can be employed to construct a corresponding spin state through

$$|\Psi_{Spin}\rangle = P_G |\Psi_{MF}\rangle, \quad (25)$$

where $|\Psi_{MF}\rangle$ is the ground state of a trial mean field Hamiltonian $H_{trial}(c, c^\dagger; a_1, \dots a_N)$, where $c_{i\sigma}^\dagger (c_{i\sigma})$ can represent either fermion or bosons and $a_1, \dots a_N$ are variational parameters determined by minimizing the energy of the parent spin Hamiltonian.² The invention of

² For historical reason the fermion representation is also called

Gutzwiller projection techniques enables us to construct a large variety of variational spin wavefunctions. The best one is the one with lowest energy.

The most important difference between fermion and boson construction is that they lead to very different sign structures in the spin wavefunction $|\Psi_{RVB}\rangle$. In a bosonic wavefunction, when two spins (note that only spin degrees of freedom remain after Gutzwiller projection) at different sites are interchanged, the wavefunction does not change, whereas the wavefunction changes sign when two spins are interchanged in a fermionic wavefunction. These different sign structures represent very different quantum entanglement structure in the corresponding RVB wavefunctions. A famous example is the Marshall's sign rule (Marshall, 1955) for AFM Heisenberg model on bipartite lattices where the Heisenberg exchange exists only between bonds linking sites in different sublattices. Marshall's theorem tells us that the ground state for such a AFM system is a spin-singlet state with positive definite coefficients in the Ising basis $\{(-1)^{N_{A\downarrow}} |\sigma_1 \cdots \sigma_N\rangle\}$, where $N_{A\downarrow}$ is the number of down spins in the sublattice A , and N is the lattice site number. Using this result, Liang, Doucot and Anderson (Liang *et al.*, 1988) proposed to use the following trial ground state RVB wavefunction for the spin-1/2 Heisenberg antiferromagnets on a square lattice,

$$|\Psi_{LDA}\rangle = \sum_{i_\alpha \in A, j_\beta \in B} h(i_1 - j_1) \cdots h(i_n - j_n) \times (-1)^{N_{A\downarrow}} |(i_1, j_1) \cdots (i_n, j_n)\rangle, \quad (26)$$

where $h(r)$ stands for a positive definite function of the bond length r . This particular wavefunction can be represented conveniently as a Gutzwiller projected wavefunction in the Schwinger boson representation. The representation of the same wavefunction by fermions is far from straightforward (Read and Chakraborty, 1989). However, it was shown that the projected BCS wavefunction in Eq.(24) will satisfy the Marshall's sign rule provided that the spatial Fourier transformation of $u_{\mathbf{k}}$ and $v_{\mathbf{k}}$ ($= u_{ij}$ and v_{ij}), only connect sites on different sublattices on a bipartite lattice (Li and Yang, 2007; Yunoki and Sorella, 2006)

It was noted by Ma (Ma, 1988) that the sum of states $|(i_1, j_1) \cdots (i_n, j_n)\rangle$ with $i_\alpha \in A, j_\beta \in B$ form an over-complete set for spin-singlet states in a bipartite lattice. Since h is a positive function, it can be interpreted as a

weight factor in a Monte-Carlo simulation based on loop gas statistics. The calculation was carried out on large lattices by Liang *et al.* (Liang *et al.*, 1988) and very accurate ground state wavefunction for the AFM Heisenberg model on square lattice was obtained. The wavefunction gives rise to both long ranged and short ranged spin correlations with different choices of $h(r)$.

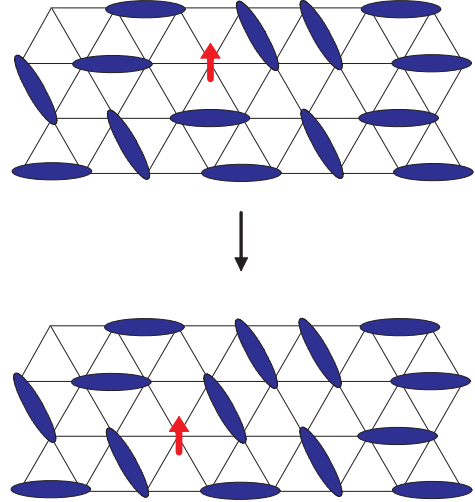


FIG. 4 A spinon excitation on the top of RVB ground state.

With a proper RVB ground state wavefunction constructed, the next natural question is what are the low energy dynamics, or elementary excitations on top of the ground states? A natural candidate of excitation is to break a singlet spin pair in the ground state to form a spin triplet excited state with two unpaired spins. For a long-ranged magnetically ordered state, it was found that the two unpaired spins will bind together closely in space and the resulting elementary excitations are localized spin triplet excitations with well defined energy and momentum. This is nothing but a spin wave or magnon excitation guaranteed by the Goldstone theorem. While for a QSL state with short ranged spin correlation, it was proposed that the two unpaired spins may interact only weakly with each other and can be considered as independent spin-1/2 elementary excitations called spinons. The existence of $S = 1/2$ spinon excitations is one of the most important predictions in QSLs and is crucial to the experimental verification of QSLs. The process that a spin-1 magnon turns into two independent spin-1/2 spinons is an example of *fractionalization*. Whether fractionalization of spin excitations actually occurs in a particular spin systems is a highly non-trivial question. A systematic way to examine whether fractionalization may happen in a spin model was first proposed by X.G. Wen (Wen, 1989, 1991) based on the concept of confinement/deconfinement in lattice gauge theory. This approach is explained in the following subsection where the gauge

the slave-boson representation and the Schwinger boson representation called the slave-fermion representation. In the context of doped Mott insulators, one can decompose the electron annihilation operator as $c_{i\sigma} = h_i^\dagger f_{i\sigma}$, where $f_{i\sigma}$ carries a charge neutral spin and h_i^\dagger is the (spinless) hole creation operator. If the spinon operator $f_{i\sigma}$ is fermionic, then the charge carrier (h_i^\dagger) is "slave-boson", and vice versa.

theory for QSLs is introduced.

III.1. RVB and Gauge Theory

A brief survey on how RVB theory is implemented in practice is given in this subsection, especially how low energy effective field theories for QSL states are constructed, which is crucial for characterizing the QSL. We shall discuss a few common examples of QSLs and explain what are the $SU(2)$, $U(1)$ and Z_2 spin liquid states. The nature of the $U(1)$ QSL will be further illuminated by connecting it to a Fermi liquid state through a Mott metal-insulator transition. We shall see that the analytical approaches have strong limitations and should be complemented by numerical approaches in practice.

A complication associated with the RVB construction is that there exists in general different mean field states $|\Psi_{MF}\rangle$ that correspond to the same RVB spin wavefunction after Gutzwiller projection. This redundancy originates from the enlarged Hilbert space in the boson/fermion representation for spins and is called *gauge redundancy* or *gauge symmetry*. Gutzwiller projection removes this redundancy resulting in a unique state in spin Hilbert space. To see how this occurs we consider the fermionic representation for $S = 1/2$ spin operators (Baskaran and Anderson, 1988; Baskaran *et al.*, 1987),

$$\vec{S}_i = \frac{1}{2} \sum_{\alpha\beta} f_{i\alpha}^\dagger \vec{\sigma}_{\alpha\beta} f_{i\beta}, \quad (27a)$$

where $\alpha, \beta = \uparrow, \downarrow$ are spin indices, $f_{i\alpha}^\dagger (f_{i\alpha})$ is the fermion creation(annihilation) operator, and $\vec{\sigma} = (\sigma^1, \sigma^2, \sigma^3)$ are Pauli matrices. It is easy to check that the three components of \vec{S}_i satisfying the $SU(2)$ Lie algebra relation, $[S_i^\lambda, S_j^\mu] = i\epsilon_{\lambda\mu\nu} S_i^\nu \delta_{ij}$, where $\lambda, \mu, \nu = 1, 2, 3$ and $\epsilon_{\lambda\mu\nu}$ is the antisymmetric tensor. Hence (27a) is a representation for $SU(2)$ spins. However, the local Hilbert space for two fermions has four Fock states $\{|0\rangle, f_\uparrow^\dagger |0\rangle = |\uparrow\rangle, f_\downarrow^\dagger |0\rangle = |\downarrow\rangle, f_\uparrow^\dagger f_\downarrow^\dagger |0\rangle = |\uparrow\downarrow\rangle\}$, which is larger than the physical spin Hilbert space for spin-1/2 = $\{|\uparrow\rangle, |\downarrow\rangle\}$ and we need to impose the single occupancy constraint

$$\sum_\alpha f_{i\alpha}^\dagger f_{i\alpha} = 1 \quad (27b)$$

to remove the unphysical states for proper representation of spins. This is what the Gutzwiller projection does. The construction (27) is equally applicable for bosons (Schwinger boson representation) since the $SU(2)$ Lie Algebra is independent of statistics of the representing particles. We shall focus on the fermion representation approach in the following because it was found to be a more fruitful approach in constructing QSLs. Readers who are interested in Schwinger boson approach may refer to reference (Arovas and Auerbach, 1988) for details.

There are more than one choices of $\{f_{i\alpha}\}$ to represent spin operators even after the single occupancy constraint is satisfied and the statistics of particles is chosen. For example, a new set of $\{f'_{i\alpha}\}$ can be obtained by an $U(1)$ gauge transformation

$$f_{i\alpha} \rightarrow f'_{i\alpha} = e^{i\theta(i)} f_{i\alpha}.$$

It is easy to verify that $\{f'_{i\alpha}\}$ forms another representation for spin operators by replacing $f_{i\alpha}$ by $f'_{i\alpha}$ in Eq.(27), independent of whether f 's are fermions or bosons. This multiplicity is called gauge redundancy or gauge symmetry in literature. We shall call it gauge redundancy here since symmetry usually refers to situations where there are more than one physically distinct states with same properties, e.g. degeneracy in energy. However, the gauge degree of freedom we discuss here is not a “real” symmetry among different physical states. Two gauge equivalent states here are the *same* state in the spin Hilbert space. They just “look” different when they are represented by particles which lives on an enlarged Hilbert space. There is no way to distinguish them physically (Wen, 2002).

The gauge redundancy in the fermion representation for $S = 1/2$ spins is beyond $U(1)$. There exists an additional $SU(2)$ gauge structure due to the particle-hole symmetry in the fermion representation which is absent in the Schwinger boson representation. An elegant way of showing this $SU(2)$ gauge structure is suggested by Affleck, Zou, Tsu and Anderson (Affleck *et al.*, 1988b) who introduced a 2×2 matrix operator

$$\Psi = \begin{pmatrix} f_\uparrow & f_\downarrow^\dagger \\ f_\downarrow & -f_\uparrow^\dagger \end{pmatrix}. \quad (28)$$

It is straightforward to show that the spin operator can be reexpressed in terms of Ψ ,

$$\vec{S}_i = \text{tr} (\Psi_i^\dagger \vec{\sigma} \Psi_i). \quad (29)$$

The single occupancy condition (27b) also leads to the identities

$$f_{i\uparrow} f_{i\downarrow} = f_{i\uparrow}^\dagger f_{i\downarrow}^\dagger = 0. \quad (30a)$$

(27b) together with Eq. (30a) can be rewritten in a compact vector form,

$$\text{tr} (\Psi_i \vec{\sigma} \Psi_i^\dagger) = 0. \quad (30b)$$

We now consider the following $SU(2)$ gauge transformation on Ψ ,

$$\Psi_i \rightarrow \Psi'_i = \Psi_i W_i, W_i \in SU(2). \quad (31)$$

The spin operators \vec{S}_i in Eq.(29) remains invariant under this transformation since $W_i W_i^\dagger = 1$. The single occupancy constraint (30b) is also invariant since $W_i \vec{\sigma} W_i^\dagger$

represents a rotation of vector $\vec{\sigma}$ but all components of $\text{tr}(\Psi_i \vec{\sigma} \Psi_i^\dagger)$ are zero, i.e. $\Psi_i \rightarrow \Psi'_i = \Psi_i W_i$ is also a valid representation for $S = 1/2$ spins.

We show now how RVB theory is implemented in an analytic fermionic approach. For concreteness we consider an AFM Heisenberg model on a lattice,

$$H = J \sum_{\langle ij \rangle} \vec{S}_i \cdot \vec{S}_j, \quad (32)$$

where $\langle ij \rangle$ denotes a nearest neighbor bond and $J > 0$. The spin exchange $\vec{S}_i \cdot \vec{S}_j$ can be written in terms of fermionic (spinon) operators,

$$\vec{S}_i \cdot \vec{S}_j = \frac{1}{4} \sum_{\alpha\beta} \left(2f_{i\alpha}^\dagger f_{i\beta} f_{j\beta}^\dagger f_{j\alpha} - f_{i\alpha}^\dagger f_{i\alpha} f_{j\beta}^\dagger f_{j\beta} \right), \quad (33)$$

where we have used the relation $\vec{\sigma}_{\alpha\beta} \cdot \vec{\sigma}_{\alpha'\beta'} = 2\delta_{\alpha\beta'}\delta_{\alpha'\beta} - \delta_{\alpha\beta}\delta_{\alpha'\beta'}$. The constraint (27b) or (30b) can be imposed by inserting delta functions in the imaginary-time path integral. The corresponding partition function is,

$$Z = \int D[f, \bar{f}] \exp[-S(f, \bar{f})] \prod_i \delta \left(\sum_{\alpha} \bar{f}_{i\alpha} f_{i\alpha} - 1 \right) \times \delta \left(\sum_{\alpha\beta} \epsilon_{\alpha\beta} f_{i\alpha} f_{i\beta} \right) \delta \left(\sum_{\alpha\beta} \epsilon_{\alpha\beta} \bar{f}_{i\alpha} \bar{f}_{i\beta} \right), \quad (34)$$

where the action $S(f, \bar{f})$ is given by

$$S(f, \bar{f}) = \int_0^\beta d\tau \left(\sum_{i\alpha} \bar{f}_{i\alpha} \partial_\tau f_{i\alpha} - H \right). \quad (35)$$

The delta functions can be represented by the integration over real auxiliary fields $a_l^l(i)$ on all sites i 's, $l = 1, 2, 3$. Using the relation $\delta(x) = \int \frac{dk}{2\pi} e^{ikx}$, we obtain

$$Z = \int D[f, \bar{f}; a] \exp[-S(f, \bar{f}; a)], \quad (36)$$

with

$$S(f, \bar{f}; a) = S(f, \bar{f}) - i \left\{ \sum_i a_0^3 \left(\sum_{\alpha} \bar{f}_{i\alpha} f_{i\alpha} - 1 \right) + \left[(a_0^1 + ia_0^2) \sum_{\alpha\beta} \epsilon_{\alpha\beta} f_{i\alpha} f_{i\beta} + h.c. \right] \right\} \quad (37)$$

It is generally believed (but not been proven) that the partition function Z will remain invariant under a Wick rotation on fields a_0^l in the path integral, namely, we can replace ia_0^l by a_0^l . Then the action becomes

$$S(f, \bar{f}; a) = S(f, \bar{f}) - \left\{ \sum_i a_0^3 \left(\sum_{\alpha} \bar{f}_{i\alpha} f_{i\alpha} - 1 \right) + \left[(a_0^1 + ia_0^2) \sum_{\alpha\beta} \epsilon_{\alpha\beta} f_{i\alpha} f_{i\beta} + h.c. \right] \right\} \quad (38)$$

The action (38) forms the starting point of theoretical analysis. The path integral is difficult to solve and approximate methods are generally needed. We start with

a mean-field theory where we assume that the path integral is dominated by saddle points characterized by equal-time expectation values of operators $\sum_{\alpha} f_{i\alpha}^\dagger f_{i\alpha}$, $\sum_{\alpha\beta} \epsilon_{\alpha\beta} f_{i\alpha} f_{i\beta}$ and $a_0^l(i)$,

$$\begin{aligned} \chi_{ij} &= \sum_{\alpha} \langle f_{i\alpha}^\dagger f_{j\alpha} \rangle, \\ \Delta_{ij} &= \sum_{\alpha\beta} \epsilon_{\alpha\beta} \langle f_{i\alpha} f_{j\beta} \rangle, \\ a_0^l &= \langle a_0^l(i) \rangle, \end{aligned} \quad (39)$$

where $\epsilon_{\alpha\beta}$ is the totally antisymmetric tensor, $l = 1, 2, 3$. It is easy to verify that χ_{ij} and Δ_{ij} satisfy the relations $\chi_{ij} = \chi_{ji}^*$ and $\Delta_{ij} = \Delta_{ji}$. Notice that time-dependent fluctuations in Δ_{ij} , χ_{ij} and $a_0^l(i)$ are ignored in mean-field theory. With these approximations, we arrive at the mean field Hamiltonian,

$$\begin{aligned} H_{MF} = & \sum_{\langle ij \rangle} -\frac{3}{8} J \left[(\chi_{ji} \sum_{\alpha} f_{i\alpha}^\dagger f_{j\alpha} \right. \\ & + \Delta_{ij} \sum_{\alpha\beta} \epsilon_{\alpha\beta} f_{i\alpha}^\dagger f_{j\beta}^\dagger + h.c.) - |\chi_{ij}|^2 - |\Delta_{ij}|^2 \left. \right] \\ & + \sum_i \left\{ a_0^3 \left(\sum_{\alpha} f_{i\alpha}^\dagger f_{i\alpha} - 1 \right) \right. \\ & \left. + \left[(a_0^1 + ia_0^2) \sum_{\alpha\beta} \epsilon_{\alpha\beta} f_{i\alpha} f_{i\beta} + h.c. \right] \right\}, \end{aligned} \quad (40)$$

where χ_{ij} , Δ_{ij} and a_0^l are determined by minimizing the ground state energy with the exact constraint condition (27b) replaced by the average constraint

$$\sum_{\alpha} \langle f_{i\alpha}^\dagger f_{i\alpha} \rangle = 1. \quad (41)$$

The spin exchange term $\vec{S}_i \cdot \vec{S}_j$ in Eq.(33) can be evaluated within mean field assumption through Wick theorem. Keeping spin rotation invariance in the calculation, we obtain

$$\langle \vec{S}_i \cdot \vec{S}_j \rangle = -\frac{3}{8} (\chi_{ij}^* \chi_{ij} + \Delta_{ij}^* \Delta_{ij}). \quad (42)$$

in mean-field theory.

Physically, the above outlined mean-field theory is equivalent to assuming that the ground state of the spin system is given by a mean-field wavefunction $|\Psi_{MF}\rangle$ without the Gutzwiller projection. The spin exchange energy (42) evaluated this way is usually not a good estimate of the energy of the "real" spin wavefunction. In practice the mean-field theory provides an effective way to obtain a BCS Hamiltonian to construct Gutzwiller projected wavefunction. Whether the spin wavefunction obtained from Gutzwiller projection is a good wavefunction for the spin Hamiltonian can only be tested by evaluating the energy of the wavefunction numerically (see section III.4).

In the following we shall assume that the Gutzwiller projected wavefunction $P_G |\Psi_{MF}\rangle$ is a good enough starting point to locate the true ground state of the spin

Hamiltonian. In this case, we expect that the ground and low energy states constructed from H_{MF} are adiabatically connected to the corresponding Gutzwiller projected wavefunctions and we may construct an effective low energy Hamiltonian/Lagrangian of the spin system from fluctuations around H_{MF} through usual path integral technique. The fluctuations in Δ_{ij}, χ_{ij} and $a_0^l(i)$ describe spin singlet excitations and are usually called *gauge fluctuations*. Before discussing gauge fluctuations we first discuss the effect of gauge redundancy on the mean-field states.

To illustrate we consider two mean-field QSL states with different structures of mean field parameters $\{\chi_{ij}, \Delta_{ij}, a_0^l(i)\}$. We shall put the states on a simple square lattice. The first state is the uniform RVB state with

$$\begin{aligned} \chi_{ij} &= 0, \\ \Delta_{ij} &= \begin{cases} \Delta, & \text{NN bonds,} \\ 0, & \text{others,} \end{cases} \\ a_0^l &= 0 \quad (l = 1, 2, 3). \end{aligned} \quad (43a)$$

The second example is the zero flux state given by

$$\begin{aligned} \chi_{ij} &= \begin{cases} \chi, & \text{NN bonds,} \\ 0, & \text{others,} \end{cases} \\ \Delta_{ij} &= 0, \\ a_0^l &= 0 \quad (l = 1, 2, 3). \end{aligned} \quad (43b)$$

Δ and χ are real numbers. We shall show that irrespective of their very different looks, these two mean field ansatz actually give rise to the same spin state after the Gutzwiller projection. The two states are gauge equivalence because they can be transformed from each other by a proper gauge transformation.

The Hamiltonian (40) keeps a local $SU(2)$ structure which originates from the gauge redundancy in the fermion representation of spin. This local $SU(2)$ symmetry becomes explicit if we introduce a doublet field $\psi = (f_\uparrow, f_\downarrow)^\top$ and a 2×2 matrix

$$u_{ij} = \begin{pmatrix} \chi_{ij} & \Delta_{ji}^* \\ \Delta_{ij} & -\chi_{ji} \end{pmatrix}.$$

The mean field Hamiltonian (40) can be written in a compact way,

$$\begin{aligned} H_{MF} &= \sum_{\langle ij \rangle} \frac{3}{8} J \left[\frac{1}{2} \text{Tr}(u_{ij}^\dagger u_{ij}) - (\psi_i^\dagger u_{ij} \psi_j + h.c.) \right] \\ &+ \sum_i a_0^l \psi_i^\dagger \tau^l \psi_i, \end{aligned} \quad (44)$$

where τ^l , $l = 1, 2, 3$ are the Pauli matrices. From Eq.(44) we see clearly that the Hamiltonian H_{MF} is invariant under a local $SU(2)$ transformation W_i :

$$\begin{aligned} \psi_i &\rightarrow W_i \psi_i, \\ u_{ij} &\rightarrow W_i u_{ij} W_j^\dagger. \end{aligned} \quad (45)$$

This $SU(2)$ gauge transformation is the same as in (31) where $\Psi = (\psi, i\sigma_2 \psi^\dagger)^T$.

Because of this $SU(2)$ gauge structure, if we regard the ansatz $(u_{ij}, a_0^l \tau^l)$ as labelling a physical spin wavefunction $|\Psi_{\text{spin}}^{(u_{ij}, a_0^l \tau^l)}\rangle = P_G |\Psi_{MF}^{(u_{ij}, a_0^l \tau^l)}\rangle$, then such a label is not a one-to-one label. Two ansatz, $(u_{ij}, a_0^l \tau^l)$ and $(u'_{ij}, a'_0 \tau^l) = (W(u_{ij}), W(a_0^l \tau^l))$, related by a $SU(2)$ gauge transformation label the same physical spin wavefunction:

$$\begin{aligned} |\Psi_{\text{spin}}(\{\alpha_i\})\rangle &= P_G |\Psi_{MF}^{(W(u_{ij}), W(a_0^l \tau^l))}\rangle \\ &= P_G |\Psi_{MF}^{(u_{ij}, a_0^l \tau^l)}\rangle \end{aligned} \quad (46)$$

where $W(u_{ij}) = W_i u_{ij} W_j^\dagger$ and $W(a_0^l(i) \tau^l) = W_i a_0^l(i) \tau^l W_i^\dagger$, $W_i \in SU(2)$. The uniform RVB state and zero-flux state discussed above denote the same physical spin state because they are related by a gauge transformation

$$W_i = \exp(i \frac{\pi}{4} \tau^2).$$

More generally, the existence of gauge redundancy implies that the low energy fluctuations in spin systems have similar redundancy. To measure gauge fluctuations, we introduce loop variables

$$P(C_i) = u_{ij} u_{jk} \cdots u_{li},$$

where i, j, k, \dots, l denotes a loop of lattice sites which pass through site i . $P(C_i)$ measures gauge fluxes and has a general form

$$P(C_i) = A(C_i) \tau^0 + \mathbf{B}(C_i) \cdot \tau,$$

where τ^0 is the identity matrix. $A(C_i)$ and $\mathbf{B}(C_i)$ measures the $U(1)$ and $SU(2)$ components of gauge fluxes, respectively. For a translational invariant mean-field state we can find a gauge with $\mathbf{B}(C_i) = \hat{n} B(C_i)$ where $A(C_i)$ and $B(C_i)$ are proportional to the area of the loop. Under a gauge transformation,

$$P(C_i) \rightarrow W_i P(C_i) W_i^\dagger,$$

and the “direction” of \hat{n} changes. The presence of gauge redundancy means that we may perform gauge transformations to change the “local” directions of \hat{n} but the physical spin state remains unchanged.

For a given mean-field state, it is useful to distinguish between two kinds of gauge transformations, those which change the mean-field ansatz $\{u_{ij}, a_0^l(i)\}$ and those which don’t. The later constitutes a subgroup of the original $SU(2)$ symmetry called invariant gauge group (IGG) (Wen, 2002),

$$\text{IGG} \equiv \left\{ W_i | W_i u_{ij} W_j^\dagger = u_{ij}, W_i \in SU(2) \right\}. \quad (47)$$

It can be shown rather generally that for a stable QSL state, physical gapless gauge excitations exist only for those fluctuations belonging to IGG of the corresponding mean field ansatz. Therefore it is important to understand the structure of IGG in spin liquid states. Within the fermionic $SU(2)$ formalism, there are only three plausible kinds of IGG, $SU(2)$, $U(1)$ and Z_2 . We call the corresponding spin liquids $SU(2)$, $U(1)$ and Z_2 spin liquids. The $SU(2)$ spin liquids have $\mathbf{B}(C_i) = 0$ with $IGG = SU(2)$. They are rather unstable because of existence of large amount of gapless $SU(2)$ gauge field fluctuations. The $U(1)$ spin liquids have $\mathbf{B}(C_i)$ pointing at only one direction for all loops C_i . The condensation of fluxes in one “direction” provides an Anderson-Higgs mechanism for $SU(2)$ fluxes in “directions” perpendicular to $\mathbf{B}(C)$ and turns the IGG into $U(1)$. The low energy fluctuations are $U(1)$ gauge field fluctuations. The Z_2 spin liquids have $\mathbf{B}(C_i)$ pointing at different directions for different loops that pass through the same site i . The gauge fluctuations are all gapped because the Anderson-Higgs mechanism applies now to fluxes in all directions. A few examples of mean-field ansatz for the three types of spin liquid states will be presented in the following.

III.2. $U(1)$ gauge fluctuations

We discuss briefly the $U(1)$ gauge theory for two examples of spin liquids which are believed to exist in nature (see section V). The first example is the zero flux state (43b) where $\Delta_{ij} = a_0^l = 0$ and $\chi_{ij} = \chi$ in the mean field ansatz.

It is easy to see that $\mathbf{B}(C_i) \equiv \mathbf{0}$ and the IGG of such a QSL is $SU(2)$, i.e., the zero flux state describes a $SU(2)$ spin liquid. The low energy fluctuations are $SU(2)$ gauge fluctuations. We shall not consider the full $SU(2)$ gauge fluctuations but shall consider only the phase fluctuations of χ_{ij} , i.e. $U(1)$ gauge fluctuations here. The consideration of $U(1)$ gauge fluctuations only for the zero flux state can be justified in a slave-rotor theory for the Hubbard model (Lee and Lee, 2005) or in a phenomenological Landau Fermi-liquid type approach for spin liquid states *near metal-insulator transition* (see next subsection).

Writing $\chi_{ij} = \chi e^{ia_{ij}}$, where a_{ij} denotes phase fluctuations, it is straightforward to see that

$$P(C_i) \propto \exp(i\Phi(C_i)\tau^3),$$

where $\Phi(C_i) = (a_{ij} + a_{jk} + \dots + a_{li})$ is the total $U(1)$ gauge flux enclosed by the loop, i.e., the phase fluctuations of χ_{ij} represents one component of the $SU(2)$ gauge fluctuations.

The effective Lagrangian describing these low energy

phase fluctuations is

$$L^{(0)} = \sum_{i\alpha} \bar{f}_{i\alpha} (\partial_\tau - a_0) f_{i\alpha} + \frac{3}{8} \sum_{\langle ij \rangle} \left(J\chi e^{ia_{ji}} \sum_\alpha \bar{f}_{i\alpha} f_{j\alpha} + h.c. \right) \quad (48)$$

and the corresponding Lagrangian in the continuum limit is

$$L^{(0)} = \int d\vec{r} \sum_\alpha \bar{f}_\alpha(\vec{r}) (\partial_\tau - a_0) f_\alpha(\vec{r}) + \frac{1}{2m^*} \bar{f}_\alpha(\vec{r}) (-i\nabla + \vec{a})^2 f_\alpha(\vec{r}), \quad (49)$$

where m^* is the effective mass for the spinon energy dispersion determined by $J\chi$, and the vector field $\vec{a}(\vec{r})$ is given by the lattice gauge field a_{ij} through

$$a_{ij} = (\vec{r}_i - \vec{r}_j) \cdot \vec{a} \left(\frac{\vec{r}_i + \vec{r}_j}{2} \right). \quad (50)$$

Thus the low energy effective field theory describes non-relativistic spin-1/2 fermions (spinons) coupled to the $U(1)$ gauge field ($a_0(\vec{r})$, $\vec{a}(\vec{r})$) in the continuum limit.

The other spin liquid state we introduce here is the π -flux state (Affleck and Marston, 1988; Kotliar, 1988) on square lattice given by $\Delta_{ij} = a_0^l = 0$, and

$$\chi_{i,i+\hat{\mu}} = \begin{cases} \chi, & \mu = x \\ i\chi(-1)^{i_x}, & \mu = y \end{cases}. \quad (51)$$

It is easy to see that $P(C_i) \propto \exp(i\pi\tau^3)$ per square plaquette in the mean-field ansatz, i.e. the π -flux state has $IGG = U(1)$ and is a $U(1)$ spin liquid.

The zero-flux and π -flux states are physically distinct states because of their different IGG. Their mean-field spinon dispersions are also qualitatively different. The zero-flux state has mean-field dispersion $E_0(\vec{k}) = -J\chi(\cos k_x + \cos k_y)$, whereas the π -flux state has $E_\pi(\vec{k}) = \pm J\chi\sqrt{\cos^2 k_x + \cos^2 k_y}$ with a reduced Brillouin zone. The continuum theory describes non-relativistic fermions with large fermi surface in the zero-flux state, and describes Dirac fermions with four Fermi points ($\mathbf{k} = (\pm\pi/2, \pm\pi/2)$) in the π -flux state (Affleck and Marston, 1988). The effective continuum theory for the π -flux state has the form

$$L^{(\pi)} = \sum_{\mu\sigma} (\bar{\psi}_{+\sigma}(\partial_\mu - ia_\mu)\tau_\mu \psi_{+\sigma} + \bar{\psi}_{-\sigma}(\partial_\mu - ia_\mu)\tau_\mu \psi_{-\sigma}), \quad (52)$$

where $\mu = 0, 1, 2$. The two-component Dirac spinor fields $\psi_{\pm\sigma}$ describe two inequivalent Dirac nodes in the spinon spectrum (Affleck and Marston, 1988). The two effective low energy Lagrangians $L^{(0)}$ and $L^{(\pi)}$ describe two different types of spin liquid states that are believed to exist in nature. We shall come back to these states again in section V.

The continuum action L forms the starting point in studying the stability and low energy properties of the spin liquid states. Integrating out the fermion fields (at each momenta shell) gives rise to a Maxwellian potential energy term of the gauge field,

$$\frac{1}{2g^2(\Lambda)}(\nabla \times \vec{a})^2,$$

where $g(\Lambda)$ is a running gauge coupling constant in the sense of renormalization group, which depends on the energy or momentum scale Λ . If $g(\Lambda) \rightarrow 0$ in the low energy and long wave length limit $\Lambda \rightarrow 0$, the gauge fluctuations become weaker and weaker. The corresponding interaction between two fermions becomes too weak to bind them together and the elementary excitations in the spin system are spin-1/2 fermionic excitations called spinons. This is called deconfinement and the ground state is a filled fermi sea of spinons. On the other hand, if $g(\Lambda) \rightarrow \infty$ in the limit $\Lambda \rightarrow 0$, two spinons are always confined together to form a magnon. This situation is called confinement. In this case the mean field QSL ground state breaks down to a spin ordered state due to the strong gauge fluctuations, and magnon excitations are recovered in the ordered state.

It is not exactly clear which kinds of mean field QSL states are stable against gauge fluctuation. It is generally believed that Z_2 QSL states are stable since Z_2 (Ising) gauge theories are deconfining (Fradkin and Shenker, 1979), while the $SU(2)$ QSL states are unstable due to presence of large gauge fluctuations. The situation of $U(1)$ QSL states are more nontrivial. The $SU(2)$ gauge group and the corresponding gauge fields are compact in spin liquid states. To reflect the compactness of the $U(1)$ gauge group one has to replace the electromagnetic field tensor $F_{\mu\nu}^2$ by $2(1 - \cos F_{\mu\nu})$. This periodic version of $U(1)$ gauge theory is called compact $U(1)$ gauge theory. A pure compact $U(1)$ pure gauge theory is always confining in two dimensions (Polyakov, 1977, 1975) but whether deconfinement is possible in the presence of matter field is an open question. Herbut *et al.* have argued that the theory is always confining in the presence of Fermi surface (Herbut *et al.*, 2003) or nodal fermions (Herbut and Seradjeh, 2003). Their conclusion depends on an approximate effective action for the gauge field obtained by integrating out the fermions to the lowest order. This approximation is questionable for gapless fermions. Indeed Hermele *et al.* (Hermele *et al.*, 2004) proved that if the spin index is generalized to N flavors, the problem of $2N$ 2-component Dirac fermions coupled to complex $U(1)$ gauge fields is deconfining for sufficiently large N , thus providing a counter example to confinement. Further renormalization group analysis for compact quantum electrodynamics in 2+1 D shows that deconfinement occurs when $N > N_c = 36/\pi^3 \simeq 1.161$, where N is the number of fermion replica. This implies the stability of a $U(1)$ spin liquid at the physical value of $N = 2$

(Nogueira and Kleinert, 2005). Moreover, by mapping the spinon Fermi surface in 2+1 D into an infinite set of 1+1 dimensional chiral fermions, Lee (Lee, 2008b) argued that an instanton has an infinite scaling dimension for any $N > 0$. Therefore, the QSL phase is stable against instantons and the noncompact $U(1)$ gauge theory is a good low energy description.

We note that other mechanism may also lead to the instability of $U(1)$ QSLs besides confinement arising from gauge fluctuations, such as Amperean pairing (Lee *et al.*, 2007b) and spin triplet pairing (Galitski and Kim, 2007) between spinons.

A non-trivial prediction of the $U(1)$ gauge theory of spin liquids is that it leads to charge excitations with a soft gap (Ng and Lee, 2007) which can be detected by their AC conductivities $\sigma(\omega)$. It was predicted that $\sigma(\omega) \sim \omega^\alpha$ in these spin liquid states with $\alpha \sim 3.33$ in the non-relativistic spin liquid and $\alpha = 2$ in the Dirac fermion spin liquid (Potter *et al.*, 2013). It is expected that this soft gap and related charge fluctuations will manifest themselves most clearly when the system is in the vicinity of metal-insulator transition (see next subsection).

Since charge fluctuations will manifest themselves in the vicinity of metal-insulator transition, the spin liquids in “weak” Mott insulators become an interesting topic (Grover *et al.*, 2010; Podolsky *et al.*, 2009; Senthil, 2008) of investigation. To study the effect of charge fluctuations near metal-insulator transition, Lee and Lee (Lee and Lee, 2005) started with the Hubbard model and developed a $U(1)$ gauge theory with the help of slave-rotor representation (Florens and Georges, 2004). A number of physical phenomena including transport properties (Nave and Lee, 2007) and Kondo effect (Ribeiro and Lee, 2011) have been studied with this framework. The charge fluctuations correspond to higher order spin ring-exchange terms in terms of spin Hamiltonian (Misguich *et al.*, 1998; Yang *et al.*, 2010).

III.2.1. Mott transition: relation between Fermi- and spin-liquids

Zhou and Ng (Zhou and Ng, 2013) proposed a different way to understand $U(1)$ spin liquids near Mott transition. They proposed that spin liquids near Mott transition can be understood as “Fermi liquids” with a constraint being imposed on the current operator. For isotropic systems, they observed that the charge current carried by quasi-particles is renormalized by the Landau parameter F_1^s in Fermi liquid theory,

$$\mathbf{J} = \frac{m}{m^*}(1 + \frac{F_1^s}{d})\mathbf{J}^{(0)}, \quad (53a)$$

but not the thermal current

$$\mathbf{J}_Q = \frac{m}{m^*}\mathbf{J}_Q^{(0)}, \quad (53b)$$

where $\mathbf{J}^{(0)}$ and $\mathbf{J}_q^{(0)}$ are the charge- and thermal- current carried by the corresponding non-interacting fermions and d is the system dimension. For systems with Galilean invariance, the charge current carried by quasi-particles is not renormalized and $\frac{m^*}{m} = 1 + \frac{F_1^s}{d}$ (Baym and Pethick, 2004). However, this is in general not valid for electrons in crystals where Galilean invariance is lost. In this case $\frac{m^*}{m} \neq 1 + \frac{F_1^s}{d}$ and the charge current carried by quasi-particles is renormalized by quasi-particle interaction. In the special case $1 + F_1^s/d \rightarrow 0$ while $\frac{m^*}{m}$ remaining finite, $\mathbf{J} \rightarrow 0$ suggesting that the fermionic system is in a special state where spin-1/2 quasi-particles do not carry charge due to interaction, but they still carry entropy. This is exactly what one expects for spinons in QSLs.

They noted that the limit $1 + F_1^s/d \rightarrow 0$ is a singular point in Fermi liquid theory, and higher order q, ω -dependent terms should be included in the Landau interaction to obtain finite results in calculating physical response functions. Expanding at small q and ω , they obtain

$$\frac{1 + F_1^s(q, \omega)/d}{N(0)} \sim \alpha - \beta\omega^2 + \gamma_t q_t^2 + \gamma_l q_l^2, \quad (54)$$

where $q_t \sim \nabla \times$ and $q_l \sim \nabla$ are associated with the transverse (curl) and longitudinal (gradient) parts of the small \vec{q} expansion. $\alpha = 0$ in the QSLs. To ensure that the system is in an incompressible (insulator) state, they found that $\gamma_l = 0$.

To show that this phenomenology actually describes fermionic spin liquids with $U(1)$ gauge fluctuations Zhou and Ng (Zhou and Ng, 2013) consider a Landau Fermi liquid with interaction parameters $F_0^s(q)$ and $F_1^s(q)$ only. The long-wavelength and low energy dynamics of the Fermi liquid is described by an effective Lagrangian

$$L_{\text{eff}} = \sum_{\mathbf{k}, \sigma} \left[c_{\mathbf{k}\sigma}^\dagger \left(i \frac{\partial}{\partial t} - \xi_{\mathbf{k}} \right) c_{\mathbf{k}\sigma} - H'(c^\dagger, c) \right], \quad (55)$$

where $c_{\mathbf{k}\sigma}^\dagger (c_{\mathbf{k}\sigma})$ are spin- σ fermion creation (annihilation) operators with momentum \mathbf{k} , and

$$H'(c^\dagger, c) = \frac{1}{2N(0)} \sum_q \left[\frac{F_1^s(q)}{v_F^2} \mathbf{j}(q) \cdot \mathbf{j}(-q) + F_0^s(q) n(q) n(-q) \right] \quad (56)$$

describes the current-current and density-density interactions between quasi-particles (Larkin, 1964; Leggett, 1965), where $q = (q, \omega)$ and $v_F = \hbar k_F/m^*$ is the Fermi velocity.

The current- and density- interactions can be decoupled by introducing fictitious gauge potentials \mathbf{a} and φ (Hubbard-Stratonovich transformation) with

$$H'(c^\dagger, c) \rightarrow \sum_q \left[\mathbf{j} \cdot \mathbf{a} + n\varphi - \frac{1}{2} \left(\frac{n}{m^*} \frac{d}{F_1^s(q)} \mathbf{a}^2 + \frac{N(0)}{F_0^s(q)} \varphi^2 \right) \right] \quad (57)$$

where n is fermion density. The equality $d(n/m^*) = N(0)v_F^2$ was used in writing down Eq. (57).

The Lagrangian (55) and (57) can be rewritten in the standard form of $U(1)$ gauge theory by noting that the fermion current is given in this representation by

$$\mathbf{j} = \frac{-i}{2m^*} \sum_{\sigma} [\psi_{\sigma}^\dagger \nabla \psi_{\sigma} - (\nabla \psi_{\sigma}^\dagger) \psi_{\sigma}] - \frac{n}{m^*} \mathbf{a},$$

where $\psi_{\sigma}(\mathbf{r}) = \int e^{-i\mathbf{k} \cdot \mathbf{r}} c_{\mathbf{k}\sigma}$ is the Fourier transform of $c_{\mathbf{k}\sigma}$. The Lagrangian can be written as

$$L = \sum_{\sigma} \int d^d \mathbf{r} \left[\psi_{\sigma}^\dagger \left(i \frac{\partial}{\partial t} - \varphi \right) \psi_{\sigma} - H(\psi_{\sigma}^\dagger, \psi_{\sigma}) \right] + L(\varphi, \mathbf{a}), \quad (58a)$$

where

$$H(\psi_{\sigma}^\dagger, \psi_{\sigma}) = \frac{1}{2m^*} |(\nabla - i\mathbf{a}) \psi_{\sigma}|^2 \quad (58b)$$

and

$$L(\varphi, \mathbf{a}) = \frac{1}{2} \int d^d \mathbf{r} \left[\frac{n}{m^*} \left(1 + \frac{d}{F_1^s} \right) \mathbf{a}^2 + \frac{N(0)}{F_0^s} \varphi^2 \right]. \quad (58c)$$

Using Eq. (54), we find that in the small q limit, the transverse part of $L(\varphi, \mathbf{a})$ is given in the spin liquid state by

$$L_t(\varphi, \mathbf{a}) = -\frac{n}{2m^*} \int d^d \mathbf{r} \left[\beta \left(\frac{\partial \mathbf{a}}{\partial t} \right)^2 - \gamma_t (\nabla \times \mathbf{a})^2 \right]. \quad (59)$$

Lagrangian (58) together with (59) is the standard Lagrangian used to describe QSLs with $U(1)$ gauge fluctuations. The analysis can be generalized to $U(1)$ spin liquid with Dirac fermion dispersion rather straightforwardly. The appearance of soft charge gap in $U(1)$ spin liquids can be understood from the phenomenological form (54) for $F_1^s(q, \omega)$ which suggests that the quasi-particles carry vanishing charges only at the limit $q, \omega \rightarrow 0$. The appearance of non-vanishing β in (54) leads to power law AC conductivity $\sigma(\omega)$. This picture is very different from theories of spin liquid states starting from simple spin models where charge fluctuations are absent at all energy scales and suggests that charge fluctuations are important at regions at the vicinity of the Mott transition. We note that charge fluctuations can be (partially) incorporated into the spin models through ring exchange terms.

The close relation between Fermi liquid and spin-liquid states suggests an alternative picture of Mott metal-insulator transition to the one proposed by Brinkman and Rice (Brinkman and Rice, 1970) who proposed that a metal-insulator (Mott) transition is characterized by diverging effective mass $\frac{m^*}{m} \rightarrow \infty$ and inverse compressibility $\kappa \rightarrow 0$ at the Mott transition point, with correspondingly a vanishing quasi-particle renormalization weight $Z \sim \frac{m}{m^*} \rightarrow 0$. The diverging effective mass and vanishing quasi-particle weight implies that the Fermi liquid

state is destroyed at the Mott transition, and the Mott insulator state is distinct from the Fermi liquid state at the metal side.

The phenomenology described here suggests an alternative picture where the Fermi surface is not destroyed but the Landau-quasiparticles are converted into spinons ($1 + \frac{F_1^s}{d} \rightarrow 0$) at the Mott transition. In particular, the effective mass m^*/m may not diverge at the metal-insulator transition although $Z \rightarrow 0$. A schematic phase diagram for the Mott (metal-QSLs) transition is presented in Fig. 5 for a generic Hubbard type Hamiltonian with hopping t and on-site Coulomb repulsion U . The system is driven to a Mott insulator state at zero temperature at $U = U_c$, where $1 + F_1^s(U > U_c)/d = 0$. This picture suggests that a $U(1)$ spin liquid state is likely to exist in insulators close to Mott transitions.

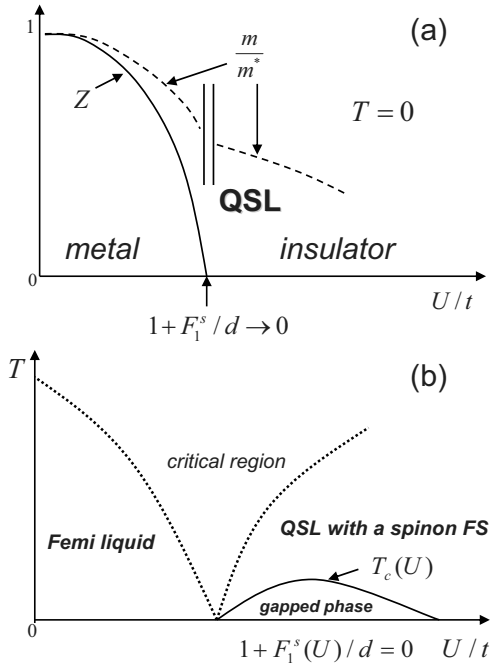


FIG. 5 (Zhou and Ng, 2013) (a) Schematic zero temperature phase diagram for Mott transition. U is the Hubbard interaction strength and t is the hopping integral. The electron quasiparticle weight and quasi-particle charge current $\sim 1 + F_1^s/d$ vanishes at the critical point while the effective mass remains finite. (b) Schematic phase diagram showing finite temperature crossovers and possible instability toward gapped phases at lower temperature. There exists a (finite temperature) critical region around U_c where the phenomenology is not applicable.

The point $1 + F_1^s/d = 0$ is a critical point in Fermi liquid theory called Pomeranchuk point. The Fermi surface is unstable with respect to deformation when $1 + F_1^s/d < 0$. The criticality of the $1 + F_1^s/d = 0$ point implies that the QSLs we obtain here are marginally stable because of large critical fluctuations. Similar conclusion is drawn from $U(1)$ gauge theory through analyzing

$U(1)$ gauge fluctuations. As a result, QSLs with large Fermi surfaces are in general susceptible to formation of other more stable QSLs at lower temperature, like the Z_2 QSLs or valence bond solid (VBS) states that gap out part or the whole Fermi surface. This is indicated schematically in the phase diagram Fig. 5(b), where the system is driven into a gapped QSL at low temperature $T < T_c(U)$ at the insulating side. The nature of the low temperature QSLs depends on the microscopic details of the system and cannot be determined from the above phenomenological consideration.

III.3. Z_2 spin liquid states

An example of Z_2 spin liquid state was first constructed by Wen (Wen, 1991) for a $J_1 - J_2$ Heisenberg model on a square lattice, J_1 and J_2 are the nearest neighbor and next nearest neighbor Heisenberg interaction, respectively. Wen considered the mean-field ansatz

$$u_{i,i+\hat{\mu}} = \begin{pmatrix} \chi & 0 \\ 0 & -\chi \end{pmatrix} \quad (60a)$$

where $\hat{\mu} = \hat{x}, \hat{y}$, and

$$u_{i,i\pm\hat{x}+\hat{y}} = u_{i,i\mp\hat{x}-\hat{y}} = \begin{pmatrix} 0 & \Delta_0 \pm i\Delta_1 \\ \Delta_0 \mp i\Delta_1 & 0 \end{pmatrix}, \quad (60b)$$

where χ, Δ_0 and Δ_1 are nonzero real numbers, and $a_0^{2,3} = 0, a_0^1 \neq 0$. It is easy to check $P(C)$ for two loops $C_1 = i \rightarrow i + \hat{x} \rightarrow i + \hat{x} + \hat{y} \rightarrow i$, and $C_2 = i \rightarrow i + \hat{y} \rightarrow i + \hat{y} - \hat{x} \rightarrow i$. We obtain

$$P(C_1) = \chi^2 (\Delta_0 \tau^1 + \Delta_1 \tau^2) \quad (61a)$$

and

$$P(C_2) = -\chi^2 (\Delta_0 \tau^1 - \Delta_1 \tau^2) \quad (61b)$$

which shows clearly that $\mathbf{B}(C_1) \neq \mathbf{B}(C_2)$ and the above spin liquid state describes a Z_2 spin liquid state. The mean-field ground state describes a half-filled spinon band with band dispersion given by $E_{\pm}(\mathbf{k}) = \pm \sqrt{\varepsilon_1(\vec{k})^2 + \varepsilon_2(\vec{k})^2 + \varepsilon_3(\vec{k})^2}$, where

$$\begin{aligned} \varepsilon_1(\vec{k}) &= 2J_1\chi(\cos(k_x) + \cos(k_y)), \\ \varepsilon_2(\vec{k}) &= 2J_2\Delta_0(\cos(k_x + k_y) + \cos(k_x - k_y)) + a_0^1, \\ \varepsilon_3(\vec{k}) &= 2J_2\Delta_1(\cos(k_x + k_y) - \cos(k_x - k_y)). \end{aligned}$$

Notice that the spinon spectrum is fully gapped.

Many other examples of Z_2 spin liquid states have been constructed in the literature. For instance, a nodal gapped Z_2 spin liquid state was proposed by Balents, Fisher and Nayak (Balents *et al.*, 1998), and Senthil and Fisher (Senthil and Fisher, 2000). The corresponding mean-field ansatz contains the nearest neighbor and next

nearest neighbor hopping and d-wave pairing on nearest neighbor bonds on the square lattice,

$$u_{i,i+\hat{x}} = \begin{pmatrix} \chi_1 & \Delta \\ \Delta & -\chi_1 \end{pmatrix} \quad (62a)$$

and

$$u_{i,i+\hat{y}} = \begin{pmatrix} \chi_1 & -\Delta \\ -\Delta & -\chi_1 \end{pmatrix} \quad (62b)$$

and

$$u_{i,i\pm\hat{x}\pm\hat{y}} = \begin{pmatrix} \chi_2 & 0 \\ 0 & -\chi_2 \end{pmatrix}, \quad (62c)$$

where χ_1 , χ_2 , and Δ are nonzero real numbers, and $a_0^{1,2} = 0$, $a_0^3 \neq 0$. The spinon dispersion is given by $E_{\pm}(\mathbf{k}) = \pm\sqrt{\varepsilon(\vec{k})^2 + \Delta(\vec{k})^2}$, where

$$\begin{aligned} \varepsilon(\vec{k}) &= 2J_1\chi_1(\cos(k_x) + \cos(k_y)) \\ &\quad + 2J_2\chi_2(\cos(k_x + k_y) + \cos(k_x - k_y)) + a_0^3, \\ \Delta(\vec{k}) &= 2J_1\Delta(\cos(k_x) - \cos(k_y)) + a_0^3, \end{aligned}$$

and is found to be gapless at four \vec{k} points with a linear dispersion. Thus this spin liquid is a Z_2 nodal spin liquid. We reiterate that Z_2 spin liquid states are expected to be most stable because the $SU(2)$ gauge fields are gapped and the fermionic spins are interacting only through short-ranged interaction.

It was pointed out by Wen (Wen, 1991) that beside spinons, a soliton-type of excitation exists in a Z_2 spin liquid. This excitation is nothing but a π flux in the Z_2 gauge field, called “ Z_2 vortex”. This Z_2 vortex can be described by a new mean-field ansatz,

$$\tilde{u}_{ij} = u_{ij}\Theta_{ij},$$

where $\Theta_{ij} = \pm 1$ generates a π flux on a lattice. One choice of Θ_{ij} is illustrated in Fig. 6, where $\Theta_{ij} = -1$ on the bonds cut by the dashed line and $\Theta_{ij} = 1$ on the other bonds. An interesting consequence of the Z_2 vortex is the spinon statistics can be changed from bosonic to fermionic and vice versa if it is bound to a vortex. Therefore, Z_2 spin liquids may contain charge neutral spin-1/2 spinons with both bosonic and fermionic statistics (Ng, 1999). The dynamics of Z_2 vortices can give rise to interesting physical consequences (Ng, 1999; Qi *et al.*, 2009).

It is worth noting that the $J_1 - J_2$ model on square lattice is well studied. The lowest energy Z_2 spin liquid state is a nodal spin liquid with four Dirac points (Capriotti *et al.*, 2001; Hu *et al.*, 2013) labeled as Z2Azz13 in the projected group symmetry classification scheme (Wen, 2002), which we will discuss in Section III.5. This nodal Z_2 spin liquid is energetically competitive with calculations by DMRG (Gong *et al.*, 2014; Jiang *et al.*, 2012b) and PEPS (Wang *et al.*, 2013).

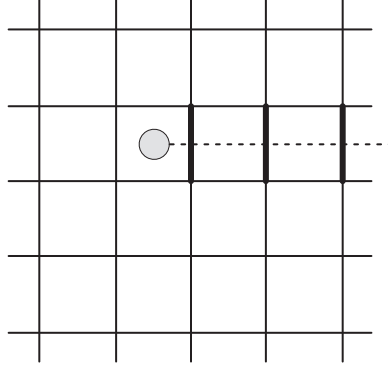


FIG. 6 A Z_2 vortex created by flipping the sign of u_{ij} along the bonds (denoted by thick lines) cut by the dashed line.

Relation to superconductivity: The RVB theory were developed not only for quantum spin liquids but also for high T_c superconductivity (Anderson, 1987). It is generally believed that Z_2 spin liquid states may become superconductors upon doping (Lee *et al.*, 2006). The superconducting state inherits novel properties from its quantum spin liquid parent and new phenomena may emerge. For instance, it was proposed that doping a Kagome system can give rise to exotic superconductor with $hc/4e$ quantized flux (opposite to usual $hc/2e$) (Ko *et al.*, 2009).

III.4. Numeric Realization of Gutzwiller Projection: Variational Monte Carlo Method and Some Results

The theories of spin liquid states rely heavily on the reliability of Gutzwiller projected wavefunctions. In this subsection, we shall discuss how the Gutzwiller projection is carried out numerically in practice and how the physical observables can be evaluated through Monte Carlo method for a given projected wavefunction $|\Psi_{RVB}\rangle = P_G |\Psi_{MF}\rangle$.

Typically, there are two types of mean-field ansatz frequently used in constructing spin liquid states. The first one only contains (fermionic) spinon hopping terms χ , and the mean-field ground state is a half-filled Fermi sea. The second one includes both hopping and pairing terms Δ , and the mean-field ground state is a BCS type state with a fermion energy gap. These two types of wavefunctions describe $U(1)$ and Z_2 spin liquid states, respectively with proper choice of hopping and pairing parameters. For a given spin Hamiltonian, we can determine these hopping and pairing parameters by optimizing the ground state energy. Therefore it is called variational Monte Carlo (VMC) method.

For a projected Fermi sea state, the mean-field ground state wavefunction on a lattice with N sites can be constructed by filling the lowest N states in the mean-field

band,

$$|\Psi_{FS}\rangle = \prod_{\sigma} \prod_{k=1}^{N/2} \psi_{k\sigma}^{\dagger} |0\rangle,$$

where $\sigma = \uparrow, \downarrow$ is the spin index and the states are sorted in ascending energy, $E_1 \leq \dots \leq E_{N/2} < E_F$. $\psi_{k\sigma}^{\dagger}$ creates an eigenstate in the mean-field band and can be expressed as

$$\psi_{k\sigma}^{\dagger} = \sum_i a_k(i) c_{i\sigma}^{\dagger},$$

where i 's denote sites and $c_{i\sigma}^{\dagger}$ is a local fermion creation operator. The eigenstate wavefunction $a_k(i)$ does not depend on spin index σ for spin-singlet states because of the spin rotational symmetry. More explicitly,

$$|\Psi_{FS}\rangle = \prod_{\sigma} \prod_{i=1}^{N/2} \left(\sum_{j=1}^N a_i(j) c_{j\sigma}^{\dagger} \right) |0\rangle, \quad (63)$$

and the Gutzwiller projected wavefunction can be written in terms of the product of three factors,

$$\begin{aligned} P_G |\Psi_{FS}\rangle &= \sum_{\{\sigma_i\}} \text{sgn} \{i_1, \dots, i_{N/2}, j_1, \dots, j_{N/2}\} \\ &\quad \times \det [A(i_1, \dots, i_{N/2})] \\ &\quad \times \det [A(j_1, \dots, j_{N/2})] |\sigma_1, \dots, \sigma_N\rangle \end{aligned} \quad (64)$$

where $|\sigma_1, \dots, \sigma_N\rangle$ is a state in the Ising basis with $N/2$ up spins locating at sites $i_1, \dots, i_{N/2}$ and $N/2$ down spins locating at sites $j_1, \dots, j_{N/2}$. $\text{sgn}\{i_1, \dots, i_{N/2}, j_1, \dots, j_{N/2}\}$ is the sign of permutation $P = \{i_1, \dots, i_{N/2}, j_1, \dots, j_{N/2}\}$. $A(i_1, \dots, i_{N/2})$ is an $N/2 \times N/2$ matrix given by

$$A(i_1, \dots, i_{N/2}) = \begin{pmatrix} a_1(i_1) & \dots & a_1(i_{N/2}) \\ \dots & \ddots & \dots \\ a_{N/2}(i_1) & \dots & a_{N/2}(i_{N/2}) \end{pmatrix}. \quad (65)$$

A BCS-type mean field ground state with spin-singlet pairing can be written as,

$$|\Psi_{BCS}\rangle = e^{\frac{1}{2} \sum_{i,j} W_{ij} (c_{i\uparrow}^{\dagger} c_{j\downarrow}^{\dagger} - c_{i\downarrow}^{\dagger} c_{j\uparrow}^{\dagger})} |0\rangle \quad (66)$$

where i and j are site indices, $W_{ij} = W_{ji}$ for fermionic spin-singlet pairing. For a system with lattice translational symmetry, W_{ij} can be written explicitly as

$$W_{ij} = - \sum_{\mathbf{k}} \frac{v_{\mathbf{k}}}{u_{\mathbf{k}}} e^{-i\mathbf{k}\cdot(\mathbf{R}_i - \mathbf{R}_j)},$$

where $u_{\mathbf{k}}$ and $v_{\mathbf{k}}$ are given by the BCS form. In the more general situation where lattice translational symmetry is lost, W_{ij} 's are determined from the Bogoliubov-de-Gennes equations. Gutzwiller projection keeps only

states with number of electrons equal to number of lattice sites and removes all the terms with more than one electrons per site, i.e.,

$$|\Psi_{RVB}\rangle = P_G \left(\sum_{i < j} W_{ij} c_{i\uparrow}^{\dagger} c_{j\downarrow}^{\dagger} \right)^{N/2} |0\rangle. \quad (67)$$

In the spin representation, the projected BCS state can be written as

$$\begin{aligned} P_G |\Psi_{BCS}\rangle &= \sum_{\{\sigma_i\}} \text{sgn} (i_1, \dots, i_{N/2}, j_1, \dots, j_{N/2}) \\ &\quad \times \det [w(i_1, \dots, i_{N/2}, j_1, \dots, j_{N/2})] \\ &\quad \times |\sigma_1, \dots, \sigma_N\rangle, \end{aligned} \quad (68)$$

where $|\sigma_1, \dots, \sigma_N\rangle$ is a state in the Ising basis with $N/2$ up spins locating at sites $i_1, \dots, i_{N/2}$ and $N/2$ down spins locating at sites $j_1, \dots, j_{N/2}$. $w(i_1, \dots, i_{N/2}, j_1, \dots, j_{N/2})$ is an $N/2 \times N/2$ matrix given by

$$w(i_1, \dots, i_{N/2}, j_1, \dots, j_{N/2}) = \begin{pmatrix} W_{i_1 j_1} & \dots & W_{i_1 j_{N/2}} \\ \dots & \ddots & \dots \\ W_{i_{N/2} j_1} & \dots & W_{i_{N/2} j_{N/2}} \end{pmatrix}. \quad (69)$$

A key observation on these two projected wavefunctions (64) and (68) is that both of them can be written as a determinant or a product of two determinants. This allows us to evaluate the projected wavefunction numerically. For large systems, the degrees of freedom increase exponentially with system size. In this case, Monte Carlo method is applied to evaluate the energy, magnetization and spin correlation for these projected wavefunctions (Gros, 1989; Horsch and Kaplan, 1983). Below we briefly describe how the MC method works. Those who are interested in the details may refer to Gros (Gros, 1989).

Expectation values of an operator Θ in a spin wavefunction $|\Psi\rangle$ system can be written as

$$\langle \Theta \rangle = \frac{\langle \Psi | \Theta | \Psi \rangle}{\langle \Psi | \Psi \rangle} = \sum_{\alpha, \beta} \langle \alpha | \Theta | \beta \rangle \frac{\langle \Psi | \alpha \rangle \langle \beta | \Psi \rangle}{\langle \Psi | \Psi \rangle}, \quad (70)$$

where the spin configurations $|\alpha\rangle$ and $|\beta\rangle$ are states in the Ising basis with $N/2$ up spins and $N/2$ down spins. This sort of expectation value is recognized to be susceptible to a Monte Carlo (MC) evaluation (Horsch and Kaplan, 1983). The expectation value in Eq. (70) can be rewritten as

$$\begin{aligned} \langle \Theta \rangle &= \sum_{\alpha} \left(\sum_{\beta} \frac{\langle \alpha | \Theta | \beta \rangle \langle \beta | \Psi \rangle}{\langle \alpha | \Psi \rangle} \right) \frac{|\langle \alpha | \Psi \rangle|^2}{\langle \Psi | \Psi \rangle} \\ &= \sum_{\alpha} f(\alpha) \rho(\alpha), \end{aligned} \quad (71)$$

with

$$f(\alpha) = \sum_{\beta} \frac{\langle \alpha | \Theta | \beta \rangle \langle \beta | \Psi \rangle}{\langle \alpha | \Psi \rangle},$$

$$\rho(\alpha) = \frac{|\langle \alpha | \Psi \rangle|^2}{\langle \Psi | \Psi \rangle}.$$

It follows that

$$\rho(\alpha) \geq 0, \sum_{\alpha} \rho(\alpha) = 1.$$

Note that for a “local operator” Θ (e.g., $\Theta = \vec{S}_i \cdot \vec{S}_j$) and a given spin configuration $|\alpha\rangle$, there are only limited number of “neighbor” configurations $|\beta\rangle$ that give rise to nonvanishing $\langle \alpha | \Theta | \beta \rangle$. As pointed out by Horsch and Kaplan (Horsch and Kaplan, 1983), the computation time for the ratio $\frac{\langle \beta | \Psi \rangle}{\langle \alpha | \Psi \rangle}$ is of order of $O(N^2)$. Therefore, $\langle \Theta \rangle$ can be evaluated by a random walk through spin configuration space with weight $\rho(\alpha)$. As in standard MC method, the transition probability $T(\alpha \rightarrow \alpha')$ from one configuration α to another configuration α' can be chosen as follows,

$$T(\alpha \rightarrow \alpha') = \begin{cases} 1, & \rho(\alpha') \geq \rho(\alpha), \\ \frac{\rho(\alpha')}{\rho(\alpha)}, & \rho(\alpha') < \rho(\alpha). \end{cases}$$

The new configuration α' is accepted with probability $T(\alpha \rightarrow \alpha')$.

Since $\langle \alpha | \Psi \rangle$ is either a determinant or a product of two determinants, the computation time for $\langle \alpha | \Psi \rangle$ is $O(N^3)$. The computation consumption of the MC weight factor $T(\alpha \rightarrow \alpha')$ is not too expensive, which makes this MC method applicable for Guzwiller Projection. Moreover, one can reduce the computation time of the ratio $T(\alpha \rightarrow \alpha')$ to $O(N^2)$ if the corresponding matrice $A(\alpha')$ or $w(\alpha')$ in Eq.(65) or (69) differs from $A(\alpha)$ or $w(\alpha)$ only by one row or column. This can be realized by properly choosing the spin update procedure, e.g. interchange of two opposite spins. This algorithm was first introduced by Ceperley *et al.* for the MC evaluation of fermionic trial wavefunction (Ceperley *et al.*, 1977).

As a variational method, VMC not only gives the upper bound of ground state energy to a spin Hamiltonian, but also provides detailed informations for the trial

ground state. These informations are useful in understanding the nature of the ground state wavefunction. In the remained part of this subsection, we shall discuss some numerical results for Gutzwiller projected wavefunction on one dimensional and two dimensional frustrated lattices.

III.4.1. One dimensional lattice

One dimensional systems usually serve as the benchmark for comparison since exact solutions are often available. It turns out that $P_G |\Psi_{FS}\rangle$, which is gauge equivalent to $P_G |\Psi_{BCS}\rangle$ in one dimension, is an excellent trial wavefunction for the ground state of the one dimensional Heisenberg model. The energy for $P_G |\Psi_{FS}\rangle$ is higher only by 0.2% than the exact ground state (Gebhard and Vollhardt, 1987; Gros *et al.*, 1987; Yokoyama and Shiba, 1987). The spin-spin correlation decays as the power law at large distance, $\langle \vec{S}_i \cdot \vec{S}_{i+r} \rangle \sim \frac{(-1)^r}{|r|}$, in agreement with the results from bosonization (Luther and Peschel, 1975). Indeed, it was shown that this Gutzwiller projected wavefunction is the exact ground state of the Haldane-Shastry model (Haldane, 1988a; Shastry, 1988),

$$H_{H-S} = \frac{J}{2} \sum_{i=1}^N \sum_{r=1}^{N-1} \frac{1}{\sin^2(\pi r/N)} \vec{S}_i \cdot \vec{S}_{i+r},$$

which describes an AFM Heisenberg chain with long-ranged coupling (a periodic version of $1/r^2$ exchange).

Excited states with $S_z = m = (N_{\uparrow} - N_{\downarrow})/2$ can also be constructed, where N_{\uparrow} and N_{\downarrow} are the numbers of up and down spins in the wavefunction, respectively. The lowest energy state in the sub-space with $S_z = m$ is given by

$$P_G |\Psi_m\rangle = P_G \prod_{|k| \leq k_F \uparrow} \psi_{k\uparrow}^{\dagger} \prod_{|k| \leq k_F \downarrow} \psi_{k\uparrow}^{\dagger} |0\rangle, \quad (72)$$

where $k_{F\sigma} = \pi(N_{\sigma} - 1)/N = \pi(N_{\sigma} - 1)/(N_{\uparrow} + N_{\downarrow})$. With the help of this trial wavefunction, the spin susceptibility χ can be calculated (Gros *et al.*, 1987). It is found that χ is close to the value from the exact solution (Griffiths, 1964). The numerical results are summarized in Table I.

TABLE I (Gros, 1989) Comparison of ground state energy and spin susceptibility in one dimension. The first row shows the results for the projected Fermi sea. The second row shows the results for the exact ground state of Heisenberg model.

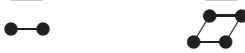
	$\langle \vec{S}_i \cdot \vec{S}_{i+1} \rangle$	χ
Gutzwiller	-0.442118 (Gebhard and Vollhardt, 1987)	0.058 ± 0.008 (Gros <i>et al.</i> , 1987)
Exact	-0.443147 (Lieb and Wu, 1968)	0.0506 (Griffiths, 1964)

III.4.2. Triangular lattice

Historically the AFM spin-1/2 Heisenberg Hamiltonian on the triangular lattice was the first proposed model for a microscopic realization of a spin liquid ground state (Fazekas and Anderson, 1974). On the other hand, the minimum energy configuration for the classical Heisenberg model on the triangular lattice is well known to be the 120° Néel state. There was a long standing debate whether the frustration together with quantum fluctuations can destroy the long-range 120° Néel order, leading to a spin liquid state. Many trial wavefunctions have been proposed as the ground state of the nearest neighbor Heisenberg model on the triangular lattice, including chiral spin liquid state (Kalmeyer and Laughlin, 1987) and 120° Néel order states with quantum mechanical corrections (Huse and Elser, 1988; Sindzingre *et al.*, 1994). In 1999, Capriotti *et al.* (Capriotti *et al.*, 1999) utilized Green's Function Monte Carlo (GFMC) method with stochastic reconfiguration technique to obtain the lowest energy state for the model to our knowledge (the ground state energy per site is 0.5458 ± 0.0001), the state exhibits 120° long-range Néel order.

It thus seems that spin liquid state is ruled out from the triangular lattice. However, the story moves on. It is found that four-spin ring exchange stabilizes the projected Fermi sea state against long-range AFM state (Motrunich, 2005). Since multi-spin ring exchange reflects the charge fluctuations in the vicinity of Mott transition, this result provides theoretical support to search for spin liquid states in a Mott insulating state close to the metal-insulator transition.

The model Hamiltonian contains both nearest neighbor Heisenberg exchange and four-spin ring exchange is

$$H_{\text{ring}} = J \sum P_{12} + J_{\text{ring}} \sum \left(P_{1234} + P_{1234}^\dagger \right), \quad (73)$$


where $P_{12} = 2\vec{S}_1 \cdot \vec{S}_2 + \frac{1}{2}$ interchanges two spins at site-1 and site-2. The four-spin exchange operators satisfy the following relations $P_{1234}^\dagger = P_{4321}$, $P_{1234} + P_{4321} = P_{12}P_{34} + P_{14}P_{23} - P_{13}P_{24} + P_{13} + P_{24} - 1$.

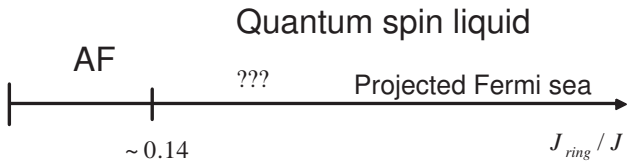


FIG. 7 (Motrunich, 2005) Variational phase diagram for the Hamiltonian (73).

By comparing the trial energies of the AF ordered states proposed by Huse and Elser (Huse and Elser, 1988) and various fermionic spin liquid states, Motrunich

found that a spin liquid ground state is favored by the ring exchange term against the AFM ordered state (Motrunich, 2005). The results is summarized in Fig.7. For small ring exchange, $J_{\text{ring}}/J \lesssim 0.14$, the ordered states have lower energy. However for $J_{\text{ring}}/J \gtrsim 0.14$, spin liquid states are energetically favored. For larger $J_{\text{ring}}/J \gtrsim 0.3 - 0.35$, the optimal spin liquid state is the projected Fermi sea state. In the intermediate regime, optimized wavefunctions with extended anisotropic *s*-wave, $d_{x^2-y^2}$, and $d_{x^2-y^2} + id_{xy}$ spinon pairings have close energies.

Recently, a novel Z_2 spin liquid state was proposed on the triangular lattice, where paired fermionic spinons preserves all symmetries of the system, and has a gapless excitation spectrum with quadratic bands that touch at $q = 0$. It is shown through VMC that this Z_2 spin liquid state has highly competitive energy when J_{ring}/J is realistic large (Mishmash *et al.*, 2013).

III.4.3. Kagome lattice

Unlike the triangular lattice, the classical Heisenberg model on the kagome lattice has an infinite number of degenerate ground states connected with one another by continuous “local” distortions of the spin configuration (Villain, J. *et al.*, 1980). This property holds on any lattices with corner sharing units such as checkerboard, kagome, and pyrochlore lattices (Moessner and Chalker, 1998). For instance, on the kagome lattice formed by corner sharing triangles, the nearest-neighbor Heisenberg Hamiltonian can be written as the sum of the square of the total spin $\vec{S}_\Delta = \vec{S}_1 + \vec{S}_2 + \vec{S}_3$ of individual triangle which share only one vertex,

$$H = J \sum_\Delta (\vec{S}_\Delta)^2.$$

Classical ground states are obtained whenever $\vec{S}_\Delta = 0$. This triangle rule fixes the relative orientations of the three classical spins of a triangle at 120° from each other in a plane but it does not fix the relative orientation of the plane of a triad with respect to the planes of the triads on neighboring triangles. These degrees of freedom lead to continuous local degeneracy for the ground states. Notice degeneracy exists even if we restrict ourselves to coplanar spin states. Two simplest examples (Sachdev, 1992) are the three sublattice planar states, $q = 0$ and $\sqrt{3} \times \sqrt{3}$ ordered states, shown in Fig. 8.

The large classical ground state degeneracy has to be lifted by quantum fluctuations. The nature of the ground state for the quantum model is highly speculative because of the huge number of degeneracy in the classical model. Many proposals exist in literature arguing for what kind of ground state is favored, and this issue is still under debate (Diep, 2004). We shall discuss in the following the $U(1)$ quantum spin liquid state which is

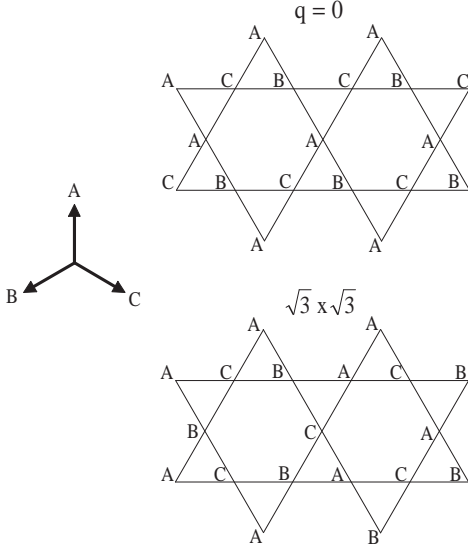


FIG. 8 Two classical planar Néel states ($q = 0$ and $\sqrt{3} \times \sqrt{3}$) on the kagome lattice. A, B and C specify three coplanar spin orientations with 120° intersection angle.

one of the promising candidates for the ground state of spin-1/2 Heisenberg antiferromagnet on kagome lattice.

Inspired by neutron scattering experiments on Herbersmithite, $\text{ZnCu}_3(\text{OH})_6\text{Cl}_2$, Ran *et al.* constructed a series of variational wavefunctions of $U(1)$ spin liquids on the kagome lattice (Ran *et al.*, 2007). Corresponding mean-field ansatz only involves fermionic spinon hopping on the nearest neighbor bonds,

$$H_{MF} = J \sum_{\langle ij \rangle \sigma} (\chi_{ij} f_{j\sigma}^\dagger f_{i\sigma} + h.c.),$$

where complex field χ_{ij} living on the links between two neighboring sites. For the Kagome lattice, the mean-field states are characterized by the $U(1)$ gauge fluxes through the triangles and the hexagons. Large-N expansion suggests several candidate mean field states (Hastings, 2000; Marston and Zeng, 1991): (i) VBS states which break translation symmetry. (ii) A spin liquid state ($\text{SL}-[\frac{\pi}{2}, 0]$) with a flux $+\pi/2$ through each triangle on Kagome lattice and zero flux through the hexagons. This is a chiral spin liquid state which breaks time-reversal symmetry. (iii) A spin liquid state ($\text{SL}-[\pm\frac{\pi}{2}, 0]$) with staggered $\pi/2$ flux through the triangles ($+\pi/2$ through up triangles and $-\pi/2$ through down triangles) and zero flux through the hexagons. (iv) A spin liquid state ($\text{SL}-[\pm\frac{\pi}{2}, \pi]$) with $+\pi/2$ flux through the triangles and π flux through the hexagons. (v) A uniform RVB spin-liquid state ($\text{SL}-[0, 0]$) with zero flux through both triangles and hexagons. This state has a spinon Fermi surface. (vi) A $U(1)$ -Dirac spin liquid state ($\text{SL}-[0, \pi]$) with zero flux through the triangles and π flux through the hexagons. This state has four flavors of two-component Dirac fermions.

By performing VMC calculation on $8 \times 8 \times 3$ and $12 \times 12 \times 3$ lattices, Ran *et al.* (Ran *et al.*, 2007) found that the $U(1)$ -Dirac spin liquid state ($\text{SL}-[0, \pi]$) has the lowest energy among the above (i)-(vi) states after the Gutzwiller projection, with ground state energy $-0.429J$ per site. Notice that there is no tunable parameter in this $U(1)$ -Dirac spin liquid state. This energy is amazingly good because the value is very close to the exact diagonalization result when extrapolated to thermodynamics limit. Comparison between the ground state energy from this VMC method and other numerical methods are present in Table II. They also found that the $U(1)$ -Dirac spin liquid state is stable against VBS ordering and chiral spin liquid with θ flux penetrating through the triangles and $(\pi - 2\theta)$ through the hexagons. Spin correlation functions have an algebraic decay with distance because of Dirac nodes in the spinon spectrum.

TABLE II Comparison of ground state energy (in units of J) of nearest neighbor Heisenberg model on Kagome lattice by different methods. In the VMC method, the $U(1)$ -Dirac spin liquid state ($\text{SL}-[0, \pi]$) is used.

Method	Energy per site
Exact diagonalization	-0.43 (Waldtmann <i>et al.</i> , 1998)
Coupled cluster method	-0.4252 (Farnell <i>et al.</i> , 2001)
Spin-wave variational method	-0.419 (Arrachea <i>et al.</i> , 2004)
VMC method	-0.429 (Ran <i>et al.</i> , 2007)

We note that exact diagonalization (Lecheminant *et al.*, 1997; Leung and Elser, 1993; Mila, 1998; Waldtmann *et al.*, 1998) and DMRG calculation (Depenbrock *et al.*, 2012; Jiang *et al.*, 2012a, 2008; Yan *et al.*, 2011) strongly indicates the existence of a spin gap, and seems to dismiss the $U(1)$ -Dirac spin liquid scenario. However, this disagreement may be a finite size effect. Exact diagonalization is limited to very small lattice, up to 36 sites, and the maximum cylinder circumferences used in DMRG is only 17 lattice spacings. Very recently, by the combination of Lanczos algorithm on projected fermionic wave functions and the Green's function Monte Carlo technique, Iqbal, Becca, Sorella, and Poilblanc (Iqbal *et al.*, 2013, 2014) found that the gapless $U(1)$ -Dirac spin liquid is competitive with the gapped Z_2 spin liquids. By performing a finite size extrapolation of the ground state energy, they obtained an energy per site $E/J = -0.4365(2)$, which is equal, within three error bars, to the estimates given by DMRG. Summarizing, the $U(1)$ -Dirac spin liquid state serves as a good candidate describing a critical phase on the kagome lattice.

III.5. Classification of spin liquid states: Quantum Order and Projective Symmetry Groups

The use of Gutzwiller projected wavefunction can be made more systematic by using a powerful approach of classifying spin liquid states according to their symmetry properties. For classical systems, it was pointed out by Landau that symmetry is a universal property shared by all the macroscopic states within the same phase, irrespective of microscopic details. Because of this, the symmetry (or broken symmetry) associated with classical order parameters serves as a powerful tool to characterize different classical phases. This approach can be generalized to quantum spin systems described by Gutzwiller projected wavefunctions with additional constraints.

For spin liquid states described by Gutzwiller projected wavefunctions, one may expect that the quantum phases can be classified by the symmetry properties of the mean-field ansatz $(u_{ij}, a_0^l \tau^l)$. However the usual classical symmetry group (SG) is insufficient in classifying these states for two reasons: (i) Because of the gauge redundancy, there exist different mean field descriptions for the same QSL state. For instance, the uniform RVB state and the zero flux state corresponds to the same spin state, and the d -wave RVB state on a square lattice is also the π -flux state. (ii) QSL states may have inherent (phase) structures contained in the mean-field ansatz $(u_{ij}, a_0^l \tau^l)$ which can not be fully distinguished by SG constructed for classical systems. For this purpose X.G. Wen invented a new mathematical object called projective symmetry group (PSG) (Wen, 2002), which generalized Landau's approach and becomes an important tool in studying QSLs and quantum phase transition between different QSL states nowadays.

Wen proposed that the symmetry of the mean-field ansatz $(u_{ij}, a_0^l \tau^l)$ is a universal property and serves as a kind of “quantum number” that characterize quantum orders in QSLs. The macroscopic properties of the ansatz is characterized by the projective symmetry group (PSG). An element of PSG is a combined operation of a symmetry transformation U followed by a local gauge transformation $G_U(i)$. The PSG of a given mean-field ansatz is formed by all the combined operations that leave the ansatz unchanged, i.e.

$$PSG \equiv \{G_U | G_U U(u_{ij}) = u_{ij}, G_U(i) \in SU(2)\}, \quad (74)$$

where $U(u_{ij}) = \tilde{u}_{ij} \equiv u_{U(i), U(j)}$, $G_U U(u_{ij}) \equiv G_U(i) \tilde{u}_{ij} G_U^\dagger(j)$, U generates the symmetry transformation (SG) and G_U is the associated gauge transformation. It is easy to see that

$$SG \equiv \frac{PSG}{IGG}$$

from this definition.

The PSG's of two mean-field ansatz related by a gauge transformation W are obviously related. From

$WG_U U(u_{ij}) = W(u_{ij})$, where $W(u_{ij}) \equiv W_i u_{ij} W_j^\dagger$, we obtain $WG_U U W^{-1} W(u_{ij}) = W(u_{ij})$. Therefore if $G_U U$ belongs to the PSG of mean-field ansatz u_{ij} , then $WG_U U W^{-1}$ belongs to the PSG of the gauge transformed ansatz $W(u_{ij})$. We see that the gauge transformation G_U associated with the transformation U changes in the following way

$$G_U(i) \rightarrow W(i) G_U(i) W(U(i))^\dagger \quad (75)$$

under a $SU(2)$ gauge transformation W . Wen proposed that mean-field ansatz with different PSG's belong to different classes of quantum spin liquid states, just as classical states with different SG's belong to different classical phases.

As examples we consider the PSG's of the zero flux state (43b) and the π -flux state (51) on square lattice. We shall consider the PSG associated with translational symmetry for illustration. First we consider the zero flux state. The mean-field ansatz (43b) is invariant under translation transformation $T_x(i \rightarrow i + \hat{x})$ and $T_y(i \rightarrow i + \hat{y})$, and gauge transformations $G(\theta) = e^{i\theta\tau^3}$. The PSG elements are $G_U U$ with $G_U = \pm G(\theta)$ and $U = (T_x)^n (T_y)^m$ where n, m are arbitrary integers. The π -flux state is different. The mean-field ansatz (51) breaks translational symmetry in x -direction by odd number of lattice site. Thus we expect naively that the PSG elements are $G_U U$ with $G_U = \pm G(\theta)$ and $U = (T_x)^{2n} (T_y)^m$. This is in fact incorrect because the two mean-field ansatz

$$\chi_{i,i+\hat{\mu}} = \begin{cases} \chi, & \mu = x \\ i\chi(-1)^{i_x}, & \mu = y \end{cases}.$$

and

$$\chi_{i,i+\hat{\mu}} = \begin{cases} \chi, & \mu = x \\ i\chi(-1)^{i_x+1}, & \mu = y \end{cases}.$$

are actually related by a gauge transformation $W_i = (-1)^{i_y} \tau^0$ and correspond to the same physical spin state. As a result, the transformations $G_{U'} U'$ with $G_{U'} = \pm G(\theta) (-1)^{i_y} \tau^0$ and $U' = (T_x)^{2n+1} (T_y)^m$ are also PSG elements of π -flux state. The zero-flux state and π -flux state have different PSG, and therefore belong to different classes of $U(1)$ quantum liquid states.

More generally, other lattice symmetry operations (reflections and rotations), such as parity transformation $P_{xy}((i_x, i_y) \rightarrow (i_y, i_x))$ and $P_{x\bar{y}}((i_x, i_y) \rightarrow (-i_y, -i_x))$ on square lattice, spin rotation transformation \mathbf{R} and time reversal transformation T are also considered in constructing PSG besides translation. Spin rotation symmetry of spin liquid states requires the mean-field ansatz to take the form

$$\begin{aligned} u_{ij} &= i\rho_{ij} W_{ij}, \\ \rho_{ij} &= \text{real number}, \\ W_{ij} &\in SU(2). \end{aligned} \quad (76)$$

We end with a brief discussion on a technique issue in the classification of PSG. For any two given symmetry transformations, their corresponding PSG elements must satisfy certain algebraic relations determined by the symmetry transformations. Solving these equations allows us to construct a PSG which will be called the *algebraic PSG*. The name algebraic PSG is introduced to distinguish them from the invariant PSG we defined above. Any invariant PSG will be a algebraic PSG. However an algebraic PSG may not be an invariant PSG unless there exists an ansatz such that the algebraic PSG is the total symmetry group of the ansatz.

We consider translations as example. The two translation elements T_x and T_y satisfy the following relation

$$T_x T_y T_x^{-1} T_y^{-1} = 1. \quad (77)$$

From the definition of PSG, we find that the two elements of PSG, $G_x T_x$ and $G_y T_y$, must satisfy the algebraic relation

$$\begin{aligned} & G_x T_x G_y T_y (G_x T_x)^{-1} (G_y T_y)^{-1} \\ &= G_x T_x G_y T_y T_x^{-1} G_x^{-1} T_y^{-1} G_y^{-1} \\ &= G_x (i) G_y (i - \hat{x}) G_x^{-1} (i - \hat{y}) G_y^{-1} (i) \in \mathcal{G}. \end{aligned} \quad (78)$$

where we denote the IGG as \mathcal{G} . Each solution $G_x T_x, G_y T_y$ of equation (78) is an algebraic PSG for T_x and T_y . By adding other symmetry transformations, we can find and classify all the algebraic PSG associated with a given symmetry group. Since an invariant PSG is always an algebraic PSG, we can check whether the algebraic PSG is an invariant PSG through constructing an explicit ansatz u_{ij} . If an algebraic PSG supports an ansatz u_{ij} with no additional symmetry, then it is an invariant PSG. Through this method, we can classify the symmetric spin liquids through PSG.

In reference (Wen, 2002) Wen utilized PSG to classify quantum spin liquid states with spin rotational symmetry, time reversal symmetry and the full lattice symmetries on square lattice. Later, the PSG classification for symmetric quantum spin liquids has been applied to triangular lattice (Zhou and Wen, 2002), star lattice (Choy and Kim, 2009), and Kagome lattice (Lu *et al.*, 2011). The PSG classification scheme can be also generalized to bosonic quantum spin liquid states (Wang, 2010b; Wang and Vishwanath, 2006) and the QSL states breaking spin rotational symmetry and time reversal symmetry (Kou and Wen, 2009).

IV. BEYOND RVB APPROACHES

There are many reasons to go beyond the simple RVB approach for $S = 1/2$ spin systems. For example the discovery of plausible spin liquid state in a spin $S = 1$ system (Zhou *et al.*, 2011) and the rise in interests of Mott insulators in systems with strong spin-orbit coupling

where rotation symmetry is broken and the ground state could not be a pure spin singlet (Jackeli and Khaliullin, 2009). What are the nature of spin liquid states in these systems? More importantly, we are interested at the possibility of exotic spin liquid states beyond the RVB description where the elementary excitations may possess exotic properties beyond the simple spinon picture.

We shall introduce some of these developments in this section. We start by introducing the generalization of RVB approach to spin systems with strong spin-orbit coupling and to $S > 1/2$ spin systems in sections IV.1 and IV.2, followed by the introduction of the Matrix Product States and Projected Entangled Pair States in section IV.3, which are totally different ways of constructing spin wave-functions compared with RVB approach. We end this section with an introduction to the Kitaev honeycomb model, which represents another different approach to constructing spin wave-functions in system with strong spin-orbit coupling with exotic properties beyond the simple spinon picture.

IV.1. RVB and its generalization to spin systems with strong spin-orbit coupling

Strong spin-orbital coupling may cause some interesting experimental consequences that are absent in systems with spin rotational symmetry. An example suggested by Zhou *et al.* (Zhou *et al.*, 2008) is presented here where strong spin-orbit coupling in Ir atoms is adopted to explain the anomalous behavior of Wilson ratio observed in $\text{Na}_4\text{Ir}_3\text{O}_8$, which was experimentally proposed (Okamoto *et al.*, 2007) to be the first candidate for 3D quantum spin liquid on hyperkagome lattice with fermionic spinons.

While the Curie-Weiss constant is estimated to be as large as $\theta_W \sim 650$ K in $\text{Na}_4\text{Ir}_3\text{O}_8$, indicating strong AFM coupling, there is no observed thermodynamics and magnetic anomaly indicative of long range spin ordering down to 2K. The specific heat ratio $\gamma = C_V/T$ shows a rather sharp peak at temperature $T_c \sim 20$ K, indicating existence of phase transition or cross-over at T_c . On the other hand, the spin susceptibility $\chi(T)$ is almost temperature independent for all temperatures $T \ll \theta_W$. Using the experimental value of spin susceptibility χ and specific heat ratio γ at the specific heat peak at ~ 20 K, one finds that the Wilson ratio $R_W = \pi^2 k_B^2 \chi / 3\mu_B^2 \gamma$ of the material is 0.88 for $T > T_c$, which is very close to that of a Fermi gas where R_W is unity. Therefore, for a wide range of temperature $T_c < T < \theta_W$, the system seems to behave as a Fermi liquid of spinons. Below T_c the specific heat decreases to zero as $C_V \sim T^2$, suggesting a line nodal gap in the low lying quasiparticle spectrum. However, this picture needs to be reconciled with the observation that the spin susceptibility χ remains almost constant, resulting in an anomalous large Wilson ratio $R_W \gg 1$ at

temperature $T < T_c$.

The spins in $\text{Na}_4\text{Ir}_3\text{O}_8$ come from the low spin $5d^5$ Ir^{4+} ions, which form a 3D network of corner shared hyperkagome lattice. It was suggested by Chen and Balents (Chen and Balents, 2008) that because of the large atomic number, spin-orbit coupling in Ir atoms is expected to be strong. In the following, we shall explain the anomalous Wilson ratio based on a modified RVB spin liquid picture where both spin-singlet and spin-triplet pairings exist in the spin-pairing wave-function.

Based on the above experimental observations Zhou et al. (Zhou *et al.*, 2008) proposed that a simple spinon hopping Hamiltonian H_0 determines the physics of the spin liquid state at $T > T_c$ where there exists a finite spinon Fermi surface, and a spinon pairing gap characterized by H_{pair} is opened up at $T < T_c$. The power law behavior $C_V \propto T^2$ observed at low temperature $T < T_c$ indicates that the gap has line node on Fermi surfaces. To determine the pairing symmetry, Zhou et al. noted that group theoretical analysis indicates that a spin triplet pairing state on a cubic lattice can create only full or point nodal gaps (Sigrist and Ueda, 1991) which seems to imply singlet pairing. However, because of broken inversion symmetry on a hyperkagome lattice (Hahn, 1996), the spin-singlet and spin-triplet pairing states are mixed together in general in the presence of spin orbit coupling (Frigeri *et al.*, 2004; Gor'kov and Rashba, 2001). ³

In terms of d -vector the gap function $\Delta_{\alpha\beta}(\mathbf{k})$ ($\alpha, \beta = \uparrow, \downarrow$) has the general matrix form (Leggett, 1975),

$$\Delta(\mathbf{k}) = i(d_0(\mathbf{k})\sigma_0 + \mathbf{d}(\mathbf{k}) \cdot \boldsymbol{\sigma})\sigma_y. \quad (79)$$

and the spinon pairing must be singlet or singlet with triplet admixture due to spin-orbit coupling in order to have line node (Zhou *et al.*, 2008).

We now consider the spin susceptibility of such mixed states. Zhou et al. showed that if both singlet and triplet pairing are present and spin-orbit scattering is much weaker than the pairing gap Δ , the k -dependent electronic contribution to spin susceptibility is given by

$$\frac{\chi_{ii}(\mathbf{k})}{\chi_N(\mathbf{k})} = 1 - \frac{d_0 d_0^* + d_i^* d_i}{d_0 d_0^* + \mathbf{d} \cdot \mathbf{d}^*} + \frac{d_0 d_0^* + d_i^* d_i}{d_0 d_0^* + \mathbf{d} \cdot \mathbf{d}^*} Y(\mathbf{k}; T),$$

where $i = x, y, z$, χ_N is the normal state contribution at $\Delta = 0$, and $Y(\mathbf{k}; T)$ is the k -dependent Yosida function (Leggett, 1975). Assuming that the d -vector is pinned

by the lattice, for a polycrystalline sample one has to average over all spatial directions, resulting in

$$\frac{\chi_s}{\chi_N} = \frac{2}{3} - \frac{2}{3} \frac{|d_0|^2}{|d_0|^2 + |\mathbf{d}|^2} + \left(\frac{1}{3} + \frac{2}{3} \frac{|d_0|^2}{|d_0|^2 + |\mathbf{d}|^2} \right) Y(T), \quad (80)$$

where $Y(T)$ is the (spatially averaged) Yosida function that vanish at zero temperature, χ_s is the spin susceptibility below T_c and χ_N is the Pauli spin susceptibility at the normal state. Therefore χ_s/χ_N reduces to $\frac{2}{3} - \frac{2}{3} \frac{|d_0|^2}{|d_0|^2 + |\mathbf{d}|^2}$ at zero temperature. If the spin-triplet pairing dominates, $\chi_s/\chi_N \rightarrow \frac{2}{3}$, while if the spin-singlet pairing dominates, $\chi_s/\chi_N \rightarrow 0$. Neither of these cases are observed in experiment, where χ hardly changes below T_c (Okamoto *et al.*, 2007). This suggested that strong spin-orbit coupling is needed to explain the absence of change in χ below $T_c \sim 20\text{K}$.

It is well known that in conventional BCS singlet superconductors, the Knight shift, which is proportional to Pauli paramagnetic susceptibility, hardly changes below T_c for heavy elements such as Sn and Hg (Androes and Knight, 1959). It was realized that this is due to the destruction of spin conservation due to the spin-orbit coupling. A clear explanation was given by Anderson (Anderson, 1959) using the notion of time reversed pairing states. We first consider the imaginary part of the spin response function $\chi''(q, \omega)$. If the total spin is conserved, the dynamics is diffusive and $\chi''(q, \omega)$ will have a central peak in ω space with width Dq^2 which goes to zero as $q \rightarrow 0$. Superconductivity gaps out all low frequency excitations, thus removing this central peak. By Kramers-Kronig relation the real part $\chi'(q = 0, \omega = 0)$ vanishes in the superconducting ground state. In the presence of spin-orbit coupling, the total spin is not conserved, but decays with a lifetime τ_s . In this case $\chi''(q = 0, \omega)$ has a central peak with a width $\frac{1}{\tau_s}$. The superconducting gap (by a pair of time reversal states) Δ cuts a hole in the $\chi''(\omega)$ for $\omega < \Delta$, but leaves the region $\omega \gg \Delta$ intact, in agreement with physical expectation that the high frequency region should be unaffected by pairing. By Kramer-Kronig relation, χ' will be reduced, but if the spin-orbit coupling is strong enough such that

$$\frac{1}{\tau_s} \gg \Delta, \quad (81)$$

the reduction will be small, i.e.

$$\frac{\chi_s}{\chi_N} = 1 - \mathcal{O}(\Delta\tau_s).$$

Eq. (81) is the strong spin-orbit coupling criterion to have very little change in the spin susceptibility below T_c . We emphasize that the criterion for strong or weak spin-orbit coupling given by Eq.(81) is totally different from usual criterion where the spin-orbit energy λ is compared with the splitting of the t_{2g} levels E_3 (Chen and Balents, 2008).

³ In general, for a many-spin system breaking spin rotational symmetry, the spin $S = 0$ state(s) will mix with spin $S \geq 1$ states even in the presence of spatial inversion symmetry. The only exception is the two-spin system, where inversion symmetry provides a good quantum number separating spin-singlet state from spin-triplet states. Since the RVB approach starts from mean-field spin wavefunctions which are superpositions of two-spin pairing states, broken inversion symmetry is needed for the construction of mixed spin-singlet and spin-triplet states.

Theoretically, the Projective Symmetry Group classification scheme has been applied to classify the spin liquid states on a Kagome lattice with Dzyaloshinskii-Moriya (DM) interaction (Dodds *et al.*, 2013). More recently, to test the validity of RVB approach in constructing wavefunctions for spin systems with strong spin-orbit coupling, Sze, Zhou and Ng (Sze *et al.*, 2016) have applied the Gutzwiller projected wave function of fermion pairing states to study the $S = 1/2$ anisotropic Heisenberg (XXZ) chain

$$H = J_z \sum_i S_i^z S_{i+1}^z + J_{\perp} \sum_i (S_i^x S_{i+1}^x + S_i^y S_{i+1}^y), \quad (82)$$

where $J_{\perp}, J_z > 0$. The model can be mapped to the isotropic (XXX) Heisenberg model with Dzyaloshinskii-Moriya (DM) interaction

$$\sum_i \mathbf{D} \cdot (\mathbf{S}_i \times \mathbf{S}_{i+1})$$

in one dimension with open boundary condition through a transformation $U = \exp(-i \sum_n \frac{n\theta}{2} S_n^z)$ with $\cos \theta = J_z/J_{\perp}$ and $D = J_{\perp} \sin \theta$, where $U^{\dagger} H_{XXX} U = H_{J+DM}$, H_J is the isotropic Heisenberg model with interaction J .

Trial mean-field wavefunctions with general pairing

$$\Delta(\mathbf{k}) = i (d_0(\mathbf{k}) \sigma_0 + \mathbf{d}(\mathbf{k}) \cdot \boldsymbol{\sigma}) \sigma_y.$$

are being considered to construct the corresponding Gutzwiller Projected wavefunctions. It was found that the trial ground state wave-functions have best energy when the d -vector has the form $d_0 = 0$ and $\mathbf{d}(k) = d_z \hat{z} = i \Delta \sin k$ for $J_z > J_{\perp}$ (Ising regime), whereas $d_0 = 0$ and $\mathbf{d}(k) = d_y \hat{y} = \Delta \sin k$ when $J_z < J_{\perp}$ (planar regime). The overlap between the trial ground state wavefunction and the exact ground state wavefunction obtained from exact diagonalization is better than 95% in all cases they consider. It is interesting to note that the pairing state with $\mathbf{d}(k) = d_y \hat{y} = \Delta \sin k$ does not conserve S_z^{tot} and is not considered in the classification scheme in (Dodds *et al.*, 2013).

IV.2. RVB approach to $S > 1/2$ systems

Historically the search for spin liquid states has concentrated at spin-1/2 systems because it has the strongest quantum mechanical fluctuation effect (see section II) when the unfrustrated Heisenberg model is considered. The situation is different when we considered spin systems with frustrated interactions (Chandra and Doucot, 1988). In this case it is not obvious whether a spin liquid state is more likely to exist in lower spin systems. In fact it was found recently that gapless spin liquid states may exist in a two-dimensional spin-1 compound $\text{Ba}_3\text{NiSb}_2\text{O}_9$ under high pressure (Cheng *et al.*, 2011). In this subsection, we examine how we can construct

spin liquid states for $S > 1/2$ systems by generalizing the RVB approach developed for $S = 1/2$ systems. It should be pointed out that there are more than one way of generalization. For example, Greiter and Thomale (Greiter and Thomale, 2009) have constructed a chiral spin liquid state using fractional quantum Hall wavefunction, while Xu *et al.* (Xu *et al.*, 2012) constructed a spin liquid state for $S = 1$ system by representing a spin-1 as the sum of two $S = 1/2$ spins. Liu, Zhou, and Ng (Liu *et al.*, 2010a,b) have constructed an alternative approach where a spin S is represented by $2S+1$ fermions. We shall consider the last approach in the following where we shall see the existence of fundamental differences between half-odd-integer spin and integer spin systems in this approach.

We begin with the fermionic representation for general spins. To generalize the fermionic representation for $S = 1/2$ spins to arbitrary spin- S , Liu, Zhou and Ng (Liu *et al.*, 2010a,b) introduce $2S+1$ species of fermionic operators c_m satisfying anti-commutation relations,

$$\{c_m, c_n^{\dagger}\} = \delta_{mn}, \quad (83)$$

where $m, n = S, S-1, \dots, -S$. The spin operator can be expressed in terms of c_m and c_n^{\dagger} 's,

$$\hat{\mathbf{S}} = C^{\dagger} \mathbf{I} C,$$

where $C = (c_S, c_{S-1}, \dots, c_{-S})^T$ and I^a ($a = x, y, z$) is a $(2S+1) \times (2S+1)$ matrix whose matrix elements are given by

$$I_{mn}^a = \langle S, m | S^a | S, n \rangle.$$

It is straightforward to show that the resulting spin operator $\hat{\mathbf{S}}$ satisfies the $SU(2)$ angular momentum algebra. Under a rotational operation, C is a spin- S “spinor” transforming as $C_m \rightarrow D_{mn}^S C_n$ and $\hat{\mathbf{S}}$ is a vector transforming as $S^a \rightarrow R_{ab} S^b$, here D^S is the $2S+1$ -dimensional irreducible representation of $SU(2)$ group generated by \mathbf{I} and R is the adjoint representation.

As in the $S = 1/2$ case, a constraint that there is only one fermion per site is needed to project the fermionic system into the proper Hilbert space representing spins, i.e.

$$(\hat{N}_i - N_f) | \text{phy} \rangle = 0, \quad (84)$$

where i is the site index and $N_f = 1$ (the particle picture, one fermion per site). Alternatively, it is straightforward to show that the constraint $N_f = 2S$ (the hole picture, a single hole per site) represents a spin equally. The $N_f = 1$ representation can be mapped to the $N_f = 2S$ representation *via a particle-hole transformation*. For $S = 1/2$, the particle picture and the hole picture are identical, reflecting an intrinsic particle-hole symmetry of the underlying Hilbert space which is absent for $S \geq 1$.

Following Affleck, Zou, Hsu and Anderson (Affleck *et al.*, 1988b), Liu, Zhou and Ng

(Liu *et al.*, 2010a) introduce another “spinor” $\bar{C} = (c_{-S}^\dagger, -c_{-S+1}^\dagger, c_{-S+2}^\dagger, \dots, (-1)^{2S} c_S^\dagger)^T$, whose components can be written as $\bar{C}_m = (-1)^{S-m} c_{-m}^\dagger$, where the index m runs from S to $-S$ as for C . Combining C and \bar{C} into a $(2S+1) \times 2$ matrix $\psi = (C, \bar{C})$, it is straightforward to see that the spin operators can be reexpressed as

$$\hat{\mathbf{S}} = \frac{1}{2} \text{Tr}(\psi^\dagger \mathbf{I} \psi) \quad (85)$$

and the constraint can be expressed as

$$\text{Tr}(\psi \sigma_z \psi^\dagger) = 2S + 1 - 2N_f = \pm(2S - 1), \quad (86)$$

where the + sign implies $N_f = 1$ and - sign implies $N_f = 2S$.

We now examine the internal symmetry group associated with the redundancy in fermion representation. The internal symmetry group is different for integer and half-odd-integer spins and is $U(1) \bar{\otimes} Z_2 = \{e^{i\sigma_z \theta}, \sigma_x e^{i\sigma_z \theta} = e^{-i\sigma_z \theta} \sigma_x; \theta \in \mathbb{R}\}$ for the former and $SU(2)$ for the latter. The reason can be qualitatively understood as follows: Notice that C and \bar{C} are not independent. The operators in the internal symmetry group “mixes” the two fermion operators in the same row of C and \bar{C} , i.e. c_S and c_{-S}^\dagger . For integer spins, c_0 and $(-1)^S c_0^\dagger$ will be “mixed”. To keep the relation $\{c_0, c_0^\dagger\} = 1$ invariant, there are only two methods of “mixing”: one is a $U(1)$ transformation, the other is interchanging the two operators. These operations form the $U(1) \bar{\otimes} Z_2$ group. For half-odd-integer spins, the pair $(c_0, (-1)^S c_0^\dagger)$ do not exist, and the symmetry group is the maximum group $SU(2)$. The difference between integer and half-odd-integer spins is a fundamental property of the fermionic representation.

Now let us see how the constraints (86) transform under the symmetry groups. For $S = 1/2$, the constraint (86) is invariant under the transformation $\psi \rightarrow \psi W$ because the right hand side vanishes (due to the particle-hole symmetry of the Hilbert space). For integer spins, if $W = e^{i\sigma_z \theta}$, then $W \sigma_z W^\dagger = \sigma_z$, and (86) is invariant. If $W = \sigma_x e^{i\sigma_z \theta}$, then $W \sigma_z W^\dagger = -\sigma_z$, meaning that the “particle” picture (+ sign in (86)) and the “hole” picture (- sign in (86)) are transformed to each other.

For a half-odd-integer spin with $S \geq 3/2$, $W \in SU(2)$ is a rotation and we may extend the constraint into a vector form similar to $S = 1/2$ case, so that Eq.(86) becomes

$$\text{Tr}(\psi \vec{\sigma} \psi^\dagger) = (0, 0, \pm(2S - 1))^T. \quad (87)$$

Under the group transformation $\psi \rightarrow \psi W$,

$$\text{Tr}(\psi \vec{\sigma} \psi^\dagger) \rightarrow (R^{-1})(0, 0, \pm(2S - 1))^T. \quad (88)$$

where $W \sigma^a W^\dagger = R_{ab} \sigma^b$, $a, b = x, y, z$, i.e. R is a 3 by 3 matrix representing a 3D rotation. The transformed constraint represents a new Hilbert subspace which is still a

$(2N + 1)$ -dimensional irreducible representation of the spin $SU(2)$ algebra. Any measurable physical quantity such as the spin \mathbf{S} remains unchanged in the new Hilbert space. Therefore, for half-odd-integer spins ($S \geq 3/2$), there exists infinitely many ways of imposing the constraint that gives rise to a Hilbert subspace representing a spin. However, for integer spins, there exists only two possible constraint representations.

The fermionic representation can be used to construct mean-field Hamiltonian for spin models with arbitrary spins after the spin-spin interaction is written down in terms of fermion operators. For spin-1/2 the Heisenberg interaction can be written as (see section III)

$$\begin{aligned} \hat{\mathbf{S}}_i \cdot \hat{\mathbf{S}}_j &= -\frac{1}{8} \text{Tr} : (\psi_i^\dagger \psi_j \psi_j^\dagger \psi_i) : \\ &= -\frac{1}{4} : (\chi_{ij}^\dagger \chi_{ij} + \Delta_{ij}^\dagger \Delta_{ij}) :, \end{aligned} \quad (89)$$

where

$$\chi_{ij} = C_i^\dagger C_j, \quad \Delta_{ij} = \bar{C}_i^\dagger C_j. \quad (90)$$

The definition of χ_{ij} and Δ_{ij} can be extended to arbitrary spins in the above form. The only difference is that for integer spin, $\chi_{ji} = \chi_{ij}^\dagger$, $\Delta_{ji} = -\Delta_{ij}$, whereas for half-odd-integer spin, $\chi_{ji} = \chi_{ij}^\dagger$, $\Delta_{ji} = \Delta_{ij}$. The parity of the pairing terms Δ_{ij} are different for integer and half-odd-integer spins (Liu *et al.*, 2010a). For $S = 1$, it can be shown after some straightforward algebra that the Hamiltonian can be written as (Liu *et al.*, 2010a)

$$\begin{aligned} \hat{\mathbf{S}}_i \cdot \hat{\mathbf{S}}_j &= -\frac{1}{2} \text{Tr} : (\psi_i^\dagger \psi_j \psi_j^\dagger \psi_i) : \\ &= : (\chi_{ij}^\dagger \chi_{ij} + \Delta_{ij}^\dagger \Delta_{ij}) :. \end{aligned} \quad (91)$$

However, for $S > 1$, we cannot write the spin-spin interaction $\hat{\mathbf{S}}_i \cdot \hat{\mathbf{S}}_j$ in terms of χ_{ij} and Δ_{ij} only. In the case of $S = 3/2$, triplet hoping and pairing terms have to be introduced to represent the Heisenberg interaction. Generally speaking, quintet and higher multipolar hoping and pairing operators are needed to represent the Heisenberg Hamiltonian when S becomes larger (Liu *et al.*, 2010a). We shall restrict ourselves to $S = 1$ systems in the following.

In this case the mean-field Hamiltonians are BCS-type Hamiltonians as in the case of $S = 1/2$ spins. The physical spin wavefunction can be obtained by applying Gutzwiller projection to the mean-field ground state. There are two major differences between $S = 1$ and $S = 1/2$ spin systems: (1) Because of the different internal symmetry group ($U(1) \bar{\otimes} Z_2$), $S = 1$ spin liquid states are either $U(1)$ or Z_2 . There are no $SU(2)$ spin liquid states for integer spin systems in the fermionic construction. Therefore we expect that in general spin liquid states for integer spin systems, if exists, are more stable against gauge fluctuations. (2) The difference in parity of pairing terms leads to the interesting possibilities of

obtaining topological spin liquid states for $S = 1$ systems which are not so easy to realize in $S = 1/2$ systems (Bieri *et al.*, 2012; Liu *et al.*, 2010b). This difference leads to the existence of Haldane phase in the bilinear-biquadratic Heisenberg spin chain in the fermionic description (Liu *et al.*, 2012).

Lastly, we point out the existence of a fundamental difference in the excitation spectrum of $S = 1$ spin systems when compared with $S = 1/2$ systems, assuming that the ground states are spin-singlets. For integer spin systems, we can form spin-singlet state in a lattice with either even or odd number of lattice sites N , as long as $N > 1$, whereas spin-singlet states can be formed only in a lattice with even number of sites for half-odd-integer spin systems. In the RVB approach, angular momentum $L = 1$ excitations of the system are formed by Gutzwiller projecting the excited states in BCS theory, i.e., by breaking a pair of spin-singlet in BCS ground state. The resulting excited state consists of two excited spinons, which are $S = 1/2$ objects for spin-1/2 systems, but are $S = 1$ objects for spin-1 systems. The two $S = 1$ spinons together form a $L = 1$ excitation in $S = 1$ spin liquids.

There is, however another way of forming $L = 1$ excitation in spin-1 spin liquids. Starting from a lattice system with N sites, we may form a $L = 1$ excitation by rearranging the spins such that the system is a product of spin-singlet ground state for $N - 1$ sites plus a single spin-1 spinon. This excitation is a non-perturbative, topological excitation which cannot be formed by simply Gutzwiller projecting a BCS excited state in the RVB construction. It was demonstrated in reference (Liu *et al.*, 2014) that the construction of these two kinds of excitations gives rise to the so-called one-magnon and two-magnon excitation spectrum in the Haldane phase of the $S = 1$ bilinear-biquadratic Heisenberg model. Similar construction is not possible for $S = 1/2$ systems.

IV.3. Matrix Product States (MPS) and Projected Entangled Pair States (PEPS)

In this subsection we discuss two approaches to spin liquid states that have completely different starting points from the RVB or Gutzwiller Projected Mean-Field Theory approach we discussed in section III. We start with the Matrix Product States (MPS) and Projected Entangled Pair States (PEPS) which represent another popular class of variational wavefunctions applicable to spin systems nowadays. Translational invariant MPS in spin chains were firstly constructed and studied by Fannes, Nachtergael and Werner (Fannes *et al.*, 1992) as an extension of the AKLT state (Affleck *et al.*, 1987), where they call them *finitely correlated states*. The term MPS was coined by Klümper, Schadschneider and Zittartz (Klümper *et al.*, 1993), who extended the AKLT state in a different way. Later, Östlund

and Rommer (Östlund and Rommer, 1995) realized that the state resulting from density matrix renormalization group (DMRG) (White, 1992) can be written as a MPS. The approach is very successful for one dimensional systems, and can be generalized to two (or higher) dimensional systems.

To begin with, let's consider the quantum wavefunction of a one-dimensional spin system which is translational invariant with a local Hamiltonian H . The wavefunction can be expressed generally as

$$|\Psi\rangle = \sum_{s_1, s_2, \dots, s_N} \phi(s_1, s_2, \dots, s_N) |s_1, s_2, \dots, s_N\rangle \quad (92)$$

where $|s_1, s_2, \dots, s_N\rangle$ represents a spin configuration with spin s_i 's on sites $i = 1, 2, \dots, N$, and $\phi(s_1, s_2, \dots, s_N)$ is the amplitude of the spin configuration at the quantum state $|\Psi\rangle$. Because of spin-spin interaction, spin configurations at far away sites are generally correlated and we cannot write $\phi(s_1, s_2, \dots, s_N) = \phi_0(s_1)\phi_0(s_2)\dots\phi_0(s_N)$ in general. The MPS is a powerful method to construct wavefunctions with non-local quantum correlations. The trick is to extend the direct-product wavefunction $\phi(s_1, s_2, \dots, s_N) = \phi_0(s_1)\phi_0(s_2)\dots\phi_0(s_N)$ to matrix products.

More explicitly, we associate for each spin state s an matrix A^s , the wavefunction amplitude $\phi(s_1, s_2, \dots, s_N)$ is then written as

$$\phi(s_1, s_2, \dots, s_N) = \text{Tr}\{A^{s_1}[1]A^{s_2}[2]\dots A^{s_N}[N]\}, \quad (93)$$

where the trace is used to impose the periodic boundary condition. As an example, we consider a $S = 1/2$ two-spin system and choose $A^\uparrow = \sigma_z, A^\downarrow = \sigma_x$, where σ 's are Pauli matrices. It is easy to see that in this case $\phi(\uparrow, \uparrow) = \phi(\downarrow, \downarrow) \neq 0$ and $\phi(\uparrow, \downarrow) = \phi(\downarrow, \uparrow) = 0$. A difference choice of $A^\uparrow = \sigma_+, A^\downarrow = \sigma_-$ gives $\phi(\uparrow, \downarrow) = \phi(\downarrow, \uparrow) \neq 0$ and $\phi(\uparrow, \uparrow) = \phi(\downarrow, \downarrow) = 0$. The correlation between the different spin states on the two sites are determined by the matrix A^s chosen to link between the sites. Extending the construction to more than two sites, one sees that the choice of matrices A^σ determines the quantum entanglement structure of the wavefunction.

Treating the MPS as variational wavefunctions, one may determine the number of variational parameters in the wavefunctions by a simple counting argument. In general, the number of parameters P entering a MPS wavefunction (93) depends on the size of the matrix A and the number of available states S per site. In general, $P \sim S \times M^2$ for a $M \times M$ matrix as long as $P < S^N$, where N is the number of sites in the system. Thus MPS wavefunctions are in general variational wavefunctions with a large number of build-in variational parameters. As the dimension $M \rightarrow \infty$, MPS can represent any quantum state of the many-body Hilbert space with arbitrary accuracy. In practice, the low energy states of gapped local Hamiltonians in one dimension can be efficiently

represented by MPS with a finite value of M (Hastings, 2007; Verstraete and Cirac, 2006). The DMRG (White, 1992) and its generalizations (Schollwöck, 2005) can be viewed as systematic approaches to construct MPS variational wavefunction when the size of the system is increased gradually.

The MPS construction can be extended in several ways. First, it can be extended to higher dimension by replacing the matrices A (= rank-2 tensor) by higher rank tensors T . These wavefunctions are called projected entangled pair states (PEPS) nowadays (Verstraete and Cirac, 2004a,b). Second, the local correlation or entanglement within a pair of sites in PEPS can be generalized to a cluster (or simplex), resulting in the states called projected entangled simplex states (PESS) (Xie *et al.*, 2014). A representative example for PESS is the simplex solid state proposed by Arovas (Arovas, 2008).

IV.3.1. Valence Bond Solid and MPS states in one dimension

The physics of the MPS or PEPS wavefunction is encoded in the tensors linking between neighboring spin states. In general, these link-tensors can be constructed optimally by DMRG or tensor-based renormalization methods (Cirac and Verstraete, 2009). In this subsection we shall discuss a simple example of tensors which represents a particular class of spin states called Valence Bond Solid (VBS) states. To start with, we introduce a well known example of Valence Bond Solid State - the Affleck-Kennedy-Lieb-Tasaki (AKLT) state (Affleck *et al.*, 1987).

The AKLT state is an example of VBS state where there is only one spin-singlet configuration allowed in the wavefunction (23). It is a one dimensional VBS state constructed for a $S = 1$ spin chain. It is represented pictorially in Fig. 9, where each grey bond represents a spin singlet formed by two $S = 1/2$ spins, i.e. Eq. (22). Each lattice site is connected to two other sites by two valence bonds and is occupied by two $S = 1/2$ spins. The AKLT wavefunction is formed by projecting the spin $1/2 \otimes 1/2 = 1 \oplus 0$ quartet states into the spin $S = 1$ triplet states. This is represented graphically in Fig. 9 by the circles which represent projection operators tying together two $S = 1/2$ spins, projecting out the spin $S = 0$ or singlet state and keeping only the spin $S = 1$ or triplet states.

For every adjacent pair of $S = 1$ spins, two of the four constituent $S = 1/2$ spins are projected into a total spin zero state by the valence bond. Therefore the pair of $S = 1$ spins is forbidden from being in a combined spin $S = 2$ state. This condition can be realized by considering a Hamiltonian which is a sum of projectors $P_{i,i+1}$ which project the pairs of $S = 1$ spins from the

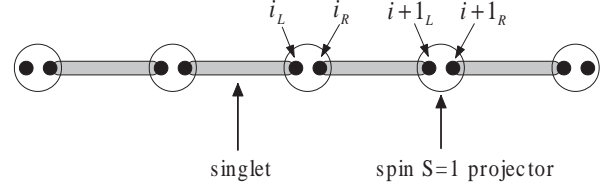


FIG. 9 A valence bond solid construction for the AKLT state.

space $1 \otimes 1 = 2 \oplus 1 \oplus 0$ into the spin $S = 2$ subspace,

$$H_{AKLT} = \sum_i P_{i,i+1}. \quad (94a)$$

Since the projection operators $P_{i,i+1}$ are positive semi-definite, the ground state satisfies $H_{AKLT}|\Psi_G\rangle = 0$ and is just the AKLT state. The projection operator $P_{i,i+1}$ can be written in terms of spin-1 operators (Affleck *et al.*, 1987),

$$P_{i,i+1} = \frac{1}{3} + \frac{1}{2}(\mathbf{S}_i \cdot \mathbf{S}_{i+1}) + \frac{1}{6}(\mathbf{S}_i \cdot \mathbf{S}_{i+1})^2. \quad (94b)$$

The AKLT state is important because it is an explicit spin wavefunction realizing the Haldane phase for integer spins (see section II). In particular, it is easy to see from Fig. 9 that an unpaired $S = 1/2$ spin will be left at the end of spin chains, which is a realization of the end state discussed in section II for $S = 1$ Heisenberg spin chains. In the following, we shall show how we can write the AKLT state as a MPS state.

The AKLT state can be constructed in two steps. Firstly we split each site i in the spin-1 chain into two sites i_L and i_R to form a spin-1/2 chain with $2N$ sites as in Fig. 9 (N = number of sites in the parent spin-1 chain) and construct a dimerized chain where spins in sites i_R and $i+1_L$ ($i = 1, 2, \dots, N$) are joined by a valence bond (Eq.(22)). The singlet bond between sites i_R and $i+1_L$ can be written as

$$(i, i+1) = \sum_{\sigma_{i_R}, \sigma_{i+1_L}} R_{\sigma_{i_R}, \sigma_{i+1_L}} |\sigma_{i_R}\rangle |\sigma_{i+1_L}\rangle \quad (95)$$

where $\sigma = \uparrow, \downarrow$ and $R_{\sigma\sigma'}$ are the components of a 2×2 matrix

$$\mathbf{R} = \begin{pmatrix} 0 & \frac{1}{\sqrt{2}} \\ -\frac{1}{\sqrt{2}} & 0 \end{pmatrix}. \quad (96)$$

In this representation the wavefunction of the dimerized spin-1/2 chain can be written as

$$|\Psi\rangle = \sum_{\sigma_{1_R}, \dots, \sigma_{N_L}} R_{\sigma_{1_R} \sigma_{2_L}} \dots R_{\sigma_{N-1_R} \sigma_{N_L}} |\sigma_{1_R}, \dots, \sigma_{N_L}\rangle. \quad (97)$$

Notice that the state is a direct product state of $S = 1/2$ RVB singlet pairs with the two end spins (σ_{1_L} and σ_{N_R}) unspecified.

Next we project the two $S = 1/2$ spins on sites i_L and i_R to the spin-1 states $|1, m\rangle$ ($m = 0, \pm 1$) with

$$\begin{aligned} |1, 1\rangle &= |\uparrow\uparrow\rangle \\ |1, 0\rangle &= \frac{1}{\sqrt{2}}(|\uparrow\downarrow\rangle + |\downarrow\uparrow\rangle) \\ |1, -1\rangle &= |\downarrow\downarrow\rangle. \end{aligned} \quad (98)$$

This projection can be expressed by three matrices, $M^{0, \pm 1}$, where

$$|1, m\rangle = \sum_{\sigma, \sigma'} M_{\sigma\sigma'}^m |\sigma\rangle |\sigma'\rangle \quad (99)$$

with

$$\mathbf{M}^1 = \begin{pmatrix} 1 & 0 \\ 0 & 0 \end{pmatrix}, \quad (100a)$$

$$\mathbf{M}^{-1} = \begin{pmatrix} 0 & 0 \\ 0 & 1 \end{pmatrix}, \quad (100b)$$

and

$$\mathbf{M}^0 = \begin{pmatrix} 0 & \frac{1}{\sqrt{2}} \\ \frac{1}{\sqrt{2}} & 0 \end{pmatrix}. \quad (100c)$$

Thus the AKLT state can be written as

$$|\Psi_{\text{AKLT}}\rangle = \sum_{s_1, s_2, \dots, s_N} \phi_{\text{AKLT}}(s_1, \dots, s_N) |s_1, s_2, \dots, s_N\rangle \quad (101)$$

where $s_i = 0, \pm 1$ and

$$\begin{aligned} \phi_{\text{AKLT}}(s_1, \dots, s_N) &= \sum_{\sigma_{1L}, \dots, \sigma_{N_L}} [M_{\sigma_{1L} \sigma_{1L}}^{s_1} R_{\sigma_{1L} \sigma_{2L}} \\ &\quad \times M_{\sigma_{2L} \sigma_{2L}}^{s_2} \dots R_{\sigma_{N-1L} \sigma_{NL}}^{s_N}] \\ &= [\mathbf{A}^{s_1} \mathbf{A}^{s_2} \dots \mathbf{A}^{s_N}]_{\sigma_{1L} \sigma_{N_L}}, \end{aligned} \quad (102a)$$

where $\mathbf{A}^s = \mathbf{M}^s \mathbf{R}$, and $\sigma_{1L}, \sigma_{N_L} = \uparrow, \downarrow$ correspond to four degenerate ground states on an open chain. Imposing the periodic boundary condition gives rise to the non-degenerate ground state with

$$\phi_{\text{AKLT}}(s_1, \dots, s_N) = \text{Tr}[\mathbf{A}^{s_1} \mathbf{A}^{s_2} \dots \mathbf{A}^{s_N}]. \quad (102b)$$

IV.3.2. PEPS states in higher dimensions and beyond

The AKLT construction can be extended to construct other types of valence bond solid states and in higher dimensions. Straightforward examples include $S = 2$ VBS states on square lattice and $S = 3/2$ VBS states on honeycomb lattice (Affleck *et al.*, 1988a). These states can be written as PEPS in the respective lattices.

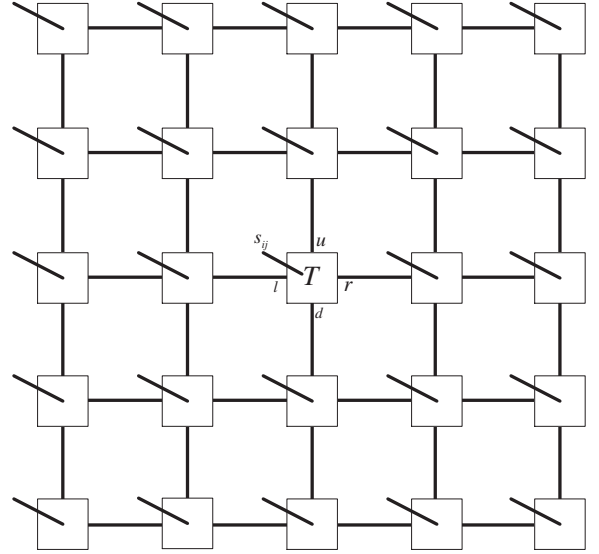


FIG. 10 Graphical representation of a PEPS in terms of contracted tensors (tensor network). Each box denotes a tensor T with components $T_{lrud}^{s_{ij}}$ at site ij , where l, u, r, d are tensor indices related to left, right, up and down bonds linking to their neighbors, the open lines represent the physical spin state s_{ij} , and connected lines represent contraction of tensors.

For instance, on the square lattice whose coordination number is 4, a generic PEPS wavefunction can be written in terms of rank-4 tensors,

$$|\Psi\rangle = \sum_{[s_{ij}]} \phi([s_{ij}]) |[s_{ij}]\rangle \quad (103a)$$

where $i, j = 1, \dots, N$ for a $N \times N$ system, $[s_{ij}] = (s_{11}, \dots, s_{1N}, s_{21}, \dots, s_{2N}, \dots, s_{N1}, \dots, s_{NN})$ denotes a spin configuration and

$$\phi([s_{ij}]) = \text{Tr}[T^{s_{11}} \dots T^{s_{1N}} T^{s_{21}} \dots T^{s_{NN}}]. \quad (103b)$$

where T^s 's are rank-4 tensors with components

$$T_{lrud}^{s_{ij}},$$

where s_{ij} is the physical spin index, l, r, u, d represent links connected to tensors in left, right, up and down neighboring sites $(i-1, j), (i+1, j), (i, j-1), (i, j+1)$, respectively and “Tr” means tensor contraction. The above mathematical expression of tensor contraction is usually represented by diagrams as shown in Fig. 10 for square lattice, where connected lines represent contraction of tensors with same index, and open lines represent the physical spin state $s_{ij} = -S, \dots, S$.

As an example the spin $S = 2$ AKLT state on the square lattice can be written in terms of PEPS as shown in Fig. 11. The tensors T^s 's can be obtained using the VBS construction with the tensors \mathbf{R} and \mathbf{M}^s as in 1D. The tensor \mathbf{R} is still defined by Eq.(96). The tensors \mathbf{M}^s , $s = 0, \pm 1, \pm 2$, project a four spin-1/2 state in the

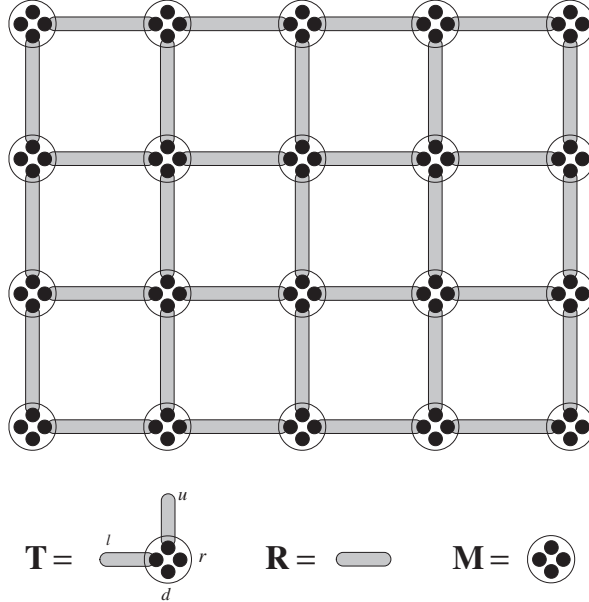


FIG. 11 (Affleck *et al.*, 1988a) The VBS construction for a $S = 2$ AKLT state on square lattice and corresponding tensors.

auxiliary Hilbert space $\frac{1}{2} \otimes \frac{1}{2} \otimes \frac{1}{2} \otimes \frac{1}{2} = 2 \oplus 1 \oplus 0$ into the physical spin space $S = 2$, whose components are given by

$$M_{\sigma_l \sigma_r \sigma_u \sigma_d}^s = \langle s | \sigma_l \sigma_r \sigma_u \sigma_d \rangle, \quad (104)$$

where $\sigma_l, \sigma_r, \sigma_u, \sigma_d = \uparrow, \downarrow$. The tensor \mathbf{T} is given by

$$T_{\sigma_l \sigma_r \sigma_u \sigma_d}^s = \sum_{\sigma_{l'}, \sigma_{u'}} M_{\sigma_l \sigma_r \sigma_{u'} \sigma_d}^s R_{\sigma_l \sigma_{l'}} R_{\sigma_u \sigma_{u'}}. \quad (105)$$

The tensor product state constructed from the above T^s 's give rises to the spin $S = 2$ AKLT state on the square lattice.

The VBS construction can be further extended by “fractionalizing” spins in more exotic ways (for example, using Majorana fermion representation for spins). In this way, we can write the toric code model (Kitaev, 2003) in the form of PEPS as well as Kitaev honeycomb model (Kitaev, 2006) (with a residual fermionic degree of freedom at each site, see section IV.4). The relation between RVB states and PEPS has also been exploited where it was shown that some RVB states can be written as PEPS (Poilblanc and Schuch, 2013; Schuch *et al.*, 2012; Verstraete *et al.*, 2006; Wang *et al.*, 2013). However, the general relation between RVB states and PEPS is still unclear.

The PEPS construction provides a way to describe entanglement among local spins based on the local pair construction and the application to geometrically frustrated lattices is limited. To go beyond this limitation people has extended the pair construction to consider entangle-

ment between more than two sites, say, a cluster or a simplex, to construct projected states. These projected entangled simplex states form the basis for more elaborate numerical approaches (Xie *et al.*, 2014). Combined with numerical techniques (tensor-based renormalization), these tensor-network methods produce an alternative way of constructing variational wavefunctions nowadays. Readers can refer to references (Cirac and Verstraete, 2009; Orus, 2014; Verstraete *et al.*, 2008) for details.

IV.4. Kitaev honeycomb model and related issues

It was previously believed that spin rotational symmetry is essential for a QSL state which supports fractional spinon excitations. If the spin rotational symmetry is broken, the system tends to approach an ordered state. Kitaev (Kitaev, 2006) provided a counter example to this view point through an unusual, exactly solvable model in two dimensions with strong spin-orbit coupling which destroys the spin rotational symmetry; but with nevertheless, deconfined spinons on top of the QSL ground states. This famous model is now called the Kitaev honeycomb model. We shall briefly review Kitaev honeycomb model to see how exotic ground states and low energy excitations emerge from this model which breaks rotation symmetry. The possible realization of Kitaev-like model in realistic materials is also discussed.

Kitaev considered a spin-1/2 model on honeycomb lattices with spin-orbit coupling (Kitaev, 2006). He divided all the nearest neighbor bonds in Honeycomb lattice into three types, called “ x -link”, “ y -link” and “ z -link” as shown in Fig. 12. The Hamiltonian is given as the following,

$$H = -J_x \sum_{x\text{-link}} K_{ij} - J_y \sum_{y\text{-link}} K_{ij} - J_z \sum_{z\text{-link}} K_{ij}, \quad (106)$$

where K_{ij} is defined as

$$K_{ij} = \begin{cases} \sigma_i^x \sigma_j^x, & \text{if } (i, j) \text{ is a } x\text{-link,} \\ \sigma_i^y \sigma_j^y, & \text{if } (i, j) \text{ is a } y\text{-link,} \\ \sigma_i^z \sigma_j^z, & \text{if } (i, j) \text{ is a } z\text{-link.} \end{cases} \quad (107)$$

Notice the strong anisotropy in the spin-spin coupling K_{ij} 's.

We first consider the following loop operators W_p defined for a hexagonal loop,

$$W_p \equiv \sigma_1^x \sigma_2^y \sigma_3^z \sigma_4^x \sigma_5^y \sigma_6^z = K_{12} K_{23} K_{34} K_{45} K_{56} K_{61}, \quad (108)$$

where p is a label of lattice plaquettes (hexgons) as shown in Fig. 13. It is easy to verify that $[W_p, K_{ij}] = 0$, therefore $[H, W_p] = 0$. Hence W_p 's serve as good quantum numbers for the Hamiltonian (106) and the total Hilbert space for spins can then be divided into direct product of sectors which are eigenspaces of $\{W_p\}$. However, the

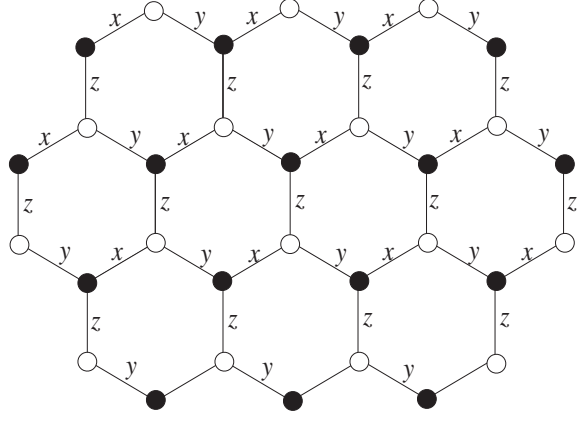


FIG. 12 (Kitaev, 2006) Kitaev honeycomb model. x , y and z denote three types of links in the honeycomb lattice.

eigenspaces of $\{W_p\}$ cannot solve the eigenvalue problem completely. Each W_p has only two eigenvalues $w_p = \pm 1$. Each plaquette contains six sites and each site is shared by three plaquettes. Therefore, the plaquette number is given by $m = N/2$, where N is the site number. It follows that the dimension of each eigenspace of $\{W_p\}$ is $2^N/2^m = 2^{N/2}$, i.e. splitting into eigenspaces of $\{W_p\}$ cannot solve the eigenvalue problem completely.

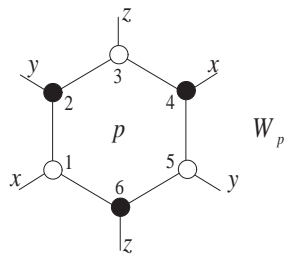


FIG. 13 (Kitaev, 2006) Loop operator $W_p = \sigma_1^x \sigma_2^y \sigma_3^z \sigma_4^x \sigma_5^y \sigma_6^z$ on a lattice plaquette (hexagon).

To solve the model Hamiltonian (106), Kitaev realized that spins can be written in terms of four Majorana fermions since a Majorana fermion can be viewed as the real or imaginary part of a complex fermion. To see how it works we rewrite the complex fermions f_\uparrow and f_\downarrow in Eq.(27) in terms of four Majorana fermions c_1 , c_2 , c_3 and c_4 ,

$$\begin{aligned} f_\uparrow &= \frac{1}{2}(c_1 + ic_2), & f_\uparrow^\dagger &= \frac{1}{2}(c_1 - ic_2), \\ f_\downarrow &= \frac{1}{2}(c_3 + ic_4), & f_\downarrow^\dagger &= \frac{1}{2}(c_3 - ic_4), \end{aligned} \quad (109a)$$

where c_α ($\alpha = 1, 2, 3, 4$) are hermitian and satisfy

$$c_\alpha c_\beta + c_\beta c_\alpha = 2\delta_{\alpha\beta}. \quad (109b)$$

Thus the three components of spin read $\sigma^x = \frac{i}{2}(c_1 c_4 - c_2 c_3)$, $\sigma^y = \frac{i}{2}(c_3 c_1 - c_2 c_4)$, and $\sigma^z = \frac{i}{2}(c_1 c_2 - c_3 c_4)$.

The single occupancy condition $f_\uparrow^\dagger f_\uparrow + f_\downarrow^\dagger f_\downarrow = 1$ (and $f_\uparrow^\dagger f_\downarrow^\dagger = f_\uparrow f_\downarrow = 0$) becomes

$$c_1 c_2 + c_3 c_4 = c_1 c_3 + c_2 c_4 = c_1 c_4 + c_3 c_2 = 0, \quad (110)$$

which can be simplified as a single equation $c_1 c_2 c_3 c_4 = 1$. Using these constraints, the spin operators can be written as $\sigma^x = ic_1 c_4$, $\sigma^y = -ic_2 c_4$, and $\sigma^z = -ic_3 c_4$. Rewriting $b_x = c_1$, $b_y = -c_2$, $b_z = -c_3$ and $c = c_4$, we arrive at the Kitaev's representation

$$\begin{aligned} \sigma^x &= ib^x c, \\ \sigma^y &= ib^y c, \\ \sigma^z &= ib^z c, \end{aligned} \quad (111)$$

with the constraint

$$D \equiv b^x b^y b^z c = 1. \quad (112)$$

The Majorana representation without constraint is redundant and enlarges the physical spin Hilbert space. Note that $D^2 = 1$ and D has two eigenvalues $D = \pm 1$, splitting the local Hilbert space into two sectors. The physical spin Hilbert space is given by the sector with all $D_j = 1$. Therefore the physical spin wavefunction $|\Psi_{\text{spin}}\rangle$ can be obtained from the Majorana fermion wavefunction $|\Psi_{\text{Majorana}}\rangle$ through the projection

$$|\Psi_{\text{spin}}\rangle = \prod_j \frac{1 + D_j}{2} |\Psi_{\text{Majorana}}\rangle, \quad (113)$$

which keeps the $D_j \equiv 1$ sector and remove all the other sectors in the enlarged Hilbert space. Note that $\frac{1+D_j}{2} = n_{j\uparrow} + n_{j\downarrow} - 2n_{j\uparrow}n_{j\downarrow}$ and Eq.(113) is nothing but the Gutzwiller projection. Notice that D_j serves as a Z_2 gauge transformation in the enlarged Hilbert space ($D_j b_j^\alpha D_j = -b_j^\alpha$, $D_j c_j D_j = -c_j$) and commutes with the spin operators ($[D_j, \sigma_j^\alpha] = 0$) ($\alpha = x, y, z$) and thus the Hamiltonian. As a result, the Gutzwiller projection is “trivial” in the sense that $\prod_j \frac{1+D_j}{2} |\Psi_{\text{Majorana}}\rangle$ is an eigenstate of H in the projected Hilbert space as long as $|\Psi_{\text{Majorana}}\rangle$ is an eigenstate of H in the “unprojected” Hilbert space and $\prod_j \frac{1+D_j}{2} |\Psi_{\text{Majorana}}\rangle \neq 0$.

In the Majorana fermion representation, K_{ij} in Eq.(107) becomes

$$K_{ij} = -i(ib_i^\alpha b_j^\alpha) c_i c_j, \quad (114)$$

where $\alpha = x, y, z$ depends on the type of link (ij) . The operator $ib_i^\alpha b_j^\alpha$ is Hermitian and we denote it as $\hat{u}_{ij} = ib_i^\alpha b_j^\alpha$. Thus, we may write

$$H = \frac{i}{4} \sum_{\langle j, k \rangle} \hat{A}_{jk} c_j c_k, \quad (115a)$$

with

$$\hat{A}_{jk} = 2J_{\alpha(jk)} \hat{u}_{jk}, \hat{u}_{jk} = ib_j^\alpha b_k^\alpha, \quad (115b)$$

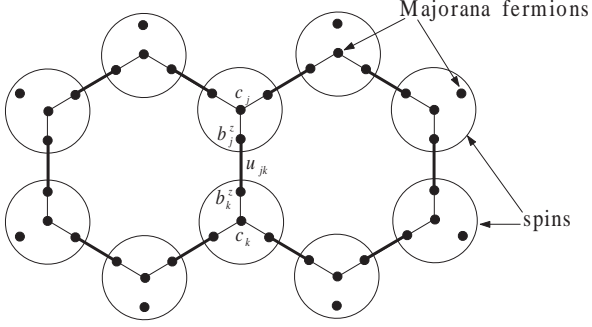


FIG. 14 (Kitaev, 2006) Graphic representation of the four Majorana fermion decomposition of Hamiltonian (106).

where $\langle j, k \rangle$ denote nearest neighbor link on Honeycomb lattice, and $\hat{u}_{jk} = -\hat{u}_{kj}$ and $\hat{A}_{jk} = -\hat{A}_{kj}$ by definition. The Hamiltonian structure in this Majorana fermion representation is shown schematically in Fig. 14. Note that $[H, \hat{u}_{jk}] = 0$ and $[\hat{u}_{jk}, \hat{u}_{j'k'}] = 0$. The enlarged Hilbert space of majorana fermions can be decomposed into common eigenspaces of $\{\hat{u}_{jk}\}$ indexed by corresponding eigenvalues $u_{jk} = \pm 1$. Thus the Hamiltonian in the invariant subspace indexed by $u = \{u_{jk}\}$ becomes

$$H_u = \frac{i}{4} \sum_{\langle j, k \rangle} A_{jk} c_j c_k, \quad A_{jk} = 2J_{\alpha(jk)} u_{jk}. \quad (116)$$

where we have replaced \hat{A}_{jk} and \hat{u}_{jk} by their eigenvalues. Notice that $u_{jk} \rightarrow -u_{jk}$ upon the Z_2 gauge transformation $u_{jk} \rightarrow D_j u_{jk} D_j$ and it is more convenient to classify the eigenstates of H by the gauge invariant loop operator $W(j_0, \dots, j_n) = K_{j_n j_{n-1}} \dots K_{j_1 j_0}$, which can be written as

$$W(j_0, \dots, j_n) = \left(\prod_{s=1}^n -i\hat{u}_{j_s j_{s-1}} \right) c_n c_0. \quad (117)$$

The close loop operator W_p (see Eq.(108)) is gauge invariant upon Z_2 transformation because $c_n = c_0$ and the gauge invariant quantities $w = \{w_p\}$ can be used to parameterize the eigenstates instead of $u = \{u_{jk}\}$, i.e.,

$$H_w = \frac{i}{4} \sum_{\langle j, k \rangle} A_{jk} c_j c_k. \quad (118)$$

For a given set of A_{ij} fixed by $\{w_p\}$, the quadratic Hamiltonian (116) and (118) can be diagonalized into the canonical form,

$$H_{\text{canonical}} = \frac{i}{2} \sum_m \epsilon_m c'_m c''_m = \sum_m \epsilon_m \left(f_m^\dagger f_m - \frac{1}{2} \right), \quad (119)$$

where $\epsilon_m \geq 0$, c'_m and c''_m are normal Majorana modes, $f_m^\dagger = \frac{1}{2}(c'_m - i c''_m)$ and $f_m = \frac{1}{2}(c'_m + i c''_m)$ are corresponding complex fermion operators. The ground state of the

Majorana system has energy

$$E = -\frac{1}{2} \sum_m \epsilon_m. \quad (120)$$

We now discuss the system of Majorana fermions on the honeycomb lattice. First we note that the global ground state energy does not depend on the signs of the exchange constants J_x, J_y, J_z . For instance, if J_z is replaced by $-J_z$, we can compensate this sign change by changing the signs of the variables u_{jk} for all the z -links through the gauge operator D_j , leaving the values of A_{jk} and w_p unchanged. Therefore as far as solving the ground state energy and the excitation spectrum is concerned, the signs of exchange constants J 's do not matter. However, this sign change affects other physical measurable quantities.

Secondly, it was proved by Lieb (Lieb, 1994) and examined by Kitaev himself numerically that the ground state of the Majorana system is achieved by the vortex free configuration, $w_p = 1$ for all plaquette p 's. In this vortex free configuration, one can solve the (fermionic) energy spectrum of the Hamiltonian by direct Fourier transforming (118) to obtain,

$$\epsilon_{\mathbf{q}} = \pm |J_x e^{i\mathbf{q} \cdot \mathbf{a}} + J_y e^{i\mathbf{q} \cdot \mathbf{b}} + J_z|, \quad (121)$$

where $\mathbf{a} = (\frac{1}{2}, \frac{\sqrt{3}}{2})$ and $\mathbf{b} = (-\frac{1}{2}, \frac{\sqrt{3}}{2})$ are two basis vectors in the xy -coordinates. The fermionic spectrum may or may not be gapped, depending on whether solution to the equation $\epsilon_{\mathbf{q}} = 0$ exists. $\epsilon_{\mathbf{q}} = 0$ has solution if and only if $|J_x|, |J_y|, |J_z|$ satisfy the triangle inequalities,

$$|J_x| \leq |J_y| + |J_z|, |J_y| \leq |J_z| + |J_x|, |J_z| \leq |J_x| + |J_y|. \quad (122)$$

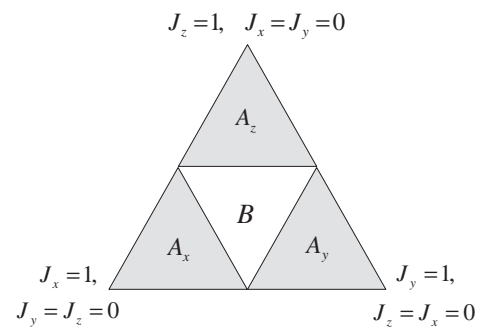


FIG. 15 (Kitaev, 2006) Phase diagram of Kitaev honeycomb model. The triangle is the section of the positive octant ($J_x, J_y, J_z \geq 0$) by the plane $J_x + J_y + J_z = 0$. A phase contains three gapped subphases (A_x, A_y, A_z) in the phase diagram. B phase is gapless.

As a result there exists two phases in the system of Majorana fermions on the honeycomb lattice, with phase diagram shown in Fig. 15. The first phase is gapped, called A phase, which contains three subphases (A_x, A_y, A_z) in the phase diagram. The second one is gapless, called B

phase. In the *A* phases, for example the A_z subphase, the Hamiltonian (106) can be mapped into Kitaev toric code model in the limit $|J_x|, |J_y| \ll |J_z|$ and the phase hosts abelian anyonic excitations. *B* phase acquires an energy gap in the presence of magnetic field. Very interestingly, it hosts stable nonabelian anyons when the energy gap is opened up by a magnetic field. The *B* phase is a very attractive state in the context of topological quantum computation. Readers can look at recent review article (Nayak *et al.*, 2008) for details.

Besides the elegant Majorana decomposition pioneered by Kitaev, there also exists other insightful approaches to the Kitaev honeycomb model. For instance, Feng, Zhang and Xiang (Feng *et al.*, 2007) and Chen and Nussinov (Chen and Nussinov, 2008) found that the original Kitaev honeycomb model can be exactly solved with the help of the Jordan-Wigner transformation. This approach provides a topological characterization of the quantum phase transition from the *A* phase to the *B* phase. A nonlocal string order parameter can be defined in one of these two phases (Chen and Nussinov, 2008; Feng *et al.*, 2007). In the appropriate dual representations, these string order parameters become local order parameters *after some singular transformation* and a description of the phase transition in terms of Landau theory of continuous phase transition becomes applicable (Feng *et al.*, 2007). The Jordan-Wigner transformation also allows a fermionization of the Kitaev honeycomb model to map it into a *p*-wave type BCS pairing problem. The spin wavefunction can be obtained from the fermion model and the anyonic character of the vortex excitations in the gapped phase has also an explicit fermionic construction (Chen and Nussinov, 2008).

The Kitaev honeycomb model can also be understood within the framework of the fermionic RVB theory. Both confinement-deconfinement transitions from spin liquid to AFM/Stripy AF/FM phases and topological quantum phase transitions between gapped and gapless spin liquid phases can be described within the framework of Z_2 gauge theory (Baskaran *et al.*, 2007; Mandal *et al.*, 2011, 2012).

Exact diagonalization has been applied to study the Kitaev honeycomb model on small lattices (Chen *et al.*, 2010). Perturbative expansion methods have been developed to study the gapped phases of the Kitaev honeycomb model and its generalization (Dusuel *et al.*, 2008; Schmidt *et al.*, 2008; Vidal *et al.*, 2008). It was pointed out in several papers (Kells *et al.*, 2009; Lee *et al.*, 2007a; Yu, 2008; Yu and Wang, 2008) that an analogy exists between the Z_2 vortices in the Kitaev honeycomb model and the vortices in *p* + *ip* superconductors.

A huge amount of efforts have been devoted to searching for exactly-solvable generalizations of Kitaev honeycomb model. It was proposed that the exact solvability would not be spoiled when the fermion gap is opened for the non-Abelian phase (Lee *et al.*, 2007a; Yu and Wang,

2008). Generalizations to other lattice models or even to three dimensions have also been developed (Baskaran *et al.*, 2009; Nussinov and Ortiz, 2009; Ryu, 2009; Tikhonov and Feigel'man, 2010; Wu *et al.*, 2009; Yang *et al.*, 2007; Yao and Kivelson, 2007; Yao and Lee, 2011; Yao *et al.*, 2009). Non-trivial emergent particles have been constructed in these exactly solvable lattice model, such as chiral fermions (Yao and Kivelson, 2007). These developments have significantly advanced our understanding of emergent phenomena based on solvable models in dimensions greater than one.

The exotic properties in Kitaev honeycomb model has triggered people to search for its realization in realistic materials. It was demonstrated by Jackeli and Khaliullin (Jackeli and Khaliullin, 2009) and Chaloupka, Jackeli and Khaliullin (Chaloupka *et al.*, 2010) that a generalization of the Kitaev honeycomb model may indeed arise in layered honeycomb lattice materials in the presence of strong spin-orbit coupling. They show that in certain iridate magnetic insulators (A_2IrO_3 , $A=Li, Na$), the effective low energy Hamiltonian for the effective $J_{eff} = 1/2$ iridium moments is given by a linear combination of the AFM Heisenberg model (H_H) and the Kitaev honeycomb model (H_K),

$$H = (1 - \alpha)H_H + 2\alpha H_K, \quad (123)$$

where α , expressed in terms of the microscopic parameters, determines the relative strength of the Heisenberg and the Kitaev interactions. It is interesting that the Kitaev honeycomb model can also be realized as the exact low energy effective Hamiltonian of spin-1/2 model with spin rotational and time reversal symmetries (Wang, 2010a). The Heisenberg-Kitaev model (123) exhibits a rich phase diagram. Readers who are interesting in these developments may refer to, for example, references (Chaloupka *et al.*, 2010; Jiang *et al.*, 2011; Kimchi and Vishwanath, 2014; Kimchi and You, 2011; Lee *et al.*, 2014; Price and Perkins, 2012; Reuther *et al.*, 2011; Schaffer *et al.*, 2012; Singh *et al.*, 2012; Yu *et al.*, 2013) for details. A comprehensive review by Nussinov and van den Brink on this aspect can be also found (Nussinov and van den Brink, 2013).

V. SPIN LIQUID STATES IN REAL MATERIALS

Experimental studies on interacting spins in geometrically frustrated lattices aim at identifying non-trivial and exotic ground states. Among these ground states, spin liquid states have been sought ever since the proposal of the RVB state (Anderson, 1973). This issue has been intensively debated in the context of the spin states behind the high-T_c superconductivity of cuprates. However, before this century, there was no direct observation of spin liquid states. The situation changes in 2003 when

an organic Mott insulator with a quasi-triangular lattice was found to exhibit no magnetic ordering even at tens mK, four orders of magnitude lower than the energy scale of the exchange interactions (Shimizu *et al.*, 2003). The low-temperature state is most likely a form of the sought-after spin liquids. Since then, what can be called spin liquids have been successively reported for quasi-triangular, kagome and hyperkagome lattices. In this section, we review the experimental studies mainly with respect to the magnetic and thermodynamic properties of the materials for which sound experimental data have been accumulated in discussing the presence of spin liquids.

V.1. Anisotropic triangular lattice systems: κ -(ET)₂Cu₂(CN)₃ and EtMe₃Sb[(Pd(dmit)₂)₂]

Both are half-filled band systems with anisotropic triangular lattices, which are isosceles for κ -(ET)₂Cu₂(CN)₃ and three different laterals for EtMe₃Sb[(Pd(dmit)₂)₂] (Kanoda, 2006; Kanoda and Kato, 2011; Kato, 2014). At ambient pressure, they are Mott insulators; however, the spins are not ordered at low temperatures on the order of tens of mK. A noticeable feature of both systems is that they undergo Mott transitions at moderate pressures 0.4 GPa for κ -(ET)₂Cu₂(CN)₃ (Furukawa *et al.*, 2015a; Komatsu *et al.*, 1996; Kurosaki *et al.*, 2005) and 0.5 GPa for EtMe₃Sb[(Pd(dmit)₂)₂] (Kato *et al.*, 2007). (Note that these pressure values indicate pressures applied at room temperature and are reduced by roughly 0.2 GPa at low temperatures.) The temperature-pressure phase diagram of κ -(ET)₂Cu₂(CN)₃ is depicted in Fig. 16. A spin liquid phase resides in proximity to the Mott transition and this feature appears to be a key to the stability of spin liquids which can be closely linked to the metal-insulator transition (Senthil, 2008; Zhou and Ng, 2013). According to the numerical studies of anisotropic triangular-lattice Hubbard model, the ground states nearby the Mott transition are controversial (Kyung and Tremblay, 2006; Laubach *et al.*, 2015; Morita *et al.*, 2002; Tocchio *et al.*, 2013; Watanabe *et al.*, 2008), implying that spin-liquid and magnetic phases are competing very closely and can be easily imbalanced by tiny perturbation.

i) κ -(ET)₂Cu₂(CN)₃

κ -(ET)₂Cu₂(CN)₃ is a layered compound, where κ -(ET)₂X has a variety of anions X and ET is bis(ethylenedithio)tetrathiafulvalene (Komatsu *et al.*, 1996). κ -(ET)₂X is composed of the ET layers with 1/2 hole per ET and the layers of monovalent anions X⁻, which have no contribution to the electronic conduction or magnetism. In the ET layer, strong ET dimers are formed (ET)₂, each of which accommodates a hole in an anti-bonding orbital of the highest occu-

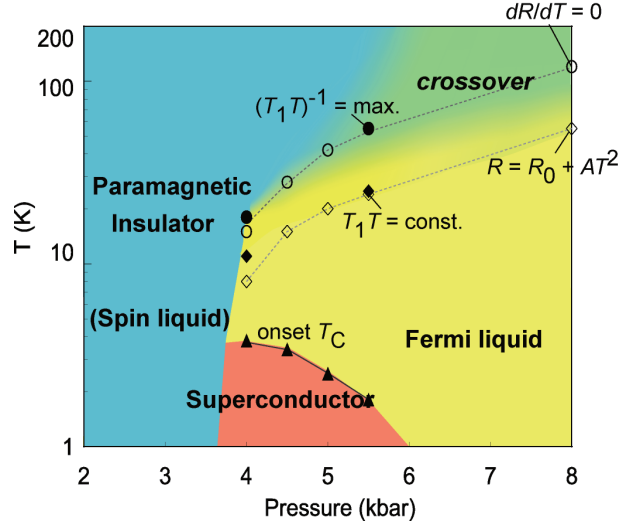


FIG. 16 (Kurosaki *et al.*, 2005) Temperature-pressure phase diagram of the spin-liquid compound with a quasi-triangular lattice, κ -(ET)₂Cu₂(CN)₃, which undergoes a Mott transition at moderate pressure.

pied molecular orbital (HOMO) of the ET. As the anti-bonding band is half-filled and the Coulomb repulsive energy is comparable to the band width, the family of κ -(ET)₂X are good model systems to study Mott physics (Kanoda, 1997a,b; Kino and Fukuyama, 1995; Powell and McKenzie, 2011; Shimizu *et al.*, 2006). The estimate of the transfer integrals between the adjacent anti-bonding orbitals on the isosceles triangular lattices, t and t' , are in a range of 50 meV, depending on the method of calculation, e.g., either the molecular orbital (MO)-based tight-binding calculation (Komatsu *et al.*, 1996; Mori *et al.*, 1984, 1999) or the first principles calculation (Kandpal *et al.*, 2009; Koretsune and Hotta, 2014; Nakamura *et al.*, 2009). Nevertheless, one can see that the values have clear systematic variation in terms of anion X as shown in Fig. 17, where the values of t and t' are calculated by the latter method: the t'/t value of κ -(ET)₂Cu[N(CN)₂]Cl is 0.75 (the MO-based calculations) and 0.44-0.52 (first principles calculations), while that of κ -(ET)₂Cu₂(CN)₃ is 1.06 and 0.80-0.99, respectively, suggestive of high geometrical frustration.

The temperature dependence of the spin susceptibility, χ , of κ -(ET)₂Cu₂(CN)₃ differs from that of the less frustrated compound κ -(ET)₂Cu[N(CN)₂]Cl, as seen in Fig. 18 (Shimizu *et al.*, 2003). An abrupt upturn at 27 K in the latter is a manifestation of the antiferromagnetic transition with a slight spin canting of approximately 0.3 degree (Miyagawa *et al.*, 1995). However, κ -(ET)₂Cu₂(CN)₃ has no anomaly in $\chi(T)$. Its overall behavior features a broad peak, which is reconciled by the triangular-lattice Heisenberg model with an exchange interaction of $J \sim 250$ K. In contrast to κ -(ET)₂Cu[N(CN)₂]Cl, the magnetic susceptibility of κ -(ET)₂Cu₂(CN)₃ is relatively flat at low temperatures and shows a gradual increase with temperature, reaching a peak around 100 K before decreasing at higher temperatures.

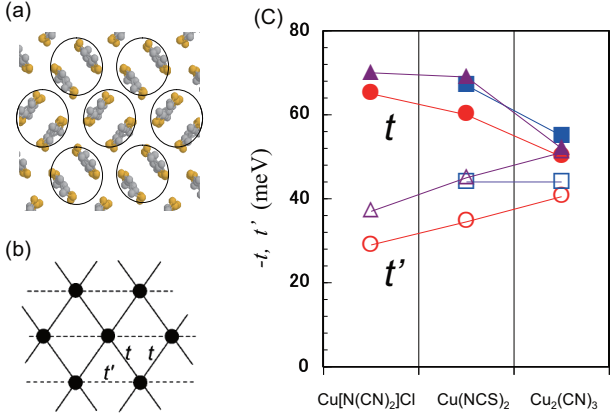


FIG. 17 (a) In-plane structure of the ET layer in κ -(ET)₂X. It is modelled to (b) an anisotropic triangular lattice. (c) First principles calculations of transfer integrals in κ -(ET)₂X for X=Cu[N(CN)₂]Cl, Cu(NCS)₂ and Cu₂(CN)₃ ; squares (Nakamura *et al.*, 2009), circles (Kandpal *et al.*, 2009), and triangles (Koretsune and Hotta, 2014).

(ET)₂Cu₂(CN)₃ may be described by the Heisenberg model because it is situated further from the Mott boundary, while κ -(ET)₂Cu[N(CN)₂]Cl undergoes a Mott transition at a low pressure (25 MPa) as it is about to enter a metallic state (Kagawa *et al.*, 2005; Lefebvre *et al.*, 2000). There is no indication of magnetic ordering in the susceptibility of κ -(ET)₂Cu₂(CN)₃, at least down to 2 K, the lowest temperature measured. Furthermore, no Curie-like upturn can be identified; the concentration of Cu²⁺ impurity spins detected by ESR is estimated to be less than 0.01 % for κ -(ET)₂Cu₂(CN)₃ (Shimizu *et al.*, 2006).

The detailed spin states can be examined by NMR measurements, which probe the static and dynamical hyperfine fields at the nuclear sites. Fig. 19 shows the single-crystal ¹H NMR spectra for the two compounds (Shimizu *et al.*, 2003). A clear line splitting in κ -(ET)₂Cu[N(CN)₂]Cl at 27 K is evidence for commensurate antiferromagnetic ordering, with the moment estimated to be 0.45 μ_B per ET dimer in separate ¹³C NMR studies (Miyagawa *et al.*, 2004). On the other hand, the spectra for κ -(ET)₂Cu₂(CN)₃ shows neither a distinct broadening nor splitting down to 32 mK, which is four orders of magnitude lower than the J value of 250 K. This indicates the absence of long-range magnetic ordering. The absence of ordering is also corroborated by zero field μ SR experiments (Pratt *et al.*, 2011). The nuclear spin lattice relaxation rate, $1/T_1$, which probes the spin dynamics, behaves similarly at the ¹H and ¹³C sites. Fig. 20 shows the $1/T_1$ at the ¹³C sites, which decreases monotonically with a square-root temperature dependence down to 10 K and exhibits a dip-like anomaly at approximately 6 K (Shimizu *et al.*, 2006). Below 6 K, the $1/T_1$ levels off down to 1 K or lower, followed by a steep decrease approximated by $T^{3/2}$ at

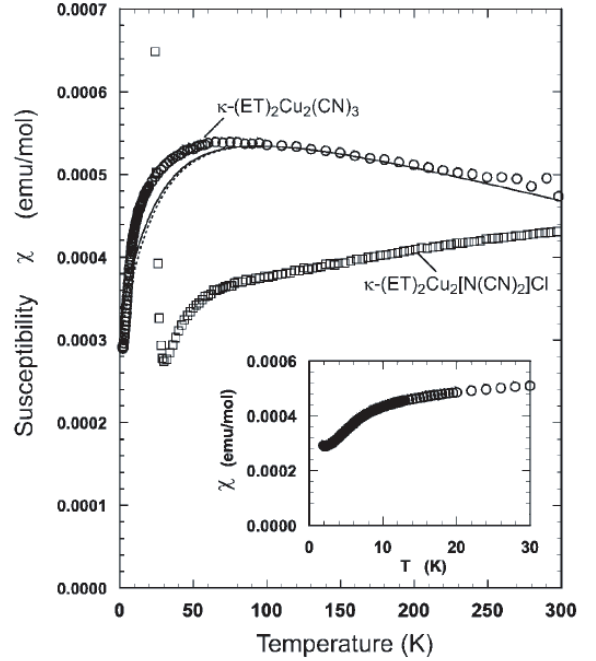


FIG. 18 (Shimizu *et al.*, 2003) Magnetic susceptibility of poly crystalline κ -(ET)₂Cu₂(CN)₃ and κ -(ET)₂Cu[N(CN)₂]Cl. The core diamagnetic susceptibility has been already subtracted. The solid and dotted lines represent the result of the series expansion of the triangular-lattice Heisenberg model using [6/6] and [7/7] PadeL approximations with $J = 250$ K. The susceptibility of κ -(ET)₂Cu₂(CN)₃ below 30 K are expanded in the inset.

even lower temperatures. The two anomalies at 6 K and 1.0 K are obvious. However, they are not so sharp as to be considered as phase transitions. Due to the large hyperfine coupling of the ¹³C sites located in the central part of ET, an electronic inhomogeneity gradually developing on cooling is captured by spectral broadening, which is enhanced at approximately 6 K and saturates below 1 K (Kawamoto *et al.*, 2006; Shimizu *et al.*, 2006). The detailed NMR (Shimizu *et al.*, 2006) and μ SR (Pratt *et al.*, 2011) measurements point to the field-induced emergence of staggered-like moments, which is distinct from the conventional magnetic order. A separate μ SR study (Nakajima *et al.*, 2012) suggests a phase separation. The degree of inhomogeneity in the ¹³C relaxation curve, which is characterized by the deviation of the exponent in the stretched exponential fitting of the relaxation curve (see Inset of Fig. 20), increases below 5-6 K (Shimizu *et al.*, 2006). The ¹H relaxation curve also starts to bend at the much lower temperatures, say, below 0.4 K and fits to a roughly equally weighed sum of two exponential functions, $1/T_1$'s of which are proportional to T and T^2 . No appreciable field dependence of the ¹³C relaxation rate is observed between 2 T and 8 T. There is no experimental indication of a finite excitation gap in any of the magnetic measurements.

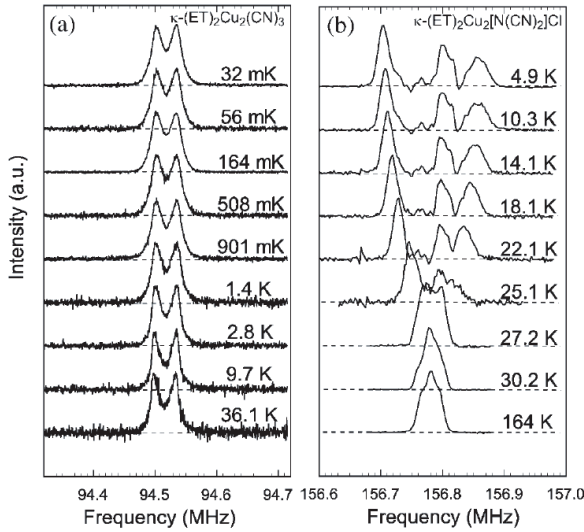


FIG. 19 (Shimizu *et al.*, 2003) ^1H NMR spectra for single crystals of $\kappa\text{-(ET)}_2\text{Cu}_2(\text{CN})_3$ and $\kappa\text{-(ET)}_2\text{Cu}[\text{N}(\text{CN})_2]\text{Cl}$.

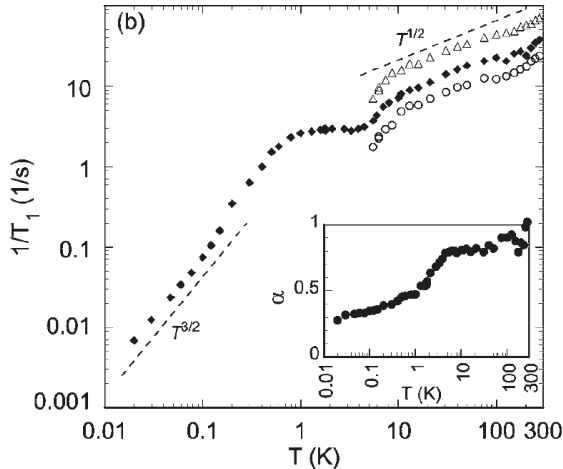


FIG. 20 (Shimizu *et al.*, 2006) ^{13}C nuclear spin-lattice relaxation rate for a single crystal of $\kappa\text{-(ET)}_2\text{Cu}_2(\text{CN})_3$. The open triangles and circles represent the relaxation rates of two separated lines coming from two non-equivalent carbon sites in a ET. At low temperatures below 5 K, the two lines merge and are not distinguished. The inset shows the exponent in the stretched exponential fitting to the relaxation curves of the whole spectra, whose relaxation rates are plotted by closed diamonds.

Thermodynamic investigations were conducted by means of the specific heat and thermal conductivity measurements. Fig. 21 shows the specific heat for $\kappa\text{-(ET)}_2\text{Cu}_2(\text{CN})_3$ and several Mott insulators with antiferromagnetic spin ordering (Yamashita *et al.*, 2008b). For all of the antiferromagnetic materials, the electronic specific heat coefficient, γ , is vanishing, as expected for insulators. For the $\kappa\text{-(ET)}_2\text{Cu}_2(\text{CN})_3$ spin liquid system, however, the extrapolation of the C/T vs. T^2 line to

absolute zero yields $\gamma=12\sim15 \text{ mJ/K}^2\text{mol}$. The linearity holds down to 0.3 K, below which a nuclear Shottky contribution overwhelms the electronic contribution to C . The finite value in spite of the Mott insulating state is a marked feature of spin liquids and suggests fermionic excitations in the spin degrees of freedom. Interestingly, the low-temperature susceptibility and the γ value give the Wilson ratio on the order of unity. A spinon Fermi sea is an intriguing model for this phenomenon (Motrunich, 2005). However, neither the $U(1)$ spin liquid, where C follows $T^{2/3}$ scaling, nor the Z_2 spin liquid, where C is gapped, reconciles the observed features in their original forms. Randomness may be an optional parameter to modify the temperature dependence. Another interesting feature is the field-insensitivity up to 8 T, which appears incompatible with the $U(1)$ spin liquid states with Dirac cones.

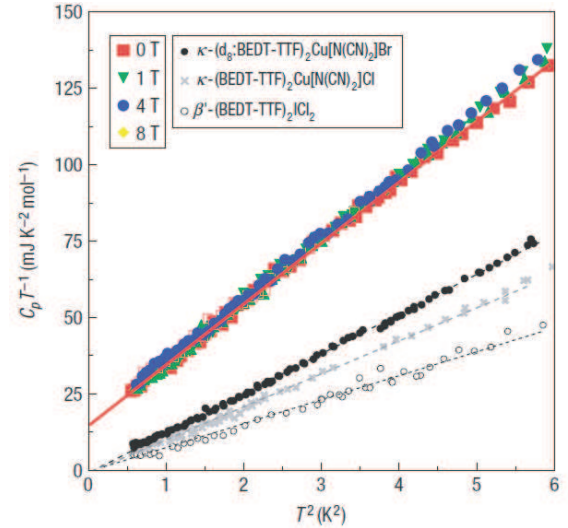


FIG. 21 (Yamashita *et al.*, 2008b) Low-temperature specific heat C_p of $\kappa\text{-(ET)}_2\text{Cu}_2(\text{CN})_3$ for several magnetic fields up to 8 T in C_p/T versus T^2 plots. Those of antiferromagnetic insulators $\kappa\text{-(ET)}_2\text{Cu}[\text{N}(\text{CN})_2]\text{Cl}$, deuterated $\kappa\text{-(ET)}_2\text{Cu}[\text{N}(\text{CN})_2]\text{Br}$ and $\beta\text{-(ET)}_2\text{ICl}_2$ are also plotted for comparison.

On the other hand, thermal transport measurements result in somewhat controversial consequences (Yamashita *et al.*, 2008a). The thermal conductivity divided by the temperature tends to vanish with decreasing temperature, as shown in Fig. 22. The gap, if one is present, is estimated to be 0.43 K, which is quite small compared with the exchange energy of 250 K. The extremely small gap may indicate a gapped Z_2 spin liquid located near a quantum critical point. The discrepancy between the thermal transport and NMR and specific heat data remains an open issue. It may be attributed to the Anderson localization of spinons.

The 6-K anomaly in the NMR spectrum and relaxation rate also manifests itself in the specific heat

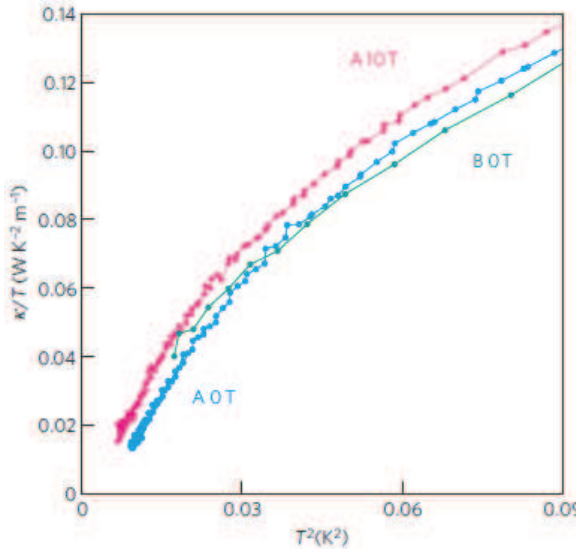


FIG. 22 (Yamashita *et al.*, 2008a) Low-temperature thermal conductivity κ of κ -(ET)₂Cu₂(CN)₃ (samples A and B) in κ/T versus T^2 plots. Sample A was investigated at 10 T applied perpendicular to the basal plane as well as at 0 T.

(Yamashita *et al.*, 2008b) and thermal conductivity (Yamashita *et al.*, 2008a) as a hump and a shoulder, respectively, indicating that the anomaly is thermodynamic as well as magnetic. Yet, the thermal expansion coefficient shows a cusp (Manna *et al.*, 2010) and the ultrasonic velocity shows a dip-like minimum, signifying lattice softening at approximately 6 K (Poirier *et al.*, 2014). In view of these results, this anomaly is likely associated with spin-lattice coupling. Instabilities of the spinon Fermi surfaces (e.g., (Galitski and Kim, 2007; Grover *et al.*, 2010; Lee and Lee, 2005; Zhou and Lee, 2011)) are among the possible origins of the anomaly.

Although the spin liquid is insulating, anomalous charge dynamics are suggested for the low-energy optical and dielectric responses. The optical gap for κ -(ET)₂Cu₂(CN)₃ is much smaller than that for κ -(ET)₂Cu[N(CN)₂]Cl, although the former system is situated further from the Mott transition than the latter (Kézsmárki *et al.*, 2006). It is proposed that gapless spinons are responsible for low-energy optical absorption inside the Mott gap (Ng and Lee, 2007). The dielectric (Abdel-Jawad *et al.*, 2010), microwave (Poirier *et al.*, 2012) and terahertz (Itoh *et al.*, 2013) responses are enhanced at low temperatures. The possible charge-imbalance excitations within the dimer are theoretically proposed (Dayal *et al.*, 2011; Hotta, 2010; Naka and Ishihara, 2010).

ii) EtMe₃Sb[(Pd(dmit)₂)₂]

This compound is a member of the A[(Pd(dmit)₂)₂] family of materials, which contain a variety of monovalent cations such as $A^+ = Et_xMe_{4-x}Z^+$ (Et = C₂H₅,

Me = CH₃, Z = N, P, As, Sb, and $x = 0, 1, 2$), where dmit is 1,3-dithiole-2-thione-4,5-dithiolate (Kato, 2014) A[(Pd(dmit)₂)₂] is a layered system composed of conducting Pd(dmit)₂ layers and insulating A layers. In the conducting layers, Pd(dmit)₂ is strongly dimerized as in κ -(ET)₂X, whereas the [Pd(dmit)₂]₂ dimer accepts an electron from cation A^+ instead of the hole in ET₂⁺. A prominent feature of the A[(Pd(dmit)₂)₂] family is that the transfer integrals of the three laterals in the triangular lattice can be finely tuned by chemical substitution of $A^+ = Et_xMe_{4-x}Z^+$ (Kato, 2014). The first principles calculations of them are shown in Fig. 23 (Tsumuraya *et al.*, 2013) The spin liquid material EtMe₃Sb[(Pd(dmit)₂)₂] is in a region where the three transfer integrals are equalized. As expected, the materials situated outside of this region have antiferromagnetic ground states. The alloying of the boundary materials offers the chance to study possible critical regions between spin liquids and ordered states (Kato, 2014). There is a charge ordered material nearby the spin liquid, suggesting that the charge cannot always be assumed to be separate degrees of freedom from the spin physics.

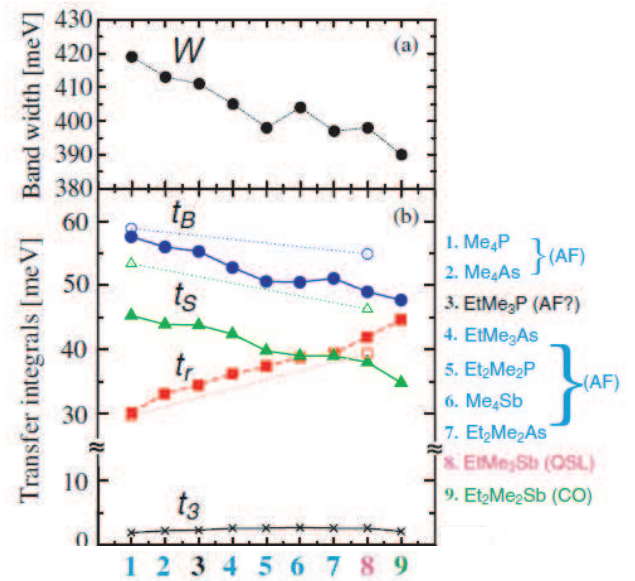


FIG. 23 (Tsumuraya *et al.*, 2013) First principles calculations of band width W (a) and transfer integrals (b) in A[(Pd(dmit)₂)₂] for various cations, A. The Pd(dmit)₂ layers are modeled to triangular lattices characterized by transfer integrals, t_B , t_S and t_r . t_3 is the interlayer transfer integral. AF, QSL and CO stand for antiferromagnet, quantum spin liquid and charge-ordered insulator.

Below, we review the properties of EtMe₃Sb[(Pd(dmit)₂)₂] and other related materials.

The magnetic susceptibility of EtMe₃Sb[(Pd(dmit)₂)₂] shows a broad peak at approximately 50 K and points to a finite value in the low-temperature limit without any anomaly down to 2 K, as shown in Fig. 24 (Kanoda and Kato, 2011; Kato, 2014), which is reminis-

cent of κ -(ET)₂Cu₂(CN)₃. The fitting of the triangular lattice Heisenberg model to the data yields an exchange interaction of 220 K to 280 K, which is nearly the same as for κ -(ET)₂Cu₂(CN)₃. Also shown, are the susceptibilities of antiferromagnetic and charge-ordered insulators, which exhibit small kink signaling of magnetic ordering and a sudden decrease indicative of a spin gapful state, respectively, despite their similar behaviors at high temperatures (Tamura and Kato, 2002). This means that the diversity in the ground states is an outcome of low-energy physics, while the same diversity is not distinguished at high energy scales.

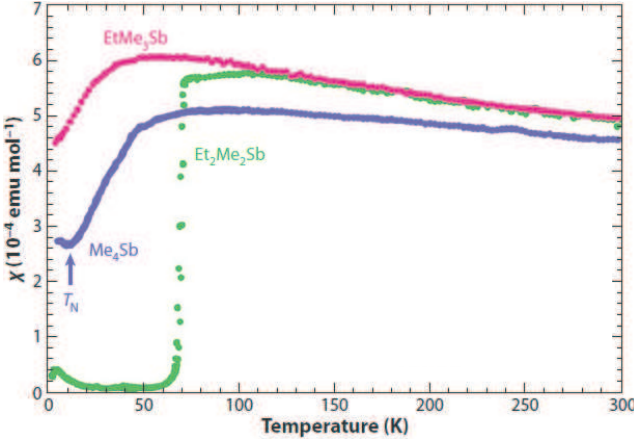


FIG. 24 (Kato, 2014) Magnetic susceptibility of an antiferromagnet $\text{Me}_4\text{Sb}[(\text{Pd}(\text{dmit})_2)_2]$, a spin liquid $\text{Et}\text{Me}_3\text{Sb}[(\text{Pd}(\text{dmit})_2)_2]$ and a charge-ordered insulator $\text{Et}_2\text{Me}_2\text{Sb}[(\text{Pd}(\text{dmit})_2)_2]$. The core diamagnetic susceptibility has been already subtracted.

The ¹³C NMR captures no signature of magnetic ordering down to 20 mK, although a slight broadening equivalent to the broadening for κ -(ET)₂Cu₂(CN)₃ is observed at low temperatures (Itou *et al.*, 2010). The temperature dependence of the ¹³C nuclear spin-lattice relaxation rate is shown in Fig. 25 (Itou *et al.*, 2010). It exhibits a non-monotonic temperature dependence. At low temperatures below 1 K, it follows a T^2 dependence, suggesting no finite gap. However, the power of 2 implies a complicated nodal gap, which is not obviously consistent with the finite susceptibility value and the thermodynamic measurements described below. Furthermore, $1/T_1$ forms a shoulder or a kink at approximately 1 K and becomes moderate in temperature dependence above 1 K. The kink temperature increases for higher magnetic fields or frequencies. The relaxation curve becomes a non-single exponential curve below 10 K but reverses below 1 K, indicating that the inhomogeneity increases below 10 K (Itou *et al.*, 2010, 2011). The reversal at 1 K can be an indication of either a recovery in the homogeneity below 1 K or the microscopic nature of the inhomogeneity, which is subject to spin-diffusion averaging of the heterogeneous relaxation time that is longer at lower temperatures. The

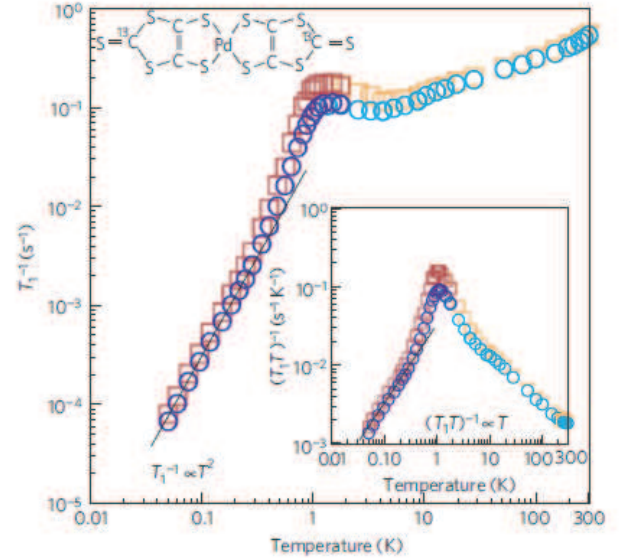


FIG. 25 (Itou *et al.*, 2010) ¹³C nuclear spin-lattice relaxation rate $1/T_1$ of $\text{Et}\text{Me}_3\text{Sb}[(\text{Pd}(\text{dmit})_2)_2]$. Inset shows the $1/T_1T$ versus T plots. The circles indicate the values determined from the stretched-exponential fitting to the relaxation curves and the squares denote the values determined from the initial decay slopes of the relaxation curves.

1-K relaxation-rate anomaly in $\text{Et}_2\text{Me}_2\text{Sb}[(\text{Pd}(\text{dmit})_2)_2]$ may be compared to the broad anomaly around nearly the same temperature for κ -(ET)₂Cu₂(CN)₃. However, they appear different in field (or frequency) dependence and spatial scale of inhomogeneity.

The thermodynamic measurements are indicative of fermionic low-energy excitations. Fig. 26 shows the temperature dependence of the specific heat (Yamashita *et al.*, 2011). The linearity of C/T versus T^2 in $\text{Et}\text{Me}_3\text{Sb}[(\text{Pd}(\text{dmit})_2)_2]$ is extrapolated to a zero Kelvin to give a finite value of γ , whereas other Mott insulators appear to have vanishing γ , as expected for conventional insulators. There is no field dependence in C/T in $\text{Et}\text{Me}_3\text{Sb}[(\text{Pd}(\text{dmit})_2)_2]$ up to 8 T, as in κ -(ET)₂Cu₂(CN)₃. The thermal conductivity results are consistent with the specific heat results, as seen in Fig. 27, where the low-temperature κ/T value for $\text{Et}\text{Me}_3\text{Sb}[(\text{Pd}(\text{dmit})_2)_2]$ is as high as 0.2 WK^{-2}m in the zero-Kelvin limit, implying the presence of gapless thermal transporters with fermionic statistics (Yamashita *et al.*, 2010). The mean free path for thermal transport is estimated to be of the order of 1 μm . κ is enhanced by the application of a magnetic field above a threshold value, suggesting that the gapped excitations coexist with the gapless excitations (Yamashita *et al.*, 2010).

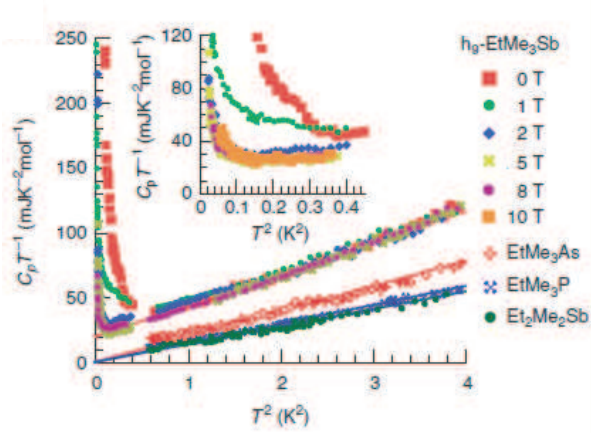


FIG. 26 (Yamashita *et al.*, 2011) Low-temperature specific heat C_p of $\text{EtMe}_3\text{Sb}[\text{Pd}(\text{dmit})_2]_2$ for several magnetic fields up to 10 T in C_p/T versus T^2 plots. The data of other insulating systems, $\text{Et}_2\text{Me}_2\text{As}[(\text{Pd}(\text{dmit})_2)_2]$, $\text{EtMe}_3\text{As}[(\text{Pd}(\text{dmit})_2)_2]$ and $\text{EtMe}_3\text{P}[(\text{Pd}(\text{dmit})_2)_2]$, are also plotted for comparison. A large upturn below 1 K is probably attributable to the rotational tunneling of Me groups. The low-temperature data are expanded in the inset.

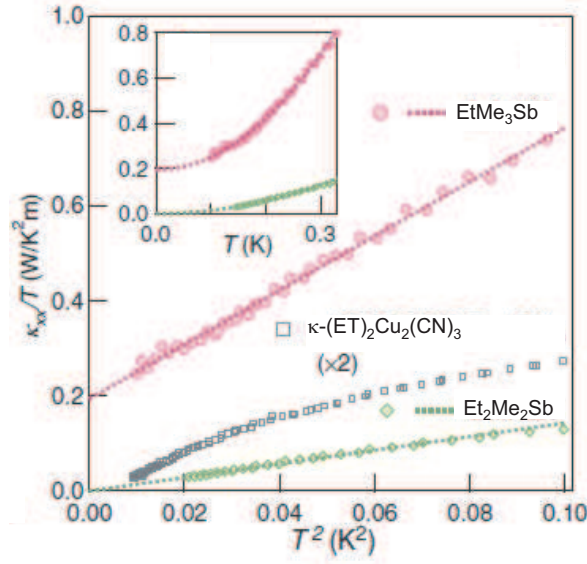


FIG. 27 (Yamashita *et al.*, 2010) Low-temperature thermal conductivity κ of $\text{EtMe}_3\text{Sb}[\text{Pd}(\text{dmit})_2]_2$ in κ/T versus T^2 and κ/T versus T (inset) plots. The data of other insulators, $\text{Et}_2\text{Me}_2\text{Sb}[\text{Pd}(\text{dmit})_2]_2$ and $\kappa-(\text{ET})_2\text{Cu}_2(\text{CN})_3$ are also plotted for comparison.

V.2. Kagome-lattice system: $\text{ZnCu}_3(\text{OH})_6\text{Cl}_2$

The kagome lattice is constructed by corner-sharing triangles in contrast to the edge-sharing in the triangular lattices, as shown in Fig. 8. Thus, the spin states in the kagome lattice have larger degeneracy than those in the triangular lattices, leading to high potential for hosting a spin liquid. Actually, the theoretical

perspective of seeking a spin liquid is more promising for the kagome-lattice Heisenberg model than for the triangular lattice (Lecheminant *et al.*, 1997; Mila, 1998; Misguich and Lhuillier, 2004; Sachdev, 1992). Among several candidates for the kagome spin systems, we select a spin-1/2 system, $\text{ZnCu}_3(\text{OH})_6\text{Cl}_2$, which is known as herbertsmithite, whose magnetism has been extensively investigated. This is a member in a family of materials with variable compositions, $\text{Zn}_x\text{Cu}_{4-x}(\text{OH})_6\text{Cl}_2$ ($0 < x < 1$). As an end material, $\text{Cu}_4(\text{OH})_6\text{Cl}_2$ has a distorted pyrochlore lattice of $S = 1/2 \text{ Cu}^{2+}$ spins, whereas the other end material, $\text{ZnCu}_3(\text{OH})_6\text{Cl}_2$, has a two-dimensional ($a - b$ plane) perfect kagome-lattice of Cu^{2+} spins separated by different crystallographic sites occupied by Zn^{2+} (Shores *et al.*, 2005). The structural symmetry changes across $x = 0.33$, above which Cu^{2+} partially occupies the Zn sites in addition to the kagome lattice. There is an argument for the mixture of Zn in the kagome sites in $\text{ZnCu}_3(\text{OH})_6\text{Cl}_2$. Magnetic susceptibility (Bert *et al.*, 2007) and specific heat (de Vries *et al.*, 2008) suggest that approximately 6% of the kagome sites are replaced by non-magnetic Zn . The same amount of Cu is assumed to invade the nominal Zn sites. Thus, significant efforts have been made to extract the intrinsic properties of the kagome lattice from the experimental data.

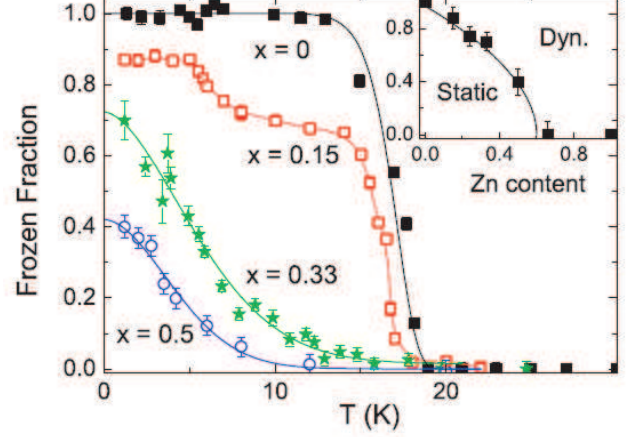


FIG. 28 (Mendels *et al.*, 2007) Temperature variation of the spin-frozen fraction determined by muon spin rotation experiments for $\text{Zn}_x\text{Cu}_{4-x}(\text{OH})_6\text{Cl}_2$. Inset shows the x -dependence of the spin-frozen fraction at a low temperature.

Experimental evidence for the absence of magnetic ordering in $\text{ZnCu}_3(\text{OH})_6\text{Cl}_2$ can be obtained from μSR experiments (Mendels *et al.*, 2007). The relaxation profile shows no internal field down to 50 mK. The experiments for a wide range of x found that the absence of an internal field was persistent in a certain range below $x = 1$ (see Fig. 28) (Mendels *et al.*, 2007). The magnetic susceptibility exhibits a Curie-Weiss behavior at high temperatures above 100 K, as shown in Fig. 29 (Helton *et al.*, 2007). The Weiss temperature is ~ 300

K, which implies an antiferromagnetic exchange interaction of $J = 17$ meV. The dc and ac magnetic susceptibility indicates no magnetic ordering down to 0.1 K and 0.05 K, respectively, which is four orders of magnitude lower than J (Helton *et al.*, 2007). The susceptibility increases progressively at lower temperatures. Two mechanisms are possible. First, impurities from Cu/Zn inter-site mixing can give a Curie-like upturn. Second, Dzyaloshinsky-Moriya interactions may be present between the adjacent sites with broken inversion symmetry as in the kagome lattice (Rigol and R. R. P. Singh, 2007). The high-field magnetization measurements suggest that the former is mainly responsible for the increasing susceptibility (Bert *et al.*, 2007).

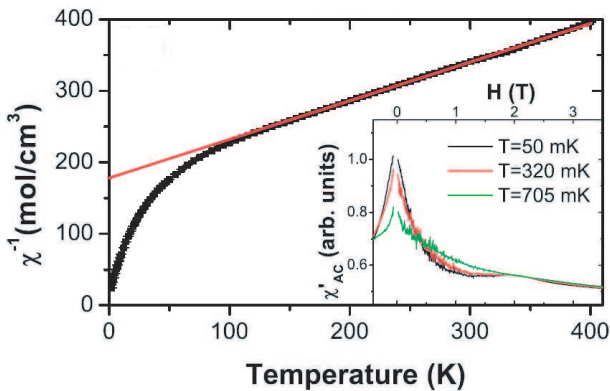


FIG. 29 (Helton *et al.*, 2007) Temperature dependence of the inverse magnetic susceptibility χ^{-1} of $\text{ZnCu}_3(\text{OH})_6\text{Cl}_2$. The line denotes a Curie-Weiss fit. Inset: ac susceptibility (at 654 Hz) at low temperatures.

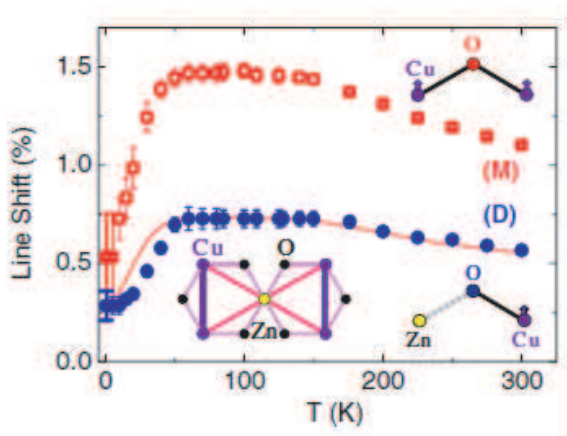


FIG. 30 (Olariu *et al.*, 2008) ^{17}O NMR shift of two lines (M and D) decomposed from the observed spectra for a powder of $\text{ZnCu}_3(\text{OH})_6\text{Cl}_2$. The M and D lines are considered to come from the oxygen sites depicted in the inset. The red curve represents the trace of a half of the value of the M line. The sketch in the lower left corner illustrates the environment of a Zn substituted on the Cu kagome plane, and thick lines represent Cu-Cu dimers.

NMR, which probes magnetism in a site-selective manner, was informative particularly for this material because the analysis of spectra allows one to distinguish the intrinsic magnetism from the extrinsic one. The NMR spectra at ^{35}Cl and ^{17}O sites are broad (Imai *et al.*, 2008; Olariu *et al.*, 2008), reflecting the inhomogeneous local fields, supposedly due to the Zn/Cu mixture. However, the smallest shift value in the broad ^{35}Cl spectrum follows a Curie-Weiss law down to 25 K, followed by a decrease at lower temperatures (Imai *et al.*, 2008). This is considered to indicate intrinsic magnetism for the kagome lattice (Imai *et al.*, 2008). The ^{17}O probes the kagome sites more preferentially than the nominal Zn sites due to larger hyperfine coupling with the kagome sites (Olariu *et al.*, 2008). The ^{17}O NMR spectra were decomposed into two components. One is from the ^{17}O sites coordinated by two Cu^{2+} ions and the other from the ^{17}O sites coordinated by a Cu^{2+} and a Zn^{2+} in the kagome plane. The relative fraction of the two components was consistent with a 6 % Zn admixture. The NMR shifts of the respective components, as shown in Fig. 30, are considered to be local susceptibilities at Cu sites with and without Zn^{2+} at the neighboring sites (Olariu *et al.*, 2008). Both decrease below 50 K and saturate to finite values, indicating the gapless nature of the spin excitations. The low-temperature decrease in the shift at the Cu site with a Zn neighbor is in contrast to the enhancement commonly observed in the neighborhood of non-magnetic impurities (Olariu *et al.*, 2008). This behavior also suggests that the Curie-like upturn in the bulk susceptibility at low temperatures is not from the kagome plane. As for the NMR relaxation rate, all of the O, Cl and Cu nuclear spins exhibit power-laws against temperature down to 0.47 K for O and 2 K or lower for Cl and Cu, indicating a gapless spin liquid (see Fig. 31) (Imai *et al.*, 2008; Olariu *et al.*, 2008). Although the power somewhat depends on the nuclear site, the relaxation profile is overall nuclear site-insensitive, which is filtered by the nuclear site-specific form-factor determined by its location relative to the kagome lattice, suggesting non-dispersive spin dynamics. Otherwise the temperature profile of the relaxation rate would be site-dependent (Olariu *et al.*, 2008). This feature is potentially relevant to the spinon excitation with the continuum. More recently, NMR experiments performed at low temperatures have revealed an anomaly in the relaxation rate at a temperature depending on the applied field, which may signify field-induced spin freezing (Jeong *et al.*, 2011). Very recently, a ^{17}O NMR experiment performed with a single crystal has found different features from those observed so far in the powder samples (Fu *et al.*, 2015). According to the analysis of NMR spectra, there is no significant contamination of Zn in the Cu sites within the kagome plane and the Knight shift shows appreciable temperature- and field-dependences suggesting a spin gap of the order of 10 K, as shown in FIG 32, in contra-

dition with the consequences of the earlier NMR and neutron (see below) experiments.

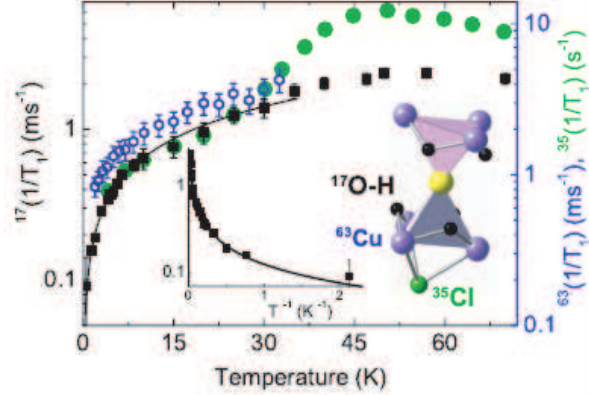


FIG. 31 (Imai *et al.*, 2008; Olariu *et al.*, 2008) ^{17}O , ^{63}Cu and ^{35}Cl nuclear spin-lattice relaxation rates $1/T_1$ for a powder of $\text{ZnCu}_3(\text{OH})_6\text{Cl}_2$. Inset shows ^{17}O $1/T_1$ versus $1/T$ plots.

The low-temperature specific heat was investigated under external magnetic fields (Helton *et al.*, 2007; de Vries *et al.*, 2008). As shown in Fig. 33(a) (Helton *et al.*, 2007), there is an enormous field dependence. The temperature dependence at a zero field is approximated by a power law T^α with α unity or smaller (see Fig. 33(b)). The broad peak present even at a zero field is shifted to higher temperatures under higher fields. Assuming that the field-dependent peak is a Schottky contribution associated with a field-induced gap, the data for different fields were analyzed in details to reveal the intrinsic specific heat of the kagome lattice (de Vries *et al.*, 2008). The deduced Schottky component is consistent with Zeeman splitting of the 6% Cu impurities in the Zn sites at higher fields and it turns out that the intrinsic C/T follows a power law T^α with $\alpha = 1.3$ as the best estimate, suggesting gapless excitations (Helton *et al.*, 2007; Shaginyan *et al.*, 2011; de Vries *et al.*, 2008).

Neutron-scattering experiments, which are capable of profiling spin excitations with respect to momentum and energy transfers, are available for herbertsmithite. One of key issues on elementally excitations in spin liquids is the possible fractionalization of $S = 1$ spin excitations into $S = 1/2$ spinons, which could manifest themselves as a continuum in the spin excitation spectrum, *i.e.*, dynamic structure factor $S(\mathbf{Q}, \omega)$, where \mathbf{Q} and ω are momentum transfer and energy transfer divided by \hbar , respectively. Such a continuum is observed in a highly anisotropic triangular-lattice system, Cs_2CuCl_4 , ($J'/J \sim 3$ and $J' \sim 0.34$ meV in FIG. 17) although it undergoes a magnetic transition into a spin-spiral order at 0.62 K (Coldea *et al.*, 2001, 2003). Several features signifying the continuum are found by neutron experiments of herbertsmithite, which were first performed for polycrys-

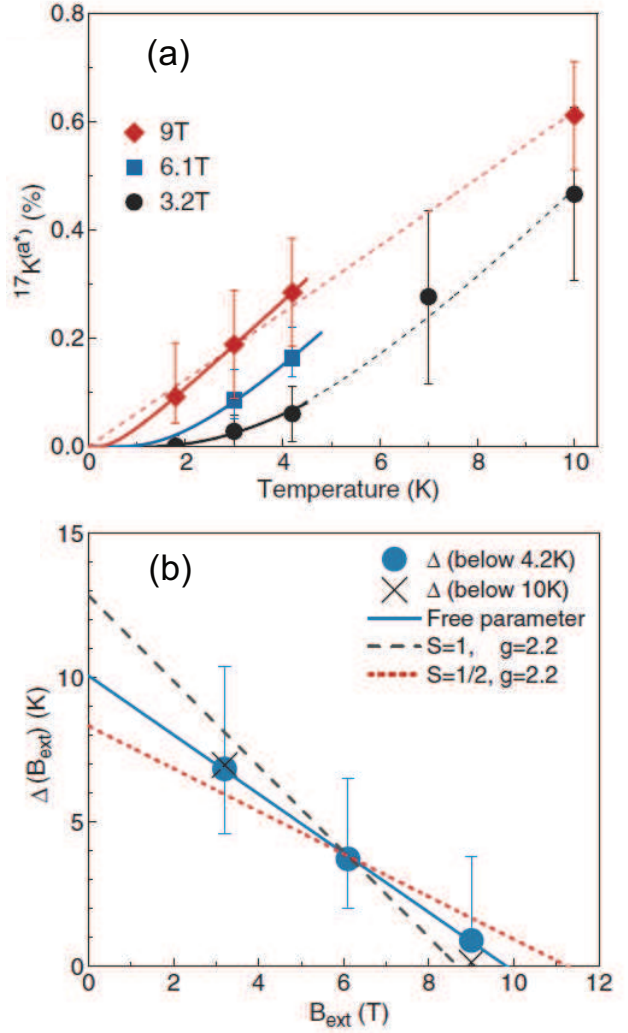


FIG. 32 (Fu *et al.*, 2015) Temperature dependence of ^{17}O Knight shift (a) and the field dependence of the spin gap deduced from the Knight shift for a single-crystal $\text{ZnCu}_3(\text{OH})_6\text{Cl}_2$.

talline or powder samples. The inelastic scattering experiments exhibit no excitation gap at least down to 0.1 meV, which corresponds to $\sim J/170$, and the insensitivity of the scattering strength to \mathbf{Q} , indicating gapless and local natures of spin fluctuations (Helton *et al.*, 2007). Furthermore, the scattering intensity is only weakly dependent on ω up to 25 meV and temperature up to 120 K, and shifts toward lower \mathbf{Q} as temperature is increased (de Vries *et al.*, 2009). Some of the results are displayed in FIG. 34. All these features are suggestive of a continuum in spin excitations and the persistence of the short-range nature of spin correlations even at low temperatures. Recent experiments on a large single crystal have succeeded in capturing the continuum nature as seen in the green area in FIG. 35. The momentum profile of the excitation intensity (dynamic structure factor), $S(\mathbf{Q}, \omega)$, is approximately reproduced by the

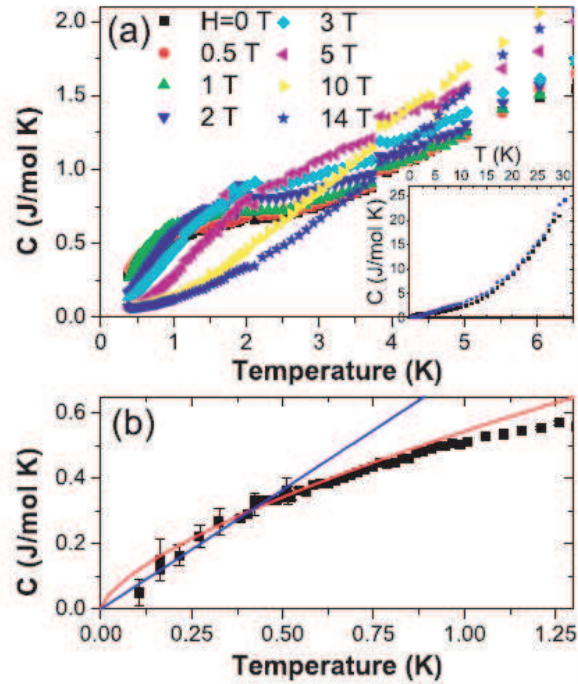


FIG. 33 (Helton *et al.*, 2007) (a) Specific heat C of $\text{ZnCu}_3(\text{OH})_6\text{Cl}_2$ in various applied fields. (b) C in a zero field at low temperatures. The lines represent power law fits.

simulated structure factor of uncorrelated dimer-singlets, which points to the short-ranged spin correlations at least down to 1.6 K (Han *et al.*, 2012). The short-range nature that persists even at low temperatures, as suggested by the powder experiments as well, is generally in favor of a gapped state, whereas there is no indication of a spin gap down to 0.25 meV at any \mathbf{Q} values in the excitation spectra (Han *et al.*, 2012). It is puzzling that spin dynamic correlation exhibits short-range RVB nature while the spectrum is gapless. One possibility is that the Herbertsmithite is in a Z_2 spin liquid in close proximity to a critical point to the $U(1)$ Dirac liquid, as indicated by some recent numerical works (Li, 2016), although the true ground state of isotropic Heisenberg model on Kagome lattice is still under debates (Iqbal *et al.*, 2016).

V.3. Hyperkagome-lattice system: $\text{Na}_4\text{Ir}_3\text{O}_8$

The hyperkagome lattice is a three-dimensional network of corner-sharing triangular lattices. In $\text{Na}_4\text{Ir}_3\text{O}_8$, Ir^{4+} ion with $5d^5$ electrons likely takes on a low-spin state. These ions locate on the corners, forming a $S=1/2$ hyperkagome lattice (Okamoto *et al.*, 2007). The resistivity of the ceramic sample is 10 Ohmcm at room temperature. The samples are semiconducting with a charge

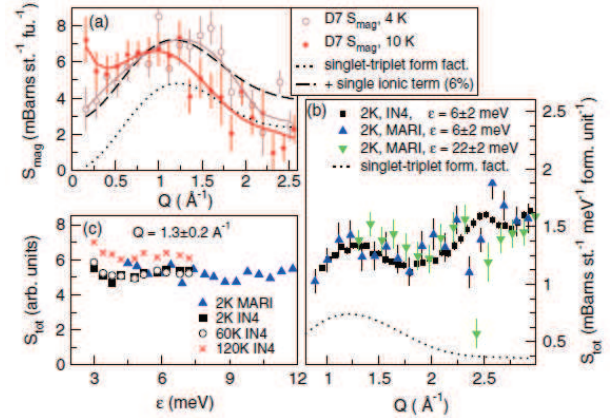


FIG. 34 (de Vries *et al.*, 2009) (a) Instantaneous magnetic correlations at 4 K and 10 K for a time scale corresponding to 6.5 meV. The solid lines are a guide to the eye. (b) The Q dependence in the dynamic correlations with the energy integration interval indicated in the legend. The dotted line in panel (a) and (b) is the structure factor for dimerlike AF correlations. The dashed line a single-ion contribution corresponding to the 6% antisite spins in this system is added. (c) The energy and temperature dependence at $Q=1.3 \text{\AA}^{-1}$. D7, IN4 and MARI in the legends stand for the types of spectrometers used.

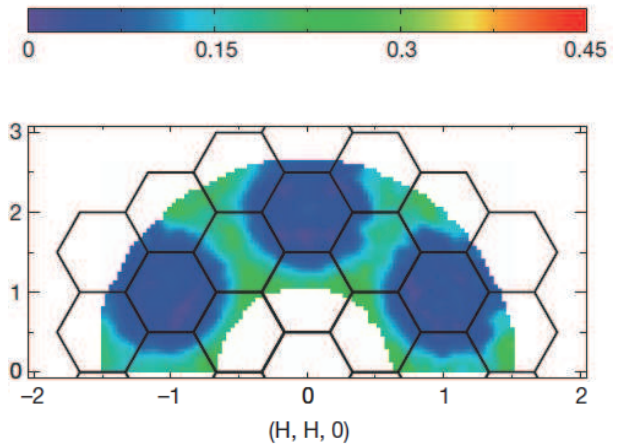


FIG. 35 (Han *et al.*, 2012) Contour plot of dynamical structure factor, $S_{\text{mag}}(\mathbf{Q}, \omega)$, integrated over $1 \leq \hbar\omega \leq 9$ meV for a single-crystal $\text{ZnCu}_3(\text{OH})_6\text{Cl}_2$ at 1.6 K. The intense scattering is extended in a green-colored region, not peaked at any specific points.

transport gap of 500 K, implying the proximity of this system to the Mott transition, which is different from the kagome materials reviewed above (Okamoto *et al.*, 2007). A connection between the spin liquid and the metal-insulator transition, similar to the case of κ - $(\text{ET})_2\text{Cu}_2(\text{CN})_3$, is pointed out (Podolsky *et al.*, 2009). A distinct feature of $\text{Na}_4\text{Ir}_3\text{O}_8$ among spin liquid candidates is its large spin-orbit coupling, which introduces additional interest to the physics of spin liquids

(Chen and Balents, 2008; Zhou *et al.*, 2008). Several theoretical papers propose that $\text{Na}_4\text{Ir}_3\text{O}_8$ is a 3D quantum spin liquid with fermionic spinons (Lawler *et al.*, 2008; Zhou *et al.*, 2008).

FIG. 36(a) shows the magnetic susceptibility of $\text{Na}_4\text{Ir}_3\text{O}_8$, which weakly increases with decreasing temperature, as characterized by the Curie-Weiss temperature of -650 K (Okamoto *et al.*, 2007). This implies an antiferromagnetic interaction of hundreds of Kelvin. There is no clear indication of magnetic ordering at least down to 2 K, whereas a small anomaly reminiscent of spin glass observed in the magnetization history against the field/temperature variation is attributed to a tiny fraction of the total spins (Okamoto *et al.*, 2007).

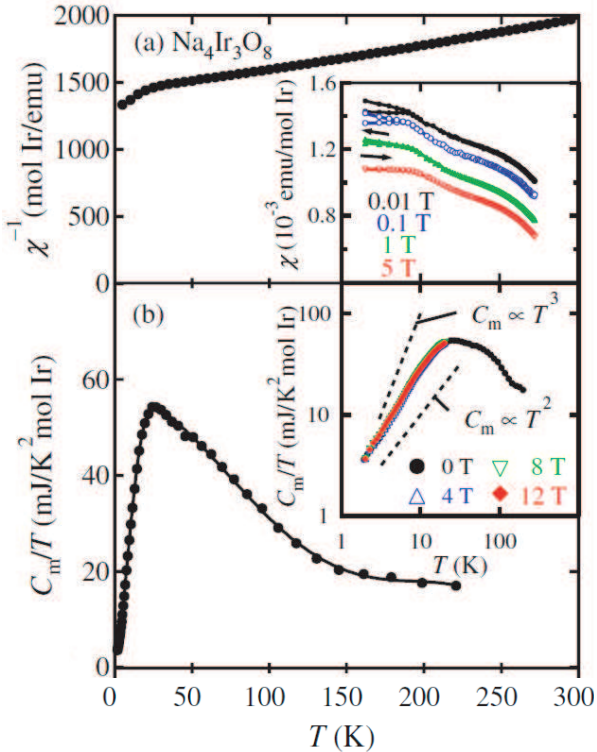


FIG. 36 (Okamoto *et al.*, 2007) (a) Temperature dependence of the inverse magnetic susceptibility χ^{-1} of polycrystalline $\text{Na}_4\text{Ir}_3\text{O}_8$ under 1 T. Inset shows magnetic susceptibility χ in various fields up to 5 T; for clarity, the curves are shifted by 3, 2, and 1×10^{-4} emu/mol Ir for 0.01, 0.1, and 1 T data, respectively. (b) Magnetic specific heat C_m divided by temperature T of polycrystalline $\text{Na}_4\text{Ir}_3\text{O}_8$. To estimate C_m , data for $\text{Na}_4\text{Sn}_3\text{O}_8$ is used as a reference of the lattice contribution. Inset shows C_m/T versus T in various fields up to 12 T.

The electronic (magnetic) contribution to the specific heat of $\text{Na}_4\text{Ir}_3\text{O}_8$, as shown in Fig. 36(b), has a broad peak at 20 K. However, no anomaly signifying magnetic ordering is apparent (Okamoto *et al.*, 2007). The magnetic entropy estimated by integrating the C/T in Fig. 36(b) reaches 70–80% of $R \ln 2$ ($= 5.7 \text{ J/molK}$) at 100 K,

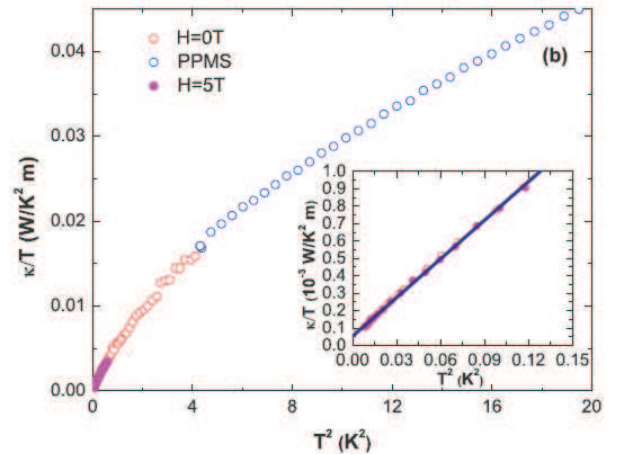


FIG. 37 (Singh *et al.*, 2013) Thermal conductivity κ of $\text{Na}_4\text{Ir}_3\text{O}_8$ in κ/T versus T^2 plots for magnetic fields of 0 T and 5 T. Inset shows the low-temperature part of the data.

a much lower temperature than the Weiss temperature of ~ 600 K, which features frustrated magnetism. The C/T is characterized by a curious T^2 dependence at the lowest temperatures. The γ term, when present, appears of the order of $1 \text{ mJ/K}^2 \text{ mol Ir}$. Recent experiments extended down to 500 m K have found that C_m/T is well approximated by a form of $\gamma + \beta T^{2.4}$ with $\gamma = 2.5 \text{ mJ/K}^2 \text{ mol Ir}$ (Singh *et al.*, 2013). As seen in the inset of Fig. 36(b), the applied field makes no influence on the specific heat, at least, up to 12 T.

The temperature dependence of thermal conductivity is shown in Fig. 37 (Singh *et al.*, 2013). At low temperatures down to 75 mK, κ/T is linear in T^2 . The κ/T value extrapolated to $T = 0$ is $6.3 \times 10^{-2} \text{ mW/K}^2 \text{ m}$, which is a vanishingly small value, compared with the value of $\text{EtMe}_3\text{Sb}[(\text{Pd}(\text{dmit})_2)_2]$, $0.2 \text{ W/K}^2 \text{ m}$, in Fig. 27. The suppression of the κ/T value by extrinsic grain-boundary effect is not ruled out (Singh *et al.*, 2013). The feature that γ is diminished and κ/T is vanishing at low temperatures while both being sizable at high temperatures of the order of Kelvin appears to be in line with a theoretical picture of spinon Fermi surfaces that undergo a pairing instability at low temperatures (Zhou *et al.*, 2008). In this context, the magnetic susceptibility keeping large even at low temperatures can be due to the large spin-orbit interactions of Ir (Zhou *et al.*, 2008).

The substitution of non-magnetic Ti^{4+} ions at Ir sites will give rise to a Curie-like tail in the spin susceptibility curve (Okamoto *et al.*, 2007), similarly to Zn substitution for Cu in high-Tc cuprates, indicating a RVB spin background. The scaling analysis of magnetic Gruneisen parameters is suggestive of the proximity of $\text{Na}_4\text{Ir}_3\text{O}_8$ to a zero-field quantum critical point (Singh *et al.*, 2013).

Very recent μSR (Dally *et al.*, 2014) and NMR experiments (Shockley *et al.*, 2015) have found some indications that are not in line with the above claims.

Both probes detected the emergence of local fields signifying the freezing of moments at low temperatures, as shown in FIG. 38. The muons are revealed to sense an inhomogeneous local field of electronic origin that appears at 6 K, where the irreversibility in magnetization occurs, and levels off to 70 G on average, which may correspond to $0.5 \mu_B$ on Ir. It is suggested, however, that the spin correlation is short-ranged (of the order of one unit-cell) and quasi-static in that the slow dynamics captured by the relaxation rate persist down to 20 mK. The quasi-static nature is also seen in the S=1 triangular-lattice system, NiGa_2S_4 (MacLaughlin *et al.*, 2008; Nakatsuji *et al.*, 2005). ^{17}O and ^{23}Na NMR lines show broadening, which is roughly scaled to the μSR results at low temperatures as seen in FIG. 38; the moment is estimated at $0.27 \mu_B$ on Ir. The NMR line pro-

file also suggests inhomogeneous spin freezing and the slow-dynamics persisting down to low temperatures although the temperature dependences of the relaxation rates on muon and ^{23}Na differ. Noticeably, the ^{23}Na relaxation rate exhibits a peak indicative of the critical slowing down at approximately 7.5 K despite no anomaly in specific heat. The nature and origin of these anomalous properties are not clear at present; however, it is likely that disorder plays a vital role in this system, which can host configurationally degenerate phases with fluctuating order (Dally *et al.*, 2014). Considering that muon, ^{17}O and ^{23}Na captured the behavior of the majority of spins in the sample, the disorder effect, if any, is such that it is not restricted in finite areas but extended over the system, being reminiscent of the quantum Griffiths effect given the inhomogeneity and slow dynamics.

V.4. Experimental summary

Owing to intensive experimental studies, unconventional thermodynamic and magnetic properties that evoke spin liquids have been found in several materials with anisotropic triangular lattices, kagome lattices and hyperkagome lattices as seen above. These materials have no indications of conventional magnetic ordering. Their magnetic and thermodynamic properties are summarized in Table III. It appears that the gapless nature is a property which a class of frustrated lattices constructed with triangles possess although the thermal conductivity of $\kappa\text{-(ET)}_2\text{Cu}_2(\text{CN})_3$ suggested a tiny excitation gap three order of magnitude smaller than J . A recent NMR work on herbertsmithite insists on gapped spin excitations, and anomalous quasi-static spin freezing has recently been revealed by μSR and NMR studies on the hyperkagome system. This feature and the successful observation of fractionalized excitations in a kagome lattice (Han *et al.*, 2012) tempt ones to think about spinons as promising elementary excitations in spin liquids. How to detect the spinon Fermi surfaces, if they exist, is a focus—smoking-gun experiments are awaited.

As seen in TABLE III, several experimental characteristics are seemingly inconsistent within given materials; how to understand the apparently contradicting data in a consistent way is a focus in clarifying the nature of the spin states. One of the key issues may be randomness present in real materials. In particular, it has long been recognized that the effect of inevitable Zn/Cu admixtures in herbertsmithite has to be separated from the intrinsic magnetism. More recently, the issue of inhomogeneous quasi-static spin correlation with slow dynamics in the hyperkagome-lattice system has emerged as a consequence of disorder. Theoretically, it was proposed that as randomness is intensified, the 120-degree Néel order

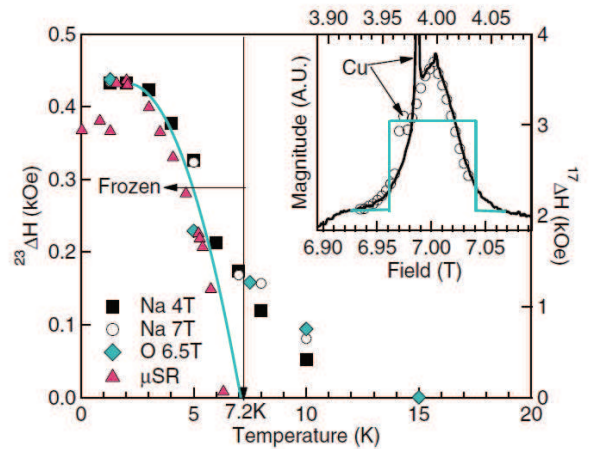


FIG. 38 (Shockley *et al.*, 2015) The line width (FWHM) of Gaussian-broadened ^{17}O and ^{23}Na NMR spectra and the mean value of the distributed local fields detected by μSR (Dally *et al.*, 2014). As for the NMR line width, its deviation from the value at 15 K is plotted. Inset: ^{23}Na spectra at 78.937 MHz for 7 T (empty circles) and 45.046 MHz for 4 T (solid line) with the horizontal axis shifted by 3.005 T at 1.3 K. The blue line shows the expected powder-pattern of spectrum with every Ir-site carrying the same moment.

in the triangular-lattice Heisenberg model is changed to a sort of random singlets but not spin glass state. It is intriguing that randomness appears to enhance the quantum nature since the singlet is a purely quantum state ((Watanabe *et al.*, 2014)). In the case of kagome lattices, it was theoretically suggested that disorder could lead to a valence-bond glass state (Singh, 2010). Furthermore, a recent NMR experiment on an organic Mott insulator, $\kappa\text{-(ET)}_2\text{Cu}[\text{N}(\text{CN})_2]\text{Cl}$, finds that the antiferromagnetic ordering in the pristine crystal, when irradiated by X-rays, disappears. Spin freezing, spin gap and critical

TABLE III Spin liquid materials summary

Material	Triangular, κ -(ET) ₂ Cu ₂ (CN) ₃	Triangular M[Pd(dmit) ₂] ₂	Kagome ZnCu ₃ (OH) ₆ Cl ₂	Hyper-Kagome, Na ₄ Ir ₃ O ₈
Susceptibility	A broad peak at 60 K, Finite at 2 K, $J = 250$ K (*1)	A broad peak at 50 K, Finite at 2 K, $J = 220 \sim$ 280 K (*7)	Curie-Weiss at high-T $\Theta_W = -300$ K, $J = 230$ K, Upturn at low-T due to impurity sites (*11, *12)	Curie-Weiss $\Theta_W = -650$ K (*19, *20)
Specific heat	Gapless, $\gamma = 15$ mJ/K ² mol, Field-independent (*2)	Gapless, $\gamma = 20$ mJ/K ² mol, Field-independent (*8)	Gapless, $C \sim T^\alpha$ $\alpha = 1.3$ at high fields (*13)	Gapless, $C \sim T^2$ (*19), $C \sim \gamma T + \beta T^{2.4}$, $\gamma = 2$ mJ/K ² mol (*20), Field-independent (*21, *22)
Thermal conductivity	Gapped; $\Delta = 0.46$ K (*3)	Gapless; finite κ/T (*9)		Vanishingly small κ/T (*22)
NMR shift	Not precisely resolved (*4)	Not precisely resolved (*10)	High-T Broad peak at 50-60 K for ¹⁷ O (*14, *15), at 25-50 K for ³⁵ Cl (*16) Low-T gapless :finite value (*14) gapped : $\Delta \sim 10$ K (*15)	¹⁷ O shift — scales to χ_{bulk} in 100 K - 300 K but levels off below 80 K (*23) ¹⁷ O, ²³ Na- inhomogeneous line broadening at low- T (*23)
NMR 1/T₁	Inhomogeneous 1/T ₁ , Power law, ¹ H 1/T ₁ ; $\sim T / \sim T^2$ at $T < 0.3$ K (two components) (*1), ¹³ C 1/T ₁ ; $\sim 1/T^{1.5}$ at $T < 0.2$ K (stretched exponential) (*4)	Inhomogeneous 1/T ₁ , Power law, ¹³ C 1/T ² at < 0.5 K (stretched exponential) (*10)	1/T ₁ $\sim T^\alpha$ $\alpha \sim 0.73$ for ¹⁷ O (*14) $\alpha \sim 0.5$ for ⁶³ O (*16) Field-induced spin freezing (*17)	²³ Na 1/T ₁ — a peak formation typical of critical slowing down at 7.5 K (*23)
μSR	No internal field at 0 T (*5, *6)		No internal field at 0 T (*18)	Emergence of distributed local fields below 6 K Quasi-static short-ranged spin freezing with slow dynamics (*24)
Neutron			Powders \sim gapless (< 0.1 meV) (*11, *19) Single crystal \sim gapless (< 0.25 meV) (*20) Continuum in dynamic structure factor (*11, *19, *20)	
References	*1 Shimizu <i>et al.</i> , 2003, *2 Yamashita <i>et al.</i> , 2008 *3 Yamashita <i>et al.</i> , 2009, *4 Shimizu <i>et al.</i> , 2006, *5 Pratt <i>et al.</i> , 2011, *6 Goto <i>et al.</i> , 2012 *6 Goto <i>et al.</i> , 2012	*7 Kato, 2014, *8 Yamashita <i>et al.</i> , 2011, *9 Yamashita <i>et al.</i> , 2010, *10 Itou <i>et al.</i> , 2010	*11 Helton <i>et al.</i> , 2007, *12 Bert <i>et al.</i> , 2007, *13 de Vries <i>et al.</i> , 2008, *14 Olariu <i>et al.</i> , 2008, *15 Imai <i>et al.</i> , 2015 *16 Imai <i>et al.</i> , 2008 *17 Jeong <i>et al.</i> , 2011, *18 Mendels <i>et al.</i> , 2007 *19 de Vries <i>et al.</i> , 2009 *20 Han <i>et al.</i> , 2012	*21 Okamoto <i>et al.</i> , 2007 *22 Singh <i>et al.</i> , 2013 *23 Shockley <i>et al.</i> , 2015 *24 Dally <i>et al.</i> , 2014

slowing down are not observed, but gapless spin excitations emerge, suggesting a novel role of disorder that brings forth a quantum spin liquid from a classical ordered state (Furukawa *et al.*, 2015b). Whether the randomness is fatal or vital to the physics of spin liquid is a non-trivial issue to be resolved.

The developments of new materials, although not touched in this article, are under way. Among them are a new type of hydrogen-bonded κ -H₃(Cat-EDT-TTF)₂ with a triangular lattice of one-dimensional anisotropy (Isono *et al.*, 2013) and κ -(ET)₂Ag₂(CN)₃, an analogue of κ -(ET)₂Cu₂(CN)₃ (Saito, 2014). Another compound with hyperkagome lattice structure, PbCuTe₂O₆, with Curie-Weiss temperature $\theta = -22$ K is also proposed to be a spin liquid candidate (Khuntia *et al.*, 2016; Koteswararao *et al.*, 2014). The entanglement of additional degrees of freedom with quantum spins may be another direction of future researches; e.g., Ba₃CuSb₂O₉ is proposed to host a spin-orbital coupled liquid state (Nakatsuji *et al.*, 2012; Zhou *et al.*, 2011).

It should be emphasized that the identification of QSL experimentally is a very important and challenging task. As a “featureless” Mott insulator, there exists no simple magnetic order for identifying QSL states and so far there exists only indirect experimental evidences for mobile fermionic spinons in some candidate compounds as discussed above.

To remedy this situation, theorists have proposed new experiments to identify QSLs through identifying nontrivial properties of spinons and gauge fields. For example, power law AC conductivity inside the Mott gap was pointed out (Ng and Lee, 2007). Giant magnetoresistance like experiment was proposed to measure mobile spinons through oscillatory coupling between two ferromagnets via a quantum spin liquid spacer (Norman and Micklitz, 2009). The thermal Hall effect in insulating quantum magnets was proposed as a probe for thermal transport of spinons, where different responses were used to distinguish between magnon- and spinon- transports (Katsura *et al.*, 2010). Raman scattering was proposed as a signature to probe $U(1)$ quantum spin liquid state (Ko *et al.*, 2010). It was also proposed that the spinon life time and mass as well as gauge fluctuations can be measured through sound attenuation experiment (Zhou and Lee, 2011), and Neutron scattering can be used to detect scalar spin chirality fluctuations in the kagome system (Lee and Nagaosa, 2013). More recently, Low energy electron spectral functions were evaluated for future ARPES experiments (Tang *et al.*, 2013) and it was proposed that spin current flow through Metal-QSL-Metal junction can be used to distinguish different QSLs (Chen *et al.*, 2013).

However, there exists important discrepancy between existing experiments and theories in some of the above experiments.

1) Specific heat: Using one-loop calculation sup-

plemented by scaling analysis (Lee and Nagaosa, 1992; Polchinski, 1994), it is found that the strong coupling between $U(1)$ gauge field and spinon Fermi surface leads to $T^{2/3}$ correction to the temperature dependence of specific heat in $U(1)$ gauge theory. This predicted $T^{2/3}$ behavior has never been observed in experiments. Instead, linear, Fermi-liquid like specific heat are found to exists in a wide range of temperature in both organic materials (κ -ET and dmit).

There exists some theories trying to explain this missing singular $T^{2/3}$ specific heat. For instance, Z_4 and Z_2 spin liquid states with spinon Fermi surface were proposed (Barkeshli *et al.*, 2013) as well as Z_2 spin liquid states with quadratic touched spinon bands (Mishmash *et al.*, 2013). However, all these proposals require fine tuned parameters. A more natural way of explaining existing experiments is still missing.

2) Thermal Hall effect: Katsura, Nagaosa and Lee (Katsura *et al.*, 2010) have investigated theoretically the thermal Hall effect induced by the external magnetic field in a $U(1)$ spin liquid with a spinon Fermi surface, and have predicted measurable electronic contributions. Their predicted sizable thermal Hall effect was never been observed in the experiment on dmit compounds (Yamashita *et al.*, 2010). This contradiction between experiment and theory remains unsolved although an explanation that depends on fine tuned parameters has been proposed (Mishmash *et al.*, 2013).

3) Power law AC conductivity: A power law AC conductivity inside the Mott gap was proposed by Ng and Lee (Ng and Lee, 2007). Indeed, power law behavior $\sigma(\omega) \sim \omega^\alpha$ has been observed in both κ -ET (Elsässer *et al.*, 2012) and Herbertsmithite (Pilon *et al.*, 2013). However the power α observed in both compounds are smaller than predicted value, indicating there exist more in-gap electronic excitations than those predicted in the $U(1)$ gauge theory.

Thus despite all the theoretical efforts, the understanding and finding of realistic “Smoking Gun” evidence for QSLs remains the biggest challenge in the study of QSLs.

VI. SUMMARY

In this article we attempt to give a pedagogical introduction to the subject of Quantum Spin Liquids and review the current status of the field. We first discuss the semi-classical approach to simple quantum antiferromagnets. We explain how it leads to the Haldane conjecture in one dimension and why it fails for frustrated spin models. We then focus on spin-1/2 systems with spin rotation symmetry and introduced the idea of RVB and the slave-particle plus Gutzwiller Projected wavefunction approaches. We explain the technical difficulties associated with the approach and why the slave-particle approaches naturally lead to gauge theo-

ries for spin liquid states. The nature of $SU(2)$, $U(1)$ and Z_2 spin liquid states are explained and the extension of the approach to systems with spin-orbit coupling and $S > 1/2$ systems are introduced. We explained that because of intrinsic limitations in the analytic slave-particle approach, many alternative approaches to spin liquid states have been developed, both numerically and analytically. These approaches complement each other and often lead to exotic possibilities not covered by the simple fermionic slave-particle approach. The experimental side of the story is also introduced where we reviewed the properties of several spin liquid candidate materials, including the anisotropic triangular lattice systems (κ -(ET)₂Cu₂(CN)₃ and EtMe₃Sb[(Pd(dmit)₂)₂]; Kagome-lattice systems (ZnCu₃(OH)₆Cl₂) and Hyperkagome-lattice systems (Na₄Ir₃O₈)). We point out several outstanding difficulties in explaining experimental results with existing theories. *These difficulties indicate that the field of QSLs is still wide open and immature, and important physics may still be missing in our present understanding of QSLs.*

To keep the article in an introductory level we are not able to cover many important developments in the study of spin liquid states and much of the technical details are left out, both theoretically and experimentally. For example, the important techniques of renormalization group and conformal field theory are left out in this article. We also have not discussed in details the many developments in MPS and/or PEPS states and the corresponding numerical DMRG technique, the understanding of spin systems that break rotational symmetry following the discovery of Kitaev state, and spin liquid physics of $S > 1/2$ systems. The role of topology in spin liquid states is not touched except that it shows up as examples in spin liquid states. These are fast evolving areas where new discoveries are expected.

In the following we outline a few other topics which are neglected in this article but have played either important historical roles in the development of the field of quantum spin liquid or shed light on the future research:

Quantum dimer model: Quantum dimer model (QDM) is a class of models defined in the Hilbert space of nearest-neighbor valence bond (or dimer) coverings over a lattice instead of the spin Hilbert space (Rokhsar and Kivelson, 1988). QDM can be obtained in certain large- N limits of $SU(N)$ or $Sp(N)$ antiferromagnets (Read and Sachdev, 1989), and provide a simplified description of RVB states. This simplification allows people to go further in analytic treatments because of their close relations to classical dimer problems, Ising models and Z_2 gauge theory (Fisher, 1961; Kasteleyn, 1961, 1963; Misguich *et al.*, 2002; Moessner and Sondhi, 2003; Moessner *et al.*, 2001). However, the QMDs focus on the dynamics in the spin-singlet subspace and ignore spin-triplet excitations by construction. Therefore they are not directly relevant to spin systems where magnetic ex-

citations are gapless.

An advantage of QDMs is that some QDMs are exactly solvable (Misguich *et al.*, 2002; Yao and Kivelson, 2012). Thus many issues on quantum spin liquid that are difficult to address, such as spinon deconfinement, Z_2 vortex and topological order, can be addressed explicitly in QDMs. It is interesting to note that some spin- $\frac{1}{2}$ Hamiltonian gives rise to sRVB ground states defined in the dimer Hilbert space when the relation between spin and dimer configuration is properly chosen (Cano and Fendley, 2010; Fujimoto, 2005; Seidel, 2009). Readers who are interested in more details on QDMs can refer to Chapter 5.5 in reference (Diep, 2004) and Chapter 17 in reference (Lacroix *et al.*, 2011).

Chiral spin liquid: Quantum spin liquid states that break parity (P) and time reversal (T) symmetry, while conserving spin rotational symmetry has been proposed by Kalmeyer and Laughlin (Kalmeyer and Laughlin, 1987, 1989). They are called chiral spin liquids.

Kalmeyer and Laughlin proposed that some frustrated Heisenberg antiferromagnet on 2D can be described by a bosonic fractional quantum Hall wave function. Soon after that Wen, Wilczek and Zee (Wen *et al.*, 1989) introduced a generic method to describe chiral spin liquids. They suggested that chiral spin states can be characterized by the spin chirality $E_{123} = \vec{S}_1 \cdot (\vec{S}_2 \times \vec{S}_3)$, defined for three different spins \vec{S}_1 , \vec{S}_2 and \vec{S}_3 . The expectation value of spin chirality in fermionic RVB theory is given by $\langle E_{123} \rangle = \frac{1}{2} \text{Im} \langle \chi_{12} \chi_{23} \chi_{31} \rangle$, where χ_{ij} 's are the short range order parameters defined in Eq. (39).

Exactly solvable Hamiltonians hosting gapful chiral spin liquid states (Laughlin, 1989; Schroeter *et al.*, 2007; Thomale *et al.*, 2009; Yao and Kivelson, 2007) as well as gapless chiral spin liquids (Chua *et al.*, 2011) have been found. There are also numerical evidence for chiral spin liquids on some 2D frustrated lattices (Bauer *et al.*, 2013; He and Chen, 2014; He *et al.*, 2014; Nielsen *et al.*, 2013; Sorella *et al.*, 2003). It was suggested that the statistics of spinons in these chiral spin liquid states can be nonabelian, e.g., see (Greiter and Thomale, 2009; Yao and Kivelson, 2007).

Characterizing spin liquid state numerically: Due to the fast advance in the power of numerical approaches to spin models, characterizing spin liquid state for specific spin models from numerical data becomes a fast evolving field. Besides the MPS and/or PEPS states and the corresponding numerical DMRG technique, Tang and Sandvik developed a method for quantum Monte Carlo to characterize spinon size and confinement length in quantum spin systems, which allows us to study spinon confinement-deconfinement issue numerically (Tang and Sandvik, 2013). Another important progress is to use entanglement entropy to characterize quantum spin liquid states. Readers may look at reference (Grover *et al.*, 2013) for a brief review.

To conclude, the field of QSLs is still wide open,

both theoretically and experimentally. The major difficulty in understanding QSLs is that they are intrinsically strongly-correlated systems where no perturbative approach is available. Theorists have been using all the available tools and are inventing new theoretical tools to understand QSLs with the hope that new emerging phenomena not covered by perturbative approaches can be uncovered. So far there are a few successes, and new experimental discoveries and theoretical ideas are appearing rapidly. However a basic mathematical framework that can be used to understand QSLs systematically is still missing. We expect that more new physics will be discovered in QSLs, and it imposes a challenge both to theorists and experimentalists to build up a basic framework to understand QSLs.

ACKNOWLEDGMENTS

Y.Z. and T.K.N. thank Patrick A. Lee, Zheng-Xin Liu, Naoto Nagaosa, Shaojin Qin, Zhaobin Su, Hong-Hao Tu, Tao Xiang, Xiao-Gang Wen, Zheng-Yu Weng, Guang-Ming Zhang, and Fu-Chun Zhang for their close collaboration on related issues over years. K. K is thankful to K. Miyagawa, Y. Shimizu, Y. Kurosaki, H. Hashiba, H. Kobashi, H. Kasahara, T. Furukawa, M. Maesato, G. Saito, F. Pratt, M. Poirier for collaboration on the spin-liquid issue. We benefitted greatly from the discussions with colleagues Yan Chen, Yin-Chen He, Bruce Normand, Fa Wang, Cenke Xu, and Hong Yao. Y.Z. is supported by National Basic Research Program of China under Grant No.2011CBA00103 and 2014CB921201, the National Natural Science Foundation of China under Grant No. 11374256. He also wants to acknowledge the hospitality of Max-Planck Institute for Physics in Complex Systems in Dresden, where this review article was finalized. K.K. is partially supported in part by JSPS KAKENHI under Grant Nos. 20110002, 25220709, and 24654101, and the US National Science Foundation under Grant No. PHYS-1066293 and the hospitality of the Aspen Center for Physics. T.K.N. acknowledges support from HKRGC through grant 603913.

Appendix A: Path integral for a single spin

We consider the Path integral for a single spin \mathbf{S} in magnetic field \mathbf{B} ($H = \mathbf{S} \cdot \mathbf{B}$) in the coherent state representation. The spin coherent states are defined by

$$\hat{\mathbf{S}}|\mathbf{n}\rangle = S\mathbf{n}|\mathbf{n}\rangle,$$

where $\hat{\mathbf{S}}$ is the spin operator. The path integral can be derived by using the identity operator

$$\mathbf{I} = \left(\frac{2S+1}{4\pi}\right) \int d^3n \delta(\mathbf{n}^2 - 1) |\mathbf{n}\rangle\langle\mathbf{n}| = \int D\mathbf{n} |\mathbf{n}\rangle\langle\mathbf{n}| \quad (\text{A1a})$$

and the corresponding inner product

$$\langle \mathbf{n}_1 | \mathbf{n}_2 \rangle = e^{iS\Phi(\mathbf{n}_1, \mathbf{n}_2, \mathbf{n}_0)} \left(\frac{1 + \mathbf{n}_1 \cdot \mathbf{n}_2}{2}\right)^S \quad (\text{A1b})$$

where \mathbf{n}_0 is a fixed unit vector usually chosen to be $\mathbf{n}_0 = \hat{z}$. $\Phi(\mathbf{n}_1, \mathbf{n}_2, \mathbf{n}_0)$ is the area of the spherical triangle with vertices $\mathbf{n}_1, \mathbf{n}_2, \mathbf{n}_0$ and $S\Phi$ is the Berry's phase acquire by a particle travel through a loop formed by the edges of the spherical triangle.

The partition function $Z = e^{-\beta H}$ can be written as a path-integral through the standard procedure

$$\begin{aligned} Z &= \lim_{N_t \rightarrow \infty, \delta t \rightarrow 0} (e^{-\delta t H})^{N_t} \\ &= \lim_{N_t \rightarrow \infty, \delta t \rightarrow 0} \left(\prod_{j=1}^{N_t} \int D\mathbf{n}_j \right) \left(\prod_{j=1}^{N_t} \langle \mathbf{n}_j | e^{-i\delta t H} | \mathbf{n}_{j+1} \rangle \right) \end{aligned} \quad (\text{A2})$$

with periodic boundary condition $|\mathbf{n}(0)\rangle = |\mathbf{n}(\beta)\rangle$.

In the limit $\delta t \rightarrow 0$, we may approximate

$$\begin{aligned} \langle \mathbf{n}_j | e^{-i\delta t H} | \mathbf{n}_{j+1} \rangle &\sim \langle \mathbf{n}_j | \mathbf{n}_{j+1} \rangle - \delta t \langle \mathbf{n}_j | H | \mathbf{n}_{j+1} \rangle \\ &\sim \langle \mathbf{n}_j | \mathbf{n}_{j+1} \rangle \left(1 - \delta t \frac{\langle \mathbf{n}_j | H | \mathbf{n}_{j+1} \rangle}{\langle \mathbf{n}_j | \mathbf{n}_{j+1} \rangle}\right) \\ &\sim e^{iS\Phi(\mathbf{n}_j, \mathbf{n}_{j+1}, \mathbf{n}_0)} \left(\frac{1 + \mathbf{n}_j \cdot \mathbf{n}_{j+1}}{2}\right)^S \\ &\quad \times (1 - \delta t S \mathbf{B} \cdot \mathbf{n}_t) \end{aligned} \quad (\text{A3})$$

valid to first order in δt . We have made use of the result $\langle \mathbf{n} | \hat{\mathbf{S}} = \langle \mathbf{n} | \mathbf{n}$ in deriving the last equality in (A3). Furthermore, we note that

$$\begin{aligned} \left(\frac{1 + \mathbf{n}_j \cdot \mathbf{n}_{j+1}}{2}\right)^S &\sim e^{S \ln(1 + \frac{\delta t}{2} \mathbf{n}(t) \cdot \partial_t \mathbf{n}(t))_{t=t_j}} \\ &\sim e^{S \delta t \partial_t [\mathbf{n}(t)]^2} = e^{(0)} \end{aligned} \quad (\text{A4})$$

to leading order in δt . Therefore,

$$\langle \mathbf{n}_j | e^{-i\delta t H} | \mathbf{n}_{j+1} \rangle \sim e^{iS\Phi(\mathbf{n}_j, \mathbf{n}_{j+1}, \mathbf{n}_0) - \delta t S \mathbf{B} \cdot \mathbf{n}_t} \quad (\text{A5})$$

and

$$Z \sim \int D\mathbf{n}(t) e^{iS\Omega(\mathbf{n}(t)) - S \int_0^\beta dt \mathbf{B} \cdot \mathbf{n}(t)} \quad (\text{A6})$$

where $\int D\mathbf{n}(t) = \lim_{N_t \rightarrow \infty, \delta t \rightarrow 0} \left(\prod_{j=1}^{N_t} \int D\mathbf{n}_j \right)$ and

$$\Omega(\mathbf{n}(t)) = \sum_j \Phi(\mathbf{n}_j, \mathbf{n}_{j+1}, \mathbf{n}_0)$$

is the total area on the surface of unit sphere covered by the (closed) path swapped out by the spin $\mathbf{n}(t)$ from $t = 0$ to $t = \beta$.

The classical action of the system at real time is given by

$$S_{cl} = S\Omega(\mathbf{n}(t)) - S \int_0^T dt \mathbf{B} \cdot \mathbf{n}(t), \quad (\text{A7a})$$

and the classical equation of motion $\frac{\delta S_{cl}}{\delta' \mathbf{n}(t)} = 0$ leads to the Euler's equation of motion

$$\mathbf{n} \times ((\mathbf{n} \times \partial_t \mathbf{n}) - \mathbf{B}) = 0 \quad (\text{A7b})$$

where we have used the result that a small variation $\delta \mathbf{n}$ leads to a change in $\Omega(C[\mathbf{n}])$ given by

$$\delta \Omega[\mathbf{n}(t)] = \int_0^\beta dt \delta \mathbf{n}(t) \cdot (\mathbf{n}(t) \times \partial_t \mathbf{n}(t)).$$

REFERENCES

Abdel-Jawad, M., I. Terasaki, T. Sasaki, N. Yoneyama, N. Kobayashi, Y. Uesu, and C. Hotta (2010), Phys. Rev. B **82**, 125119.

Affleck, I. (1986), Nucl. Phys. B **265** (3), 409.

Affleck, I. (1990), *Field Theory Methods and Quantum Critical Phenomena*, edited by E. Brezin and J. Zinn-Justin (North-Holland, Amsterdam).

Affleck, I., T. Kennedy, E. Lieb, and H. Tasaki (1988a), Commun. Math. Phys. **115** (3), 477.

Affleck, I., T. Kennedy, E. H. Lieb, and H. Tasaki (1987), Phys. Rev. Lett. **59**, 799.

Affleck, I., and J. B. Marston (1988), Phys. Rev. B **37**, 3774.

Affleck, I., Z. Zou, T. Hsu, and P. W. Anderson (1988b), Phys. Rev. B **38**, 745.

Anderson, P. (1973), Mater. Res. Bull. **8** (2), 153.

Anderson, P. W. (1959), Phys. Rev. Lett. **3**, 325.

Anderson, P. W. (1987), Science **235**, 1196.

Androes, G. M., and W. D. Knight (1959), Phys. Rev. Lett. **2**, 386.

Arovas, D. P. (2008), Phys. Rev. B **77**, 104404.

Arovas, D. P., and A. Auerbach (1988), Phys. Rev. B **38**, 316.

Arrachea, L., L. Capriotti, and S. Sorella (2004), Phys. Rev. B **69**, 224414.

Auerbach, A. (1994), *Interacting Electrons and Quantum Magnetism* (Springer-Verlag New York, Inc.).

Balents, L. (2010), Nature **464**, 199.

Balents, L., M. P. A. Fisher, and C. Nayak (1998), Int. J. Mod. Phys. B **12** (10), 1033.

Barkeshli, M., H. Yao, and S. A. Kivelson (2013), Phys. Rev. B **87**, 140402.

Baskaran, G., and P. W. Anderson (1988), Phys. Rev. B **37**, 580.

Baskaran, G., S. Mandal, and R. Shankar (2007), Phys. Rev. Lett. **98**, 247201.

Baskaran, G., G. Santhosh, and R. Shankar (2009), arXiv:0908.1614.

Baskaran, G., Z. Zou, and P. Anderson (1987), Solid State Commun. **63** (11), 973.

Bauer, B., B. P. Keller, M. Dolfi, S. Trebst, and A. W. W. Ludwig (2013), arXiv preprint arXiv:1303.6963.

Baym, G., and C. Pethick (2004), *Landau Fermi-Liquid Theory: Concepts and Applications* (WILEY-VCH Verlag GmbH & Co. KGaA, Weinheim).

Berry, M. V. (1984), Proc. Roy. Soc. London A **392** (1802), pp. 45.

Bert, F., S. Nakamae, F. Ladieu, P. L'Hôte, D. and Bonville, F. Duc, J.-C. Trombe, and M. P. (2007), Phys. Rev. B **76**, 132411.

Bieri, S., M. Serbyn, T. Senthil, and P. A. Lee (2012), Phys. Rev. B **86**, 224409.

Brézin, E., and J. Zinn-Justin (1976), Phys. Rev. B **14**, 3110.

Brinkman, W. F., and T. M. Rice (1970), Phys. Rev. B **2**, 4302.

Cano, J., and P. Fendley (2010), Phys. Rev. Lett. **105**, 067205.

Capriotti, L., F. Becca, A. Parola, and S. Sorella (2001), Phys. Rev. Lett. **87**, 097201.

Capriotti, L., A. E. Trumper, and S. Sorella (1999), Phys. Rev. Lett. **82**, 3899.

Ceperley, D., G. V. Chester, and M. H. Kalos (1977), Phys. Rev. B **16**, 3081.

Chaloupka, J. c. v., G. Jackeli, and G. Khaliullin (2010), Phys. Rev. Lett. **105**, 027204.

Chandra, P., and B. Doucot (1988), Phys. Rev. B **38**, 9335.

Chen, C. Z., Q. F. Sun, F. Wang, and X. C. Xie (2013), Phys. Rev. B **88**, 041405.

Chen, G., and L. Balents (2008), Phys. Rev. B **78**, 094403.

Chen, H. D., and Z. Nussinov (2008), J. Phys. A: Math. Theor. **41** (7), 075001.

Chen, H. D., B. Wang, and S. Das Sarma (2010), Phys. Rev. B **81**, 235131.

Chen, X., Z. C. Gu, Z. X. Liu, and X. G. Wen (2012), Science **338** (6114), 1604.

Chen, X., Z. C. Gu, and X. G. Wen (2011a), Phys. Rev. B **83**, 035107.

Chen, X., Z. C. Gu, and X. G. Wen (2011b), Phys. Rev. B **84**, 235128.

Cheng, J. G., G. Li, L. Balicas, J. S. Zhou, J. B. Goodenough, C. Xu, and H. D. Zhou (2011), Phys. Rev. Lett. **107**, 197204.

Choy, T. P., and Y. B. Kim (2009), Phys. Rev. B **80**, 064404.

Chua, V., H. Yao, and G. A. Fiete (2011), Phys. Rev. B **83**, 180412.

Cirac, J. I., and F. Verstraete (2009), J. Phys. A: Math. Theor. **42** (50), 504004.

Coldea, R., D. A. Tennant, A. M. Tsvelik, and Z. Tyliczynski (2001), Phys. Rev. Lett. **86**, 1335.

Coldea, R., D. A. Tennant, and Z. Tyliczynski (2003), Phys. Rev. B **68**, 134424.

Dally, R., T. Hogan, A. Amato, H. Luetkens, C. Baines, J. Rodriguez-Rivera, M. J. Graf, and S. D. Wilson (2014), Phys. Rev. Lett. **113**, 247601.

Dayal, S., R. T. Clay, H. Li, and S. Mazumdar (2011), Phys. Rev. B **83**, 245106.

Depenbrock, S., I. P. McCulloch, and U. Schollwöck (2012), Phys. Rev. Lett. **109**, 067201.

Diep, H. T. (2004), *Frustrated spin systems* (World Scientific).

Dodds, T., S. Bhattacharjee, and Y. B. Kim (2013), Phys. Rev. B **88**, 224413.

Dombre, T., and N. Read (1988), Phys. Rev. B **38**, 7181.

Dusuel, S., K. P. Schmidt, J. Vidal, and R. L. Zaffino (2008), Phys. Rev. B **78**, 125102.

Eggert, S., and I. Affleck (1992), Phys. Rev. B **46**, 10866.

Elsässer, S., D. Wu, M. Dressel, and J. A. Schlueter (2012), Phys. Rev. B **86**, 155150.

Fannes, M., B. Nachtergaele, and R. F. Werner (1992), Commun. Math. Phys. **144** (3), 443.

Farnell, D. J. J., R. F. Bishop, and K. A. Gernoth (2001), Phys. Rev. B **63**, 220402.

Fazekas, P., and P. Anderson (1974), Philos. Mag. **30** (2), 423.

Feng, X. Y., G. M. Zhang, and T. Xiang (2007), Phys. Rev. Lett. **98**, 087204.

Fisher, M. E. (1961), Phys. Rev. **124**, 1664.

Florens, S., and A. Georges (2004), Phys. Rev. B **70**, 035114.

Fradkin, E., and S. H. Shenker (1979), Phys. Rev. D **19**, 3682.

Fradkin, E., and M. Stone (1988), Phys. Rev. B **38**, 7215.

Frigeri, P. A., D. F. Agterberg, A. Koga, and M. Sigrist (2004), Phys. Rev. Lett. **92**, 097001.

Fu, M., T. Imai, T.-H. Han, and Y. S. Lee (2015), Science **350**, 655.

Fujimoto, S. (2005), Phys. Rev. B **72**, 024429.

Furukawa, T., K. Miyagawa, H. Taniguchi, R. Kato, and K. Kanoda (2015a), Nature Physics **11**, 221.

Furukawa, T., K. Miyagawa, H. Taniguchi, R. Kato, and K. Kanoda (2015b), Physical Review Letters **115**, 077001.

Galitski, V., and Y. B. Kim (2007), Phys. Rev. Lett. **99**, 266403.

Gebhard, F., and D. Vollhardt (1987), Phys. Rev. Lett. **59**, 1472.

Giamarchi, T. (2003), *Quantum Physics in One Dimension* (Oxford University Press).

Glarum, S. H., S. Geschwind, K. M. Lee, M. L. Kaplan, and J. Michel (1991), Phys. Rev. Lett. **67**, 1614.

Gong, S.-S., W. Zhu, D. N. Sheng, O. I. Motrunich, and M. P. A. Fisher (2014), Phys. Rev. Lett. **113**, 027201.

Gor'kov, L. P., and E. I. Rashba (2001), Phys. Rev. Lett. **87**, 037004.

Greiter, M., and R. Thomale (2009), Phys. Rev. Lett. **102**, 207203.

Griffiths, R. B. (1964), Phys. Rev. **133**, A768.

Gros, C. (1989), Ann. Phys. (N.Y.) **189** (1), 53.

Gros, C., R. Joynt, and T. M. Rice (1987), Phys. Rev. B **36**, 381.

Grover, T., N. Trivedi, T. Senthil, and P. A. Lee (2010), Phys. Rev. B **81**, 245121.

Grover, T., Y. Zhang, and A. Vishwanath (2013), New J. Phys **15**, 025002.

Gu, Z. C., and X. G. Wen (2009), Phys. Rev. B **80**, 155131.

Hahn, T. (1996), *International tables for crystallography, Volume A, Space-Group Symmetry*, 4th ed., Vol. A (Kluwer Academic Publishers, Dordrecht, Netherlands).

Haldane, F. (1985), J. Appl. Phys. **57** (8), 3359.

Haldane, F. D. M. (1983a), Phys. Lett. A **93** (9), 464.

Haldane, F. D. M. (1983b), Phys. Rev. Lett. **50**, 1153.

Haldane, F. D. M. (1988a), Phys. Rev. Lett. **60**, 635.

Haldane, F. D. M. (1988b), Phys. Rev. Lett. **61**, 1029.

Han, T.-H., J. S. Helton, S. Chu, D. G. Nocera, J. A. Rodriguez-Rivera, C. Broholm, and Y. S. Lee (2012), Nature **492**, 406.

Hastings, M. B. (2000), Phys. Rev. B **63**, 014413.

Hastings, M. B. (2007), J. Stat. Mech. **2007**, P08024.

He, Y. C., and Y. Chen (2014), arXiv preprint arXiv:1407.2740.

He, Y. C., D. Sheng, and Y. Chen (2014), Phys. Rev. Lett. **112**, 137202.

Helton, J. S., K. Matan, M. P. Shores, E. A. Nytko, B. M. Bartlett, Y. Yoshida, Y. Takano, A. Suslov, Y. Qiu, J. H. Chung, D. G. Nocera, and Y. S. Lee (2007), Phys. Rev. Lett. **98**, 107204.

Herbut, I. F., and B. H. Seradjeh (2003), Phys. Rev. Lett. **91**, 171601.

Herbut, I. F., B. H. Seradjeh, S. Sachdev, and G. Murthy (2003), Phys. Rev. B **68**, 195110.

Hermele, M., T. Senthil, M. P. A. Fisher, P. A. Lee, N. Nagaosa, and X. G. Wen (2004), Phys. Rev. B **70**, 214437.

Horsch, P., and T. A. Kaplan (1983), J. Phys. C **16** (35), L1203.

Hotta, C. (2010), Phys. Rev. B **82**, 241104.

Hu, W.-J., F. Becca, A. Parola, and S. Sorella (2013), Phys. Rev. B **88**, 060402.

Huse, D. A., and V. Elser (1988), Phys. Rev. Lett. **60**, 2531.

Imai, T., E. A. Nytko, B. Bartlett, S. M.P., and D. G. Nocera (2008), Phys. Rev. Lett. **100**, 077203.

Iqbal, Y., F. Becca, S. Sorella, and D. Poilblanc (2013), Phys. Rev. B **87**, 060405.

Iqbal, Y., D. Poilblanc, and F. Becca (2014), Phys. Rev. B **89**, 020407.

Iqbal, Y., D. Poilblanc, and F. Becca (2016), arXiv:1606.02255 , 5.

Isono, T., H. Kamo, A. Ueda, A. Takahashi, K. Nakao, R. Kumanai, H. Nakano, K. Kobayashi, Y. Murakami, and H. Mori (2013), Nature Commun. **4**, 1344.

Itoh, K., H. Itoh, M. Naka, S. Saito, I. Hosako, N. Yoneyama, S. Ishihara, T. Sasaki, and S. Iwai (2013), Phys. Rev. Lett. **110**, 106401.

Itou, T., A. Oyamada, S. Maegawa, and R. Kato (2010), Nature Phys. **6**, 673.

Itou, T., A. Oyamada, S. Maegawa, M. Tamura, and R. Kato (2008), Phys. Rev. B **77**, 104413.

Itou, T., K. Yamashita, M. Nishiyama, A. Oyamada, S. Maegawa, K. Kubo, and R. Kato (2011), Phys. Rev. B **84**, 094405.

Jackeli, G., and G. Khaliullin (2009), Phys. Rev. Lett. **102**, 017205.

Jeong, M., F. Bert, P. Mendels, F. Duc, J. C. Trombe, M. A. de Vries, and A. Harrison (2011), Phys. Rev. Lett. **107**, 237201.

Jiang, H. C., Z. C. Gu, X. L. Qi, and S. Trebst (2011), Phys. Rev. B **83**, 245104.

Jiang, H. C., Z. Wang, and L. Balents (2012a), Nature Phys. **8** (12), 902.

Jiang, H. C., Z. Y. Weng, and D. N. Sheng (2008), Phys. Rev. Lett. **101**, 117203.

Jiang, H.-C., H. Yao, and L. Balents (2012b), Phys. Rev. B **86**, 024424.

Kagawa, F., K. Miyagawa, and K. Kanoda (2005), Nature **436**, 534.

Kalmeyer, V., and R. B. Laughlin (1987), Phys. Rev. Lett. **59**, 2095.

Kalmeyer, V., and R. B. Laughlin (1989), Phys. Rev. B **39**, 11879.

Kandpal, H. C., I. Opahle, Y.-Z. Zhang, H. O. Jeschke, and R. Valenti (2009), Phys. Rev. Lett. **103**, 067004.

Kanoda, K. (1997a), Physica C **287**, 299.

Kanoda, K. (1997b), Hyperfine Interact. **104**, 235.

Kanoda, K. (2006), J. Phys. Soc. Jpn. **75**, 051007.

Kanoda, K., and R. Kato (2011), Annu. Rev. Condens. Matter Phys. **2**, 167.

Kasteleyn, P. (1961), Physica **27** (12), 1209 .

Kasteleyn, P. (1963), **4**, 10.1063/1.1703953.

Kato, R. (2014), Bull. Chem. Soc. Jpn. **87**, 355.

Kato, R., A. Tajima, A. Nakao, A. Tajima, and M. Tamura (2007), *Multifunctional Conducting Molecular Materials*, p. 32. *Erratum: Caption of Fig. 4 in p. 35 should be corrected for right; 'Cation =EtMe₃Sb left; Cation=EtMe₃As'.* (RSC, Cambridge).

Katsura, H., N. Nagaosa, and P. A. Lee (2010), Phys. Rev. Lett. **104**, 066403.

Kawamoto, A., Y. Honma, K. Kumagai, N. Matsunaga, and K. Nomura (2006), Phys. Rev. B **74**, 212508.

Kells, G., J. K. Slingerland, and J. Vala (2009), Phys. Rev. B **80**, 125415.

Kézsmárki, I., Y. Shimizu, G. Mihály, Y. Tokura, K. Kanoda, and G. Saito (2006), Phys. Rev. B **74**, 201101.

Khuntia, P., F. Bert, P. Mendels, B. Koteswararao, A. V. Mahajan, M. Baenitz, F. C. Chou, C. Baines, A. Amato, and Y. Furukawa (2016), Phys. Rev. Lett. **116**, 107203.

Kimchi, I., and A. Vishwanath (2014), Phys. Rev. B **89**, 014414.

Kimchi, I., and Y. Z. You (2011), Phys. Rev. B **84**, 180407.

Kino, H., and H. Fukuyama (1995), J. Phys. Soc. Jpn. **64**, 2726.

Kitaev, A. (2003), Ann. Phys. **303** (1), 2.

Kitaev, A. (2006), Ann. Phys. **321** (1), 2, january Special Issue.

Klümper, A., A. Schadschneider, and J. Zittartz (1993), Europhys. Lett. **24** (4), 293.

Ko, W. H., P. A. Lee, and X. G. Wen (2009), Phys. Rev. B **79**, 214502.

Ko, W. H., Z. X. Liu, T. K. Ng, and P. A. Lee (2010), Phys. Rev. B **81**, 024414.

Komatsu, Y., N. Matsukawa, T. Inoue, and G. Saito (1996), J. Phys. Soc. Jpn. **65**, 1340.

Koretsune, T., and C. Hotta (2014), Phys. Rev. B **89**, 045102.

Koteswararao, B., R. Kumar, P. Khuntia, S. Bhowal, S. K. Panda, M. R. Rahman, A. V. Mahajan, I. Dasgupta, M. Baenitz, K. H. Kim, and F. C. Chou (2014), Phys. Rev. B **90**, 035141.

Kotliar, G. (1988), Phys. Rev. B **37**, 3664.

Kou, S. P., and X. G. Wen (2009), Phys. Rev. B **80**, 224406.

Kurosaki, Y., Y. Shimizu, K. Miyagawa, and K. Kanoda (2005), Phys. Rev. Lett. **95**, 177001.

Kyung, B., and A.-M. S. Tremblay (2006), Phys. Rev. Lett. **97**, 046402.

Lacroix, C., P. Mendels, and F. Mila (2011), *Introduction to Frustrated Magnetism: Materials, Experiments, Theory*, Vol. 164 (Springer).

Larkin, A. I. (1964), Sov. Phys. JETP **19** (6), 1478.

Laubach, M., R. Thomale, C. Platt, W. Hanke, and G. Li (2015), Phys. Rev. B **91**, 245125.

Laughlin, R. B. (1989), Annals of Physics **191** (1), 163.

Lawler, M. J., A. Paramekanti, Y. B. Kim, and L. Balents (2008), Phys. Rev. Lett **101**, 197202.

Lecheminant, P., B. Bernu, C. Lhuillier, L. Pierre, and P. Sindzingre (1997), Phys. Rev. B **56**, 2521.

Lee, D. H., G. M. Zhang, and T. Xiang (2007a), Phys. Rev. Lett. **99**, 196805.

Lee, E. K. H., R. Schaffer, S. Bhattacharjee, and Y. B. Kim (2014), Phys. Rev. B **89**, 045117.

Lee, P. A. (2008a), Science **321**, 1306.

Lee, P. A., and N. Nagaosa (1992), Phys. Rev. B **46**, 5621.

Lee, P. A., and N. Nagaosa (2013), Phys. Rev. B **87**, 064423.

Lee, P. A., N. Nagaosa, and X.-G. Wen (2006), Rev. Mod. Phys. **78**, 17.

Lee, S.-S. (2008b), Phys. Rev. B **78**, 085129.

Lee, S. S., and P. A. Lee (2005), Phys. Rev. Lett. **95**, 036403.

Lee, S. S., P. A. Lee, and T. Senthil (2007b), Phys. Rev. Lett. **98**, 067006.

Lefebvre, S., P. Wzietek, S. Brown, C. Bourbonnais, D. Jerome, C. Mezire, M. Fourmigue, and P. Batail (2000), Phys. Rev. Lett. **85**, 5420.

Leggett, A. J. (1965), Phys. Rev. **140**, A1869.

Leggett, A. J. (1975), Rev. Mod. Phys. **47**, 331.

Leung, P. W., and V. Elser (1993), Phys. Rev. B **47**, 5459.

Li, T. (2016), arXiv:1601.0216 , 5.

Li, T., and H.-Y. Yang (2007), Phys. Rev. B **75**, 172502.

Liang, S., B. Doucot, and P. W. Anderson (1988), Phys. Rev. Lett. **61**, 365.

Lieb, E. H. (1994), Phys. Rev. Lett. **73**, 2158.

Lieb, E. H., and F. Y. Wu (1968), Phys. Rev. Lett. **20**, 1445.

Liu, Z. X., Y. Zhou, and T. K. Ng (2010a), Phys. Rev. B **82**, 144422.

Liu, Z. X., Y. Zhou, and T. K. Ng (2010b), Phys. Rev. B **81**, 224417.

Liu, Z. X., Y. Zhou, and T. K. Ng (2014), New J. Phys. **16**, 083031.

Liu, Z. X., Y. Zhou, H. H. Tu, X. G. Wen, and T. K. Ng (2012), Phys. Rev. B **85**, 195144.

Lu, Y. M., Y. Ran, and P. A. Lee (2011), Phys. Rev. B **83**, 224413.

Luther, A., and I. Peschel (1975), Phys. Rev. B **12**, 3908.

Ma, M. (1988), Phys. Rev. B **38**, 6813.

MacLaughlin, D. E., Y. Nambu, S. Nakatsuji, R. H. Heffner, L. Shu, O. O. Bernal, and K. Ishida (2008), Phys. Rev. B **78**, 220403.

Mandal, S., S. Bhattacharjee, K. Sengupta, R. Shankar, and G. Baskaran (2011), Phys. Rev. B **84**, 155121.

Mandal, S., R. Shankar, and G. Baskaran (2012), J. Phys. A **45** (33), 335304.

Manousakis, E. (1991), Rev. Mod. Phys. **63**, 1.

Marshall, W. (1955), Proc. Roy. Soc. London A. **232** (1188), 48.

Marston, J., and C. Zeng (1991), J. Appl. Phys. **69** (8), 5962.

Mendels, P., F. Bert, M. A. de Vries, A. Olariu, A. Harrison, F. Duc, J. C. Trombe, J. S. Lord, and A. a. C. B. Amato (2007), Phys. Rev. Lett. **98**, 077204.

Mermin, N. D., and H. Wagner (1966), Phys. Rev. Lett. **17**, 1133.

Mila, F. (1998), Phys. Rev. Lett. **81**, 2356.

Misguich, G., B. Bernu, C. Lhuillier, and C. Waldtmann (1998), Phys. Rev. Lett. **81**, 1098.

Misguich, G., and C. Lhuillier (2004), *Frustrated spin systems*, edited by T. H. Diep (World Scientific, Singapore).

Misguich, G., D. Serban, and V. Pasquier (2002), Phys. Rev. Lett. **89**, 137202.

Mishmash, R. V., J. R. Garrison, S. Bieri, and C. Xu (2013), Phys. Rev. Lett. **111**, 157203.

Miyagawa, K., K. Kanoda, and A. Kawamoto (2004), Chem. Rev. **104**, 5635.

Miyagawa, K., A. Kawamoto, Y. Nakazawa, and K. Kanoda (1995), Phys. Rev. Lett. **75**, 1174.

Moessner, R., and J. T. Chalker (1998), Phys. Rev. Lett. **80**, 2929.

Moessner, R., and S. L. Sondhi (2003), Phys. Rev. B **68**, 054405.

Moessner, R., S. L. Sondhi, and E. Fradkin (2001), Phys. Rev. B **65**, 024504.

Mori, T., A. Kobayashi, Y. Sasaki, H. Kobayashi, G. Saito, and H. Inokuchi (1984), Bull. Chem. Soc. Jpn **57**, 627.

Mori, T., H. Mori, and S. Tanaka (1999), Bull. Chem. Soc. Jpn **72**, 179.

Morita, H., S. Watanabe, and M. Imada (2002), J. Phys. Soc. Jpn. **71**, 2109.

Motrunich, O. I. (2005), Phys. Rev. B **72**, 045105.

Naka, M., and S. Ishihara (2010), J. Phys. Soc. Jpn. **79**, 063707.

Nakajima, S., T. Suzuki, Y. Ishii, K. Ohishi,

I. Watanabe, T. Goto, A. Oosawa, N. Yoneyama, N. Kobayashi, F. L. Pratt, and T. Sasaki (2012), *J. Phys. Soc. Jpn.* **81**, 063706.

Nakamura, K., Y. Yoshimoto, T. Kusugi, R. Arita, and I. M. (2009), *J. Phys. Soc. Jpn.* **78**, 083710.

Nakatsuji, S., K. Kuga, K. Kimura, R. Satake, N. Katayama, E. Nishibori, H. Sawa, R. Ishii, M. Hagiwara, F. Bridges, T. U. Ito, W. Higemoto, M. Karaki, Y. Halim, A. A. Nugroho, J. A. Rodriguez-Rivera, and C. B. M. A. Green (2012), *Science* **336**, 559.

Nakatsuji, S., Y. Nambu, H. Tonomura, O. Sakai, S. Jonas, C. Broholm, H. Tsunetsugu, Y. Qiu, and Y. Maeno (2005), *Science* **309**, 1697.

Nave, C. P., and P. A. Lee (2007), *Phys. Rev. B* **76**, 235124.

Nayak, C., S. H. Simon, A. Stern, M. Freedman, and S. Das Sarma (2008), *Rev. Mod. Phys.* **80**, 1083.

Ng, T. K. (1994), *Phys. Rev. B* **50**, 555.

Ng, T. K. (1999), *Phys. Rev. Lett.* **82**, 3504.

Ng, T. K., and P. A. Lee (2007), *Phys. Rev. Lett.* **99**, 156402.

Nielsen, A. E., G. Sierra, and J. I. Cirac (2013), *Nature communications* **4**.

Nogueira, F. S., and H. Kleinert (2005), *Phys. Rev. Lett.* **95**, 176406.

Norman, M. R., and T. Micklitz (2009), *Phys. Rev. Lett.* **102**, 067204.

Nussinov, Z., and Z. van den Brink (2013), arXiv:1303.5922 .

Nussinov, Z., and G. Ortiz (2009), *Phys. Rev. B* **79**, 214440.

Okamoto, Y., M. Nohara, H. Aruga-Katori, and H. Takagi (2007), *Phys. Rev. Lett.* **99**, 137207.

Olariu, A., P. Mendels, F. Bert, F. Duc, J. C. Trombe, M. A. de Vries, and A. Harrison (2008), *Phys. Rev. Lett.* **100**, 087202.

Orus, R. (2014), *Ann. Phys.* **349**, 117.

Östlund, S., and S. Rommer (1995), *Phys. Rev. Lett.* **75**, 3537.

Pauling, L. (1949), *Proc. Roy. Soc. London A.* **196** (1046), 343.

Pilon, D. V., C. H. Lui, T. H. Han, D. Shrekenhamer, A. J. Frenzel, W. J. Padilla, Y. S. Lee, and N. Gedik (2013), *Phys. Rev. Lett.* **111**, 127401.

Podolsky, D., A. Paramekanti, Y. B. Kim, and T. Senthil (2009), *Phys. Rev. Lett.* **102**, 186401.

Poilblanc, D., and N. Schuch (2013), *Phys. Rev. B* **87**, 140407.

Poirier, M., M. de Lafontaine, K. Miyagawa, K. Kanoda, and Y. Shimizu (2014), *Phys. Rev. B* **89**, 045138.

Poirier, M., S. Parent, A. Cote, K. Miyagawa, K. Kanoda, and Y. Shimizu (2012), *Phys. Rev. B* **85**, 134444.

Polchinski, J. (1994), *Nucl. Phys. B* **422** (3), 617.

Pollmann, F., E. Berg, A. M. Turner, and M. Oshikawa (2012), *Phys. Rev. B* **85**, 075125.

Polyakov, A. (1977), *Nucl. Phys. B* **120** (3), 429 .

Polyakov, A. (1987), *Gauge Fields and Strings (Contemporary Concepts in Physics)* (Harwood Academic Publishers, Switzerland).

Polyakov, A. M. (1975), *Phys. Lett. B* **59** (1), 79.

Potter, A. C., T. Senthil, and P. A. Lee (2013), *Phys. Rev. B* **87**, 245106.

Powell, B. J., and R. H. McKenzie (2011), *Reports Prog. Phys.* **74**, 056501.

Pratt, F. L., P. J. Baker, S. J. Blundell, T. Lancaster, S. Ohira-Kawamura, C. Baines, Y. Shimizu, K. Kanoda, I. Watanabe, and G. Saito (2011), *Nature* **471**, 612.

Price, C. C., and N. B. Perkins (2012), *Phys. Rev. Lett.* **109**, 187201.

Qi, Y., C. Xu, and S. Sachdev (2009), *Phys. Rev. Lett.* **102**, 176401.

Qin, S., T. K. Ng, and Z. B. Su (1995), *Phys. Rev. B* **52**, 12844.

Ran, Y., M. Hermele, P. A. Lee, and X. G. Wen (2007), *Phys. Rev. Lett.* **98**, 117205.

Read, N., and B. Chakraborty (1989), *Phys. Rev. B* **40**, 7133.

Read, N., and S. Sachdev (1989), *Nucl. Phys. B* **316** (3), 609 .

Read, N., and S. Sachdev (1990), *Phys. Rev. B* **42**, 4568.

Reuther, J., R. Thomale, and S. Trebst (2011), *Phys. Rev. B* **84**, 100406.

Ribeiro, P., and P. A. Lee (2011), *Phys. Rev. B* **83**, 235119.

Rigol, M., and R. R. P. R. P. Singh (2007), *Nature Phys.* **98**, 207204.

Rokhsar, D. S., and S. A. Kivelson (1988), *Phys. Rev. Lett.* **61**, 2376.

Ryu, S. (2009), *Phys. Rev. B* **79**, 075124.

Sachdev, S. (1992), *Phys. Rev. B* **45**, 12377.

Saito, G. (2014), unpublished.

Schaffer, R., S. Bhattacharjee, and Y. B. Kim (2012), *Phys. Rev. B* **86**, 224417.

Schmidt, K. P., S. Dusuel, and J. Vidal (2008), *Phys. Rev. Lett.* **100**, 057208.

Schollwöck, U. (2005), *Rev. Mod. Phys.* **77**, 259.

Schroeter, D. F., E. Kapit, R. Thomale, and M. Greiter (2007), *Phys. Rev. Lett.* **99**, 097202.

Schuch, N., D. Poilblanc, J. I. Cirac, and D. Pérez-García (2012), *Phys. Rev. B* **86**, 115108.

Seidel, A. (2009), *Phys. Rev. B* **80**, 165131.

Senthil, T. (2008), *Phys. Rev. B* **78**, 045109.

Senthil, T., and M. P. A. Fisher (2000), *Phys. Rev. B* **62**, 7850.

Shaginyan, V. R., A. Z. Msezane, and K. G. Popov (2011), *Phys. Rev. B* **84**, 0640401(R).

Shankar, R., and N. Read (1990), *Nucl. Phys. B* **336** (3), 457.

Shastry, B. S. (1988), *Phys. Rev. Lett.* **60**, 639.

Shimizu, Y., K. Miyagawa, K. Kanoda, M. Maesato, and G. Saito (2003), *Phys. Rev. Lett.* **91**, 107001.

Shimizu, Y., K. Miyagawa, K. Kanoda, M. Maesato, and G. Saito (2006), *Phys. Rev. B* **73**, 140407.

Shockley, A. C., F. Bert, J.-C. Orain, Y. Okamoto, and P. Mendels (2015), *Phys. Rev. Lett.* **115**, 047201.

Shores, M. P., E. A. Nytka, B. M. Bartlett, and D. G. Nocera (2005), *J. Am. Chem. Soc.* **127**, 13462.

Sigrist, M., and K. Ueda (1991), *Rev. Mod. Phys.* **63**, 239.

Sindzingre, P., P. Lecheminant, and C. Lhuillier (1994), *Phys. Rev. B* **50**, 3108.

Singh, R. R. P. (2010), *Phys. Rev. Lett.* **104**, 177203.

Singh, Y., S. Manni, J. Reuther, T. Berlijn, R. Thomale, W. Ku, S. Trebst, and P. Gegenwart (2012), *Phys. Rev. Lett.* **108**, 127203.

Singh, Y., Y. Tokiwa, J. Dong, and P. Gegenwart (2013), *Phys. Rev. B* **88**, 220413.

Sorella, S., L. Capriotti, F. Becca, and A. Parola (2003), *Phys. Rev. Lett.* **91**, 257005.

Stephenson, J. (1970), *J. Math. Phys.* **11** (2), 420.

Sze, W. P., Y. Zhou, and T.-K. Ng (2016), *Phys. Rev. Lett.* ..

Tamura, M., and R. Kato (2002), *J. Phys. Condens. Matter* **14**, L729.

Tang, E., M. P. A. Fisher, and P. A. Lee (2013),

Phys. Rev. B **87**, 045119.

Tang, Y., and A. W. Sandvik (2013), Phys. Rev. Lett. **110**, 217213.

Thomale, R., E. Kapit, D. F. Schroeter, and M. Greiter (2009), Phys. Rev. B **80**, 104406.

Tikhonov, K. S., and M. V. Feigel'man (2010), Phys. Rev. Lett. **105**, 067207.

Tocchio, L. F., H. Feldner, F. Becca, V. R., and C. Gros (2013), Phys. Rev. B **87**, 035143.

Toulouse, G. (1977), Commun. Phys **2** (4), 115.

Tsumuraya, T., H. Seo, H. Tsuchizuru, R. Kato, and T. Miyazaki (2013), J. Phys. Soc. Jpn. **82**, 033709.

Vannimenus, J., and G. Toulouse (1977), J. Phys. C **10** (18), L537.

Verstraete, F., and J. I. Cirac (2004a), arXiv:0407066 .

Verstraete, F., and J. I. Cirac (2004b), Phys. Rev. A **70**, 060302.

Verstraete, F., and J. I. Cirac (2006), Physical Review B **73**, 094423.

Verstraete, F., V. Murg, and J. Cirac (2008), Adv. Phys. **57** (2), 143.

Verstraete, F., M. M. Wolf, D. Perez-Garcia, and J. I. Cirac (2006), Phys. Rev. Lett. **96**, 220601.

Vidal, J., K. P. Schmidt, and S. Dusuel (2008), Phys. Rev. B **78**, 245121.

Villain, J., Bidaux, R., Carton, J.-P., and Conte, R. (1980), J. Phys. France **41** (11), 1263.

de Vries, M. A., K. V. Kamenev, W. A. Kockelmann, J. Sanchez-Benitez, and A. Harrison (2008), Phys. Rev. Lett **100**, 157205.

de Vries, M. A., J. R. Stewart, P. P. Deen, J. O. Piatek, G. J. Nilsen, H. M. Rønnow, and A. Harrison (2009), Phys. Rev. Lett **103**, 237201.

Waldtmann, C., H. U. Everts, B. Bernu, C. Lhuillier, P. Sindzingre, P. Lecheminant, and L. Pierre (1998), Eur. Phys. J. B **2** (4), 501.

Wang, F. (2010a), Phys. Rev. B **81**, 184416.

Wang, F. (2010b), Phys. Rev. B **82**, 024419.

Wang, F., and A. Vishwanath (2006), Phys. Rev. B **74**, 174423.

Wang, L., D. Poilblanc, Z. C. Gu, X. G. Wen, and F. Verstraete (2013), Phys. Rev. Lett. **111**, 037202.

Wannier, G. H. (1950), Phys. Rev. **79**, 357.

Watanabe, D., M. Yamashita, S. Tonegawa, Y. Oshima, H. Yamamoto, R. Kato, I. Sheikin, K. Behnia, T. Terashima, S. Uji, *et al.* (2012), Nature Commun. **3**, 1090.

Watanabe, K., H. Kawamura, H. Nakano, and T. Sakai (2014), J. Phys. Soc. Jpn. **83**, 034714.

Watanabe, T., H. Yokoyama, Y. Tanaka, and J. Inoue (2008), Phys. Rev. B **77**, 214505.

Wen, X. G. (1989), Phys. Rev. B **39**, 7223.

Wen, X. G. (1991), Phys. Rev. B **44**, 2664.

Wen, X. G. (2002), Phys. Rev. B **65**, 165113.

Wen, X. G., F. Wilczek, and A. Zee (1989), Phys. Rev. B **39**, 11413.

Wen, X. G., and A. Zee (1988), Phys. Rev. Lett. **61**, 1025.

White, S. R. (1992), Phys. Rev. Lett. **69**, 2863.

Wu, C., D. Arovas, and H.-H. Hung (2009), Phys. Rev. B **79**, 134427.

Wu, T. T., and C. N. Yang (1976), Nucl. Phys. B **107** (3), 365.

Xie, Z., J. Chen, J. F. Yu, X. Kong, B. Normand, and T. Xiang (2014), Phys. Rev. X **4**, 011025.

Xu, C., F. Wang, Y. Qi, L. Balents, and M. P. A. Fisher (2012), Phys. Rev. Lett. **108**, 087204.

Yamashita, M., N. Nakata, Y. Kasahara, T. Sasaki, N. Yoneyama, N. Kobayashi, S. Fujimoto, T. Shibauchi, and Y. Matsuda (2008a), Nature Phys. **5** (1), 44.

Yamashita, M., N. Nakata, Y. Senshu, M. Nagata, H. M. Yamamoto, R. Kato, T. Shibauchi, and Y. Matsuda (2010), Science **328** (5983), 1246.

Yamashita, S., Y. Nakazawa, M. Oguni, Y. Oshima, H. Nojiri, Y. Shimizu, K. Miyagawa, and K. Kanoda (2008b), Nature Phys. **4** (6), 459.

Yamashita, S., T. Yamamoto, Y. Nakazawa, M. Tamura, and R. Kato (2011), Nature Commun. **2** (Aug), 275.

Yan, S., D. Huse, and S. White (2011), Science **332** (6034), 1173.

Yang, H. Y., A. M. Läuchli, F. Mila, and K. P. Schmidt (2010), Phys. Rev. Lett. **105**, 267204.

Yang, S., D. L. Zhou, and C. P. Sun (2007), Phys. Rev. B **76**, 180404.

Yao, H., and S. A. Kivelson (2007), Phys. Rev. Lett. **99**, 247203.

Yao, H., and S. A. Kivelson (2012), Phys. Rev. Lett. **108**, 247206.

Yao, H., and D. H. Lee (2011), Phys. Rev. Lett. **107**, 087205.

Yao, H., S.-C. Zhang, and S. A. Kivelson (2009), Phys. Rev. Lett. **102**, 217202.

Yokoyama, H., and H. Shiba (1987), J. Phys. Soc. Jpn. **56**, 3570.

Yu, Y. (2008), Nucl. Phys. B **799** (3), 345 .

Yu, Y., L. Liang, Q. Niu, and S. Qin (2013), Phys. Rev. B **87**, 041107.

Yu, Y., and Z. Wang (2008), EPL **84**, 57002.

Yunoki, S., and S. Sorella (2006), Phys. Rev. B **74**, 014408.

Zhou, H. D., E. S. Choi, G. Li, L. Balicas, C. R. Wiebe, Y. Qiu, J. R. D. Copley, and J. S. Gardner (2011), Phys. Rev. Lett. **106**, 147204.

Zhou, Y., and P. A. Lee (2011), Phys. Rev. Lett. **106**, 056402.

Zhou, Y., P. A. Lee, T. K. Ng, and F. C. Zhang (2008), Phys. Rev. Lett. **101**, 197201.

Zhou, Y., and T. K. Ng (2013), Phys. Rev. B **88**, 165130.

Zhou, Y., and X.-G. Wen (2002), arXiv:cond-mat/0210662 .